UNIVERSITY OF CALIFORNIA, SAN DIEGO

# Lysophosphatidic Acid (LPA) Signaling in the Etiology of Fetal Hydrocephalus

A dissertation submitted in partial satisfaction of the
requirements for the degree Doctor of Philosophy

in

Biomedical Sciences

by

Yun C. Yung

Committee in charge:

Professor Jerold Chun, Chair
Professor Joan Heller Brown, Co-Chair
Professor Katerina Akassoglou
Professor Joseph Gleeson
Professor Bruce Hamilton

2010

The Dissertation of Yun C. Yung is approved, and it is acceptable in quality and form for publication on microfilm and electronically:

_____

_____

_____

_____
Co-Chair

_____
Chair

University of California, San Diego

2010

# DEDICATION

*This dissertation is dedicated with love and gratitude*
*to my wife Tevy Tith,*
*my sister Christine Yung Yusi,*
*and my parents Ching-Jing and Yueh-Neu Yung,*
*and in fond memory of my grandmother Maan-Tuan Chang Yung (1926-2005)*

*Also, I dedicate this dissertation to the patients and families*
*who are impacted by the neurological disorder I present here.*
*May they find comfort in the onward progress of medicine.*

EPIGRAPH

"If I have seen further than others,
it is by standing upon the shoulders of giants."

*Sir Isaac Newton*

*On making discoveries:*

"By always thinking unto them.
I keep the subject constantly before me
and wait till the first dawnings open
little by little into the full light."

*Sir Isaac Newton*

TABLE OF CONTENTS

LIST OF FIGURES

Chapter I



Chapter II

Chapter III



Appendix A



Appendix B

LIST OF TABLES

Chapter II



Chapter III



Appendix A



Appendix B

ACKNOWLEDGEMENTS

I thank Dr. Jerold Chun for giving me the opportunity to conduct my doctoral work in his laboratory these many years. His unwavering support, enthusiasm, and intellectual and personal guidance as both mentor and chair of my committee have been invaluable and encouraged me to embark on intellectually exciting and ultimately rewarding studies. I started my Ph.D. career broadly oriented towards neuroscience, but Jerold's interdisciplinary interests have given me an excellent roadmap to many fields and, in particular, allowed me to surf a fine line between neurobiology and lipid science. I will miss the weekly meetings and the impromptu discussions but look forward to many more years of scientific collaboration and friendship.

I would also like to thank the other members of my dissertation committee for their guidance: Dr. Joan Heller Brown as the co-chair of my committee and for help on GPCR signaling; Dr. Bruce Hamilton for asking hard but necessary questions and always encouraging me towards better science; Dr. Joseph Gleeson for perspectives on neurological disorders, helpful suggestions regarding cilia, and introduction to UCSD as my faculty host; and Dr. Katerina Akassoglou for expanding my awareness of neuroinflammation and her commitment to my professional development despite being a flight away.

It is sometimes little appreciated how extensively one's environment influences their trajectory in life. I would like to gratefully acknowledge past and present members of the Chun lab for their technical assistance, camaraderie, and friendship that has made this time so rewarding. I thank Drs. Marcy Kingsbury and

Stevens Rehen for sharing their enthusiasm for both the LPA and aneuploidy projects and being so supportive, which ultimately lead me to pursue both avenues of work. I thank Dr. Tetsuji Mutoh for his intellectual discussions and partnership in examining lysophospholipid effects on the developing cortex. He was also a source of inspiration for my foray into marathon running. I also thank Grace Kennedy for invaluable all-around help; she was a treasure trove of knowledge and taught me much histology and microscopy. I will miss her stories! I would also like to thank Drs. Richard Rivera and Deron Herr for all their advice, help with molecular biology, and introduction to fine beer. To each "beer sensei": gan-bei! I am also grateful to Keira S.T. Teo, who made both life inside and outside of lab so much fun! Because of her, I will never think twice about "restaurant hopping." Special thanks also go to Dr. Xiaoqin Ye for her advice, scientific discussions, and inspirational grit and determination. In addition to Stevens, I would also like to thank members of the aneuploidy crew - Drs. Suzanne Peterson and Willem Westra – for their support during the days of FISH spot counting. Special thanks also go to Danielle Letourneau and Victoria Hedquist for administrative help and friendship. In particular, I thank Danielle for preparing me for parenthood. Finally, I thank all the remaining members of the lab for great memories: Drs. Kyoko Noguchi, Ji Woong Choi, Chang-Wook Lee, Amy Yang, Michael McConnell, Adrienne Dubin, Brigitte Anliker, Eric Birgbauer, and Alycia Mosley, as well as Mu-en Lin, Diane Bushman, Hope Mirendil, Kristine Park, and Christine Westra.

I would also like to thank various members of the laboratories within the Dorris Neuroscience Center and the Scripps Research Institute for their generous sharing of reagents, protocols, and equipment in keeping with the cherished spirit of scientific openness. This was truly a special place, with extensive resources and expert personnel, to develop and train as a young scientist. In particular I would like to acknowledge crucial help from Dusko Trajkovic in histology; Dr. Kathryn Spencer for indispensable help with microscopy; Dr. Alan Saluk and members of the TSRI flow cytometry core for help with sorting experiments; and Dr. Malcolm Wood at the TSRI microscopy core for help with EM imaging.

I also acknowledge the many classmates in the Biomedical Sciences Program that I came to know and befriend, especially Drs. Benjamin Sachs, Lisa Gallegos, Lindsey Lewellyn, David Peters, Thomas Gallegos, and Jason Goode.

Family is the most important anchor in my life, and I want to thank my parents Dr. Ching-Jing and Yueh-Neu Yung for their encouragement to pursue what I love, a freedom I cherish deeply. I want to also thank my sister Christine for her support over the years and listening to my ideas. I am happy that we are finally on the same coast. I also thank my late grandmother Maan-Tuan Chang Yung who was such a strong woman with a generous heart.

Finally, words cannot adequately express how grateful I am to have the loving and unfailing support of my best friend and wife, Tevy. I cannot imagine going through graduate school or any other major challenge without her. I thank her for her

patience with my irregular schedule, uncertain time table, and vacillating moods; she accepted it all with grace, kindness, and humor.

Chapter II has been submitted for publication of the material. Yung, YC; Mutoh, T; Lin, M-E; Noguchi, K; Rivera, RR; Choi, JW; Kingsbury, MA; Chun, J. The dissertation author was the primary investigator and co-author of this material.

Appendix A is a reprint, in full, of the material as it appears in Constitutional Aneuploidy in the Normal Human Brain in the Journal of Neuroscience, 2005. Rehen SK, Yung YC, McCreight MP, Kaushal D, Yang AH, Almeida BS, Kingsbury MA, Cabral KM, McConnell MJ, Anliker B, Fontanoz M, Chun J. The dissertation author was a primary investigator and co-author of this paper.

Appendix B is a reprint, in full, of the material as it appears in Identification of Neural Programmed Cell Death through the Detection of DNA in situ and by PCR in Current Protocols Neuroscience, 2009. Yung, YC; Kennedy, G Chun, J. The dissertation author was the primary investigator and author of this paper.

## CURRICULUM VITAE

### EDUCATION

| | |
|---|---|
| 2010 | Ph.D. in Biomedical Sciences<br>School of Medicine, University of California, San Diego |
| 2003-2010 | Graduate Student, Biomedical Sciences Program<br>School of Medicine, University of California, San Diego<br>Advisor: Dr. Jerold Chun |
| 2000-2003 | Research Fellow<br>Stanford University School of Medicine<br>Laboratory of Dr. Victor Tse |
| 1999 | A.B., Molecular and Cell Biology<br>University of California, Berkeley |
| 1999 | A.B., Cognitive Sciences<br>University of California, Berkeley |

### SCHOLARSHIPS AND AWARDS

| | |
|---|---|
| 2010-2012 | Hydrocephalus Association Mentored Young Investigator<br>The Scripps Research Institute<br>Laboratory of Dr. Jerold Chun |
| 2005-2008 | NSF Predoctoral Fellowship<br>Laboratory of Dr. Jerold Chun |
| 2001-2003 | ECS Brain Tumor Research Fellowship<br>Laboratory of Dr. Victor Tse |

### PUBLICATIONS

*~ Articles ~*

**Yung YC**, Mutoh T, Lin M-E, Noguchi K, Rivera RR, Choi JW, Kingsbury MA, Chun J. Lysophosphatidic acid (LPA) signaling as an initiating cause of fetal hydrocephalus. (*manuscript submitted*)

Choi JW, Gardell SE, Herr DR, Rivera RR, Lee CW, Noguchi K, Teo ST, **Yung YC**, Melissa Lu, Grace Kennedy, and Jerold Chun. FTY720 (fingolimod) efficacy in an animal model of multiple sclerosis requires astrocyte S1P1 modulation. (*manuscript submitted*)

Westra JW, Rivera RR, Bushman DM, **Yung YC**, Peterson SE, Barral S, Chun J. Neuronal DNA content variation (DCV) with regional and individual differences in the human brain. J Comp Neurol. 2010 Oct 1;518(19):3981-4000.

Westra JW, Peterson SE, **Yung YC**, Mutoh T, Barral S, Chun J. Aneuploid mosaicism in the developing and adult cerebellar cortex. J Comp Neurol. 2008 Apr 20;507(6):1944-51.

Lunyak VV, Prefontaine GG, Nunez E, Cramer T, Ju BG, Ohgi KA, Hutt K, Roy R, Garcia-Diaz A, Zhu X, **Yung Y**, Montoliu L, Glass CK, Rosenfeld MG. Developmentally regulated activation of a SINE B2 repeat as a domain boundary in organogenesis. Science. 2007 Jul 13;317(5835):248-51.

Santarelli JG, Udani V, **Yung YC**, Cheshier S, Wagers A, Brekken RA, Weissman I, Tse V. Incorporation of bone marrow-derived Flk-1-expressing CD34+ cells in the endothelium of tumor vessels in the mouse brain. Neurosurgery. 2006 Aug;59(2):374-82; discussion 374-82.

Santarelli JG, Udani V, **Yung YC**, Cheshier S, Wagers A, Brekken RA, Weissman I, Tse V. Preuss Resident Research Award: bone marrow-derived Flk-1-expressing CD34+ cells contribute to the endothelium of tumor vessels in mouse brain. Clin Neurosurg. 2005;52:384-8.

Huhn SL, **Yung YC**, Cheshier S, Harsh G, Ailles L, Weissman I, Vogel H, Tse VK. Identification of phenotypic neural stem cells in a pediatric astroblastoma. J Neurosurgery (5 Suppl Pediatrics) 2005. 103:446-450.

**Yung YC**, Rehen SK, McCreight MP, Yang AH, Almeida BSV, Kingsbury MA, Cabral KMS, Kaushal D, McConnell MJ, Anliker B, Fontanoz M, Chun J. Constitutional Aneuploidy in the Normal Human Brain. J Neurosci. 2005 Mar 2;25(9):2176-80. [J. Neuroscience cover art]

Udani V, Santarelli J, **Yung Y**, Cheshier S, Andrews A, Kasad Z, Tse V. Differential expression of angiopoietin-1 and angiopoietin-2 may enhance recruitment of bone marrow-derived endothelial precursor cells into brain tumors. Neurol Res 2005 Dec;27(8):801-6.

Udani VM, Santarelli JG, **Yung YC**, Wagers AJ, Weissman IL, Cheshier S, Tse V. Hematopoietic Stem Cells Give Rise to Perivascular Endothelial-like Cells during Brain Tumor Angiogenesis. Stem Cells & Dev. 2005 Oct;14(5):478-86.

**Yung YC**, Cheshier S, Santarelli JG, Huang Z, Wagers A, Weissman IL, Tse VK. Incorporation of Naïve Bone Marrow Derived Cells into the Vascular Architecture of Brain Tumor. Microcirculation, 2004. Dec; 11(8): 699-708.

Tse VK, **Yung YC**, Xu L, Huang Z, Hsaio M, Yancopoulos G, Silverberg G. Effects of Tumor Suppressor Gene p53 on Brain Tumor Angiogenesis and Expression of Angiogenic Modulators. Anticancer Research, 2004 Jan-Feb; 24(1):1-10.

Tse V, Xu L, **Yung YC**, Santarelli JG, Juan D, Fabel K, Silverberg G, Harsh G. The temporal-spatial expression of VEGF, angiopoietins-1 and 2, and Tie-2 during tumor angiogenesis and their functional correlation with tumor neovascular architecture. Neurological Research, 2003 Oct; 25(7):729-738.

*~ Reviews ~*

Choi JW, Herr DR, Noguchi K, **Yung YC**, Lee CW, Mutoh T, Lin ME, Teo ST, Park KE, Mosley AN, Chun J. LPA Receptors: Subtypes and biological actions. Annu Rev Pharmacol Toxicol. 2010;50:157-86.

Teo ST, **Yung YC**, Herr D, Chun J. Lysophosphatidic Acid in Vascular Development and Disease. IUBMB Life. 2009 Jul 20; 61(8):791-799.

**Yung YC**, Kennedy G, Chun J. Identification of Neural Programmed Cell Death through the Detection of DNA Fragmentation in situ and by PCR. Curr Protoc Neurosci. 2009 Jul;Chapter 3:Unit3.8.

Peterson SE, Rehen SK, Westra W, **Yung Y**, Chun J. Spectral Karyotyping and Fluorescent in situ Hybridization. In Human Stem Cell Manual: A Laboratory Guide. Chapter 7, pp. 71-84. Loring JF (Ed.). Elsevier Science & Technology Books (2007)

Kingsbury MA, **Yung YC**, Peterson SE, Westra JW, Chun J. Aneuploidy in the normal and diseased brain. Cell Mol Life Sci. 2006 Nov;63(22):2626-41.

*~ Posters & Presentations ~*

**Yung YC**, Mutoh T, Lin M-E, Kingsbury MA, Chun J. Lysophosphatidic acid signaling through $LPA_1$ receptor in fetal hydrocephalus. $4^{th}$ Global COE International

Symposium jointly with 19th Hot Spring Harbor Symposium: Molecular Evolution and Bioinformatics (2009).

**Yung YC**, Mutoh T, Lin M-E, Kingsbury MA, Chun J. Lysophosphatidic acid signaling through $LPA_1$ receptor in fetal hydrocephalus. Society for Neuroscience (2009).

**Yung YC**, Mutoh T, Lin M-E, Webb B, Kingsbury MA, Teo ST, Chun J. Lysophosphatidic acid signaling through $LPA_1$ receptor in fetal hydrocephalus. FASEB SRC (2009).

Peterson SE, Yang AH, Westra JW, **Yung YC**, Mutoh T, Rehen SK, Chun J. Non-uniform changes in mosaic aneuploidies of the developing cortex following caspase inhibition. Society for Neuroscience (2007).

**Yung YC**, Zhu L, Westra JW, Peterson SE, Mutoh T, Chun J. Analysis of mosaic aneuploidies in the Down syndrome brain. Society for Neuroscience (2007).

Udani V, Santarelli J, Andrews A, Kasad Z, **Yung Y**, Tse V. Involvement of bone marrow derived cells with angiopoietins in brain tumor angiogenesis. Association of Neurological Surgeons 72st annual meeting (2004).

Huhn S, **Yung Y**, Juan D, Cheshier S, Tse V. Identification of phenotypic neural stem cells in pediatric brain tumor. AANS/CNS Pediatric Neurosurgery Joint meeting (2003).

Hou L, Juan D, Cheshier S, **Yung Y**, Silverberg G, Tse V. The role of sonic hedgehog protein in tumor angiogenesis. Association of Neurological Surgeons 71st annual meeting (2003).

Cheshier S, **Yung Y**, Hou L, Wagers A, Weissman I, Tse V. The involvement of bone marrow derived cells in tumor angiogenesis. Association of Neurological Surgeons 71st annual meeting (2003).

Tse V, Xu L, Huang Z, **Yung Y**, Silverberg G. The influence of tumor suppressor gene p53 on the expression of angiopoietin-1 and 2: Its role(s) in inhibiting tumor angiogenesis. CNS 52nd annual meeting (2002).

ABSTRACT OF THE DISSERTATION

Lysophosphatidic Acid (LPA) Signaling in the Etiology of Fetal Hydrocephalus

by

Yun C. Yung

Doctor of Philosophy in Biomedical Sciences

University of California, San Diego, 2010

Professor Jerold Chun, Chair
Professor Joan Heller Brown, Co-Chair

Lysophosphatidic acid (LPA) is a small, ubiquitous phospholipid that acts as an extracellular signaling molecule through at least six cognate G protein-coupled receptors $LPA_{1-6}$. These receptors mediate diverse biological responses, including developmental, physiological, and pathophysiological effects. The embryonic nervous system is a major site of LPA presence and action through its receptors, although the precise cellular and mechanistic roles are not well understood. To study the role of LPA signaling in an intact developing cortex, I developed an *in utero* injection

paradigm targeting mouse brain and used histology and immunochemistry in combination with pharmacological perturbation and LPA receptor null mutants to study this system. Overactivation of $LPA_1$ via a single LPA bolus exposure causes disruption of neuroprogenitor cells (NPCs) residing in the ventricular zone of the fetal brain, numerous accompanying histological changes - including ventricular dilation, formation of neurorosettes and heterotopias, mitotic displacement, loss of ependymal cells, ciliary defects, and $3^{rd}$ ventricular occlusion - and subsequently fetal hydrocephalus (FH). In addition, exposure to blood derivatives and components such as serum and plasma through hemorrhage, two major sources of LPA, also cause FH. This modeled disorder can be prevented using both $LPA_1$ null mutants and pharmacological antagonism. This novel role of LPA in the etiology of FH is consistent with multiple, independent hydrocephalic models and clinical observations, suggesting common mechanistic pathways and, importantly, potential therapeutic targets for the amelioration of this disorder.

# CHAPTER I

General Introduction

Proper formation of the cerebral cortex is vital for cognition and behavior. In humans, cortical malformations result in debilitating neurological disorders with numerous personal and societal costs. Understanding the mechanisms that underlie both normal and pathological development, therefore, provides insight into the basis of such disorders and may facilitate their future amelioration and treatment. Recent, intriguing observations that bioactive lipids, such as LPA, can considerably alter cortical structure, lead to the intense exploration of its effect on the development of the cerebral cortex described here.

## 1.1 Development of the cerebral cortex

The study of the nervous system has preoccupied numerous philosophers and scientists since ancient times. Evidence of detailed studies can be found in early treatises by individuals such as Hippocrates and Galen (1). Subsequent invention of the microscope permitted observations that lead to the collective recognition that organisms are composed of cells, a theory first postulated by Theodor Schwann in 1839 (2). Further refinements in microscopy, coupled with the critical discovery of a selective staining method by Camillo Golgi, permitted his contemporary Santiago Ramòn y Cajal to make detailed morphological observations of single neural cells over 100 years ago (3, 4). Since then, exponential technological progress in various forms of imaging and labeling techniques have lead to a fundamental understanding of all parts of the nervous system, importantly the cerebral cortex (5).

The cerebral cortex of the brain is distinctly unique in humans. Structurally, it is a bilateral sheet of neural tissue approximately 1 - 4.5 mm thick (6) on the outermost brain surface with strong gyrification patterns and arranged in a laminar pattern with up to six horizontal layers with different cellular and connective compositions (7). The cerebral cortex is composed of neurons, astrocytes, oligodendrocytes, immune cells, and blood vessels (7). Most importantly, the cerebral cortex plays critical roles in memory, thought, language, reason, creativity, and consciousness (8).

Broadly speaking, corticogenesis follows a stereotyped, continuous sequence of progressive and regressive events that involve cell proliferation, patterning, neuronal migration, synapse formation, and cell death (7). From the embryo, the neural tube arises from the ectoderm, rapidly expands by cell proliferation and forms the telencephalon (forebrain, including the cerebral cortex), the mesencephalon (midbrain), and rhombencephalon (hindbrain) (9, 10). The cortex develops through an inside-out process: early proliferating cells generate the preplate; further dividing cells migrate and divide the preplate into the subplate and marginal zone; and finally future cells generated in the dividing ventricular zone (VZ) layer migrate past settled cell layers (11, 12). Thus, the earliest born cells reside deep in the cortex and later born cells inhabit more superficial positions.

Generation of daughter cells with distinct identities involves two essential, entwined processes: interkinetic nuclear migration (13) and cell division (14). Neuroblasts within the ventricular zone are attached to both the apical ventricular and

pial surfaces; during cell cycle progression, these elongated, fusiform-shaped progenitors undergo S-phase and synthesize their DNA within the subventricular zone (14). They then translocate their nuclei downwards to the apical ventricular surface, round up, and divide by mitosis (15). Dividing neuroblasts can undergo either symmetric or asymmetric division, producing classes of progenitor cells that include neuroepithelial cells, radial glia, and basal progenitors (16, 17). In symmetric division, the parental cell gives rise to two progeny cells that remain as neuroprogenitors – ready to divide again – or as two terminally differentiated neuronal cells that can migrate to their final settled position, whereas asymmetric division produces one of each cell type (18). During this period of rapid cell generation, numerous cells are pruned through a process termed proliferative cell death (please refer to Appendix B), whereby an average of 50% of cells are dying at any given period (19). While the purpose of this cell death is unclear, the validated detection of variable genetic content at the chromosomal level in individual cells during this time - termed neural aneuploidy (please refer to Appendix A) (20-25) – may suggest one possible reason: a Darwinian strategy to promote neural diversity and fitness. Other concurrent and subsequent developmental processes, including vasculogenesis (26) and angiogenesis (27), gliogenesis (28, 29), synaptic wiring, and cell pruning through programmed cell death (30, 31), contribute to and complete the overall formation of the cerebral cortex .

**Development of the cerebroventricular system**

An additional aspect of brain development pertains to the fluid-filled ventricular cavity immediately ventral to the neuroproliferative layer. As the cerebral cortex and other brain structures are formed, the central lumen of the neural tube enlarges and forms the hollow chambers and narrow passages that emerge as the lateral, 3$^{rd}$, and 4$^{th}$ ventricles and connecting aqueducts (32). The development of the ventricular system depends, in part, on the contractility of the overlying neuroepithelium (33). The ventricular system of the brain is filled with cerebrospinal fluid (CSF) - composed of water, ions, and bioactive factors produced by choroid plexi – that flows posteriorly and is reabsorbed into the draining sinuses of the head (34). The specialized ependymal cell eventually forms a single-cell barrier between cortical tissue and the underlying flowing CSF (35, 36). Multi-ciliated ependymal cells arise during mid to late neurogenesis, differentiating and maturing by early post-natal life in the mouse (37). Coordinated beating of cilia contributes to CSF flow within the ventricles, which is thought to be important for removal of wastes, and more recently, proper formation of neural structures (38-41).

**Lysophosphatidic acid biology**

Recently, many molecular cues that govern the formation of the cerebral cortex have been identified, among them a quantitatively minor but bioactive fraction of lipids termed lysophospholipids (LPs). While lipids, in general, have been

traditionally regarded as energy storage and structural molecules, a growing body of work identify the importance of LPs in basic cell processes such as growth, movement, communication, and death.

There are several classes of LPs, among them lysophosphatidic acid (LPA) (Figure 1.1), which signals through a family of at least 6 G-protein coupled receptors, $LPA_{1-6}$ (42, 43) (Figure 1.2), which mediate a wide variety of biological processes. In 1996, the first cognate, cell-surface receptor for LPA was identified ($LPA_1$) (44). The mammalian *LPAR1* gene (human chromosomal locus 9q31.3) encodes an approximately 41-kDa protein consisting of 364 amino acids with 7 putative transmembrane domains. In mice, the opening reading frame is encoded on two of five exons with a conserved intron (shared with *Lpar2* and *Lpar3*).

While *Lpar1* expression is widespread in adult tissues such as brain, uterus, testis, and spleen (42), it is more spatially restricted during embryonic development, with strong expression in the nervous system (45, 46). In the cerebral cortex, *Lpar1* expression is limited to the VZ and superficially in the meninges and layer 1 (Figure 2.S8) (44). Although the VZ disappears at the end of cortical neurogenesis, just prior to birth, *Lpar1* continues in the postnatal brain, where it is found in oligodendrocytes and Schwann cells, the myelinating cells of the central nervous system (CNS) and peripheral nervous system (PNS), respectively (47, 48). The spatiotemporal expression pattern of *Lpar1* suggests potential involvement with neuroprogenitor development and perhaps cerebral cortical formation.

oleoyl LPA

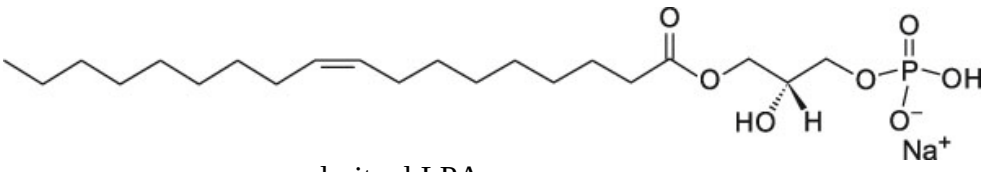


palmitoyl LPA

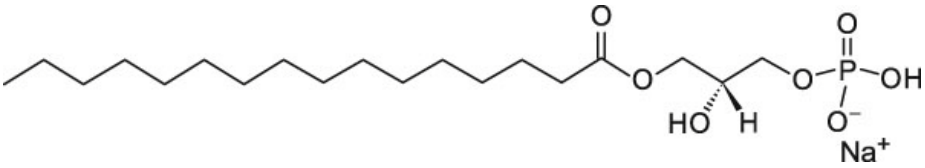


arachidonoyl LPA

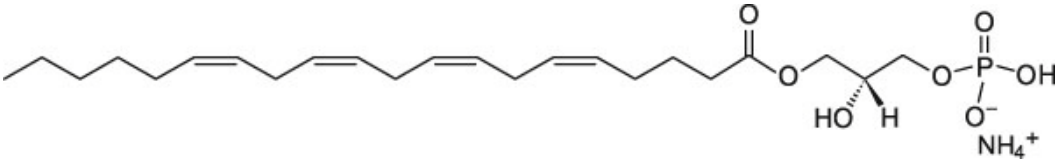


**Figure 1.1: Chemical structures of several common forms of lysophosphatidic acid (LPA).** LPA is composed of a glycerol backbone, a phosphate group, and an acyl chain of varying length and degree of saturation. Oleoyl LPA, also commonly known as 18:1 LPA, exists naturally in organisms, is commonly used as a laboratory reagent, and is the main reagent in the studies presented here. Other forms include palmitoyl (16:0) and arachidonoyl (20:4) LPA.

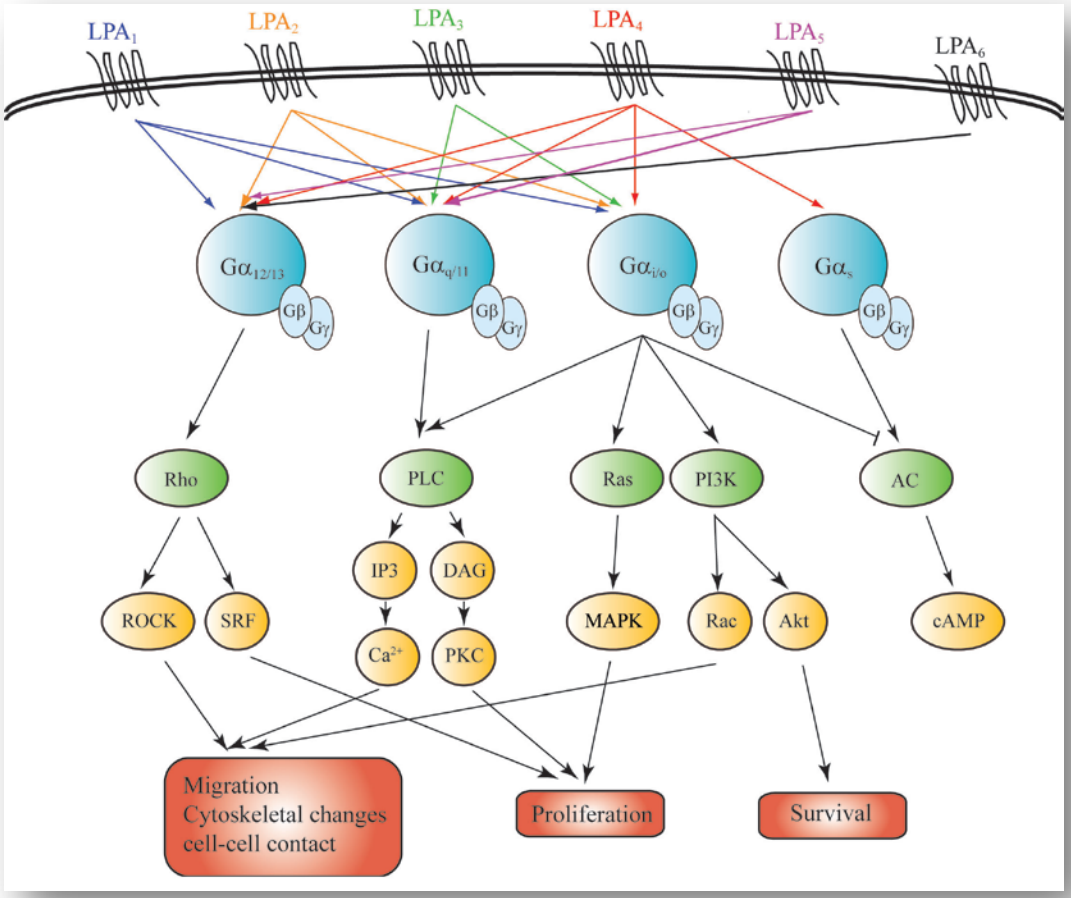


**Figure 1.2: Downstream signaling pathways activated by $LPA_{1-6}$ G protein-coupled receptors.**

*LPAR2* (chromosome locus 19p12) encodes a protein with a predicted amino acid sequence of 348 residues (~39 kDa) (49). *Lpar2* has 60% amino acid similarity to *Lpar1*. In the adult, *Lpar2* is more restricted in its expression pattern compared with *Lpar1*, with high levels in kidney, uterus, and testis and to a lesser extent in lung, stomach, spleen, thymus, heart, and brain (50). In the embryonic cortex, *Lpar2* is present at moderate levels, quantitatively less than *Lpar1* (46), with a more diffuse expression pattern throughout the cortical wall (Figure 2.S9) (51).

$LPA_1$ and $LPA_2$ couple to and activate three types of G proteins: $G\alpha_{i/o}$, $G\alpha_{q/11}$, and $G\alpha_{12/13}$ (52, 53) which signal downstream and produce $Ca^{2+}$ mobilization; adenylyl cyclase inhibition; and activation of various intracellular mediators such as mitogen-activated protein kinase, Rac, phospholipase C, Akt, and Rho (Figure 1.2) (reviewed in (50, 54, 55)). A range of cellular responses ensue: cytoskeletal reorganization, process retraction, cell proliferation and survival, cell migration, and cell differentiation (55-57). These LPA-mediated processes influence numerous biological processes, including nervous system function, vascular development, immune system function, cancer, reproduction, and obesity (42).

Genetic deletion of these receptors has revealed numerous disruptions in various systems. *Lpar1*$^{-/-}$ mice show 50% perinatal lethality in a mixed (C57Bl/6J x 129) genetic background. Survivors have a reduced body size, craniofacial dysmorphism with blunted snouts, and increased apoptosis in sciatic nerve Schwann

cells (58, 59). Defective suckling, attributed to olfactory defects, likely accounts for perinatal lethality. Small fractions of *Lpar1*$^{-/-}$ embryos have exencephaly (~5%) or frontal cephalic hemorrhage (~2.5%). In addition, an *Lpar1*$^{-/-}$ substrain arose spontaneously during colony expansion, which is called the "Màlaga variant" and exhibits more severe developmental brain defects (60). *Lpar2*$^{-/-}$ mice unexpectedly are viable, grossly normal, and born at normal Mendelian ratios (61). Examination of *Lpar1*$^{-/-}$ *Lpar2*$^{-/-}$ double null mice reveals no additional defects relative to the original *Lpar1*$^{-/-}$ mice, except for an increased incidence of perinatal frontal hematoma (61).

**LPA and development of the cerebral cortex**

High levels of LPA receptor expression exist within the nervous system and is present in most cell types here, including neural progenitors, primary neurons, astrocytes, microglia, oligodendrocytes, and Schwann cells (reviewed in (62)). The putative ligand LPA also exists in the brain at relatively high concentrations at both embryonic (Figure 2.S3) and adult ages (63).

The restricted expression of $LPA_1$ within the proliferative cortical VZ of the embryonic brain (44, 52) indicates a significant role of LPA signaling in the development of VZ neuroprogenitor (NPC) cells, which express *Lpar1* and *Lpar2*. Heterologous expression studies in NPC lines have revealed changes in cellular morphology due to LPA receptors (55, 62), while LPA signaling also significantly alters the morphology of primary NPCs via promotion of neurite retraction and

compaction in the VZ via actomyosin rearrangement (58, 64-67). Furthermore, LPA signaling can also stimulate proliferation and differentiation of primary NPCs (52, 68) and neurosphere cultures (69) via $LPA_1$ and differentiation of immortalized hippocampal progenitor cells via $LPA_4$ (70). Additionally, LPA can stimulate ionic conductance changes in cortical NPCs earlier than L-glutamate or GABA, with contribution mainly from $LPA_1$ and $LPA_2$ (46, 71). Thus, LPA mediates a diverse range of neurodevelopmentally relevant effects in many validated *in vitro* systems.

What are the effects of LPA on corticogenesis in an intact brain? Initially, this was examined using an *ex vivo* whole cortical hemisphere culture system (72, 73). Exogenous LPA exposure increased terminal mitosis of NPCs, resulting in cortical thickening and folding that resembled gyri. These effects were absent in embryonic cerebral cortices from *Lpar1*$^{-/-}$ *Lpar2*$^{-/-}$ double null mice exposed to LPA, demonstrating that these changes were dependent on both LPA receptors. Surprisingly, LPA exposure did not increase NPC proliferation (as was seen during *in vitro* studies), but instead resulted in decreased cell death and early cell cycle exit, which lead to increased terminal mitosis. This study provided evidence for a considerable role of LPA signaling in corticogenesis via perturbation of a variety of NPC functions and through alteration of gross cortical structure.

Companion studies examining the genetic loss of *Lpar1*, *Lpar2*, or *Lpar1 Lpar2* double null mice found only minor cellular defects in brain development (58, 61). This was a surprising finding based on known influences of LPA signaling and since dissociated cultures of fibroblast cells derived from these single or double null

mice showed receptor-dependent deficits in the LPA signaling pathways. Recently, several studies which examined the Màlaga $LPA_1$ null variant reported significant, pronounced defects in cortical development, including reduced proliferative populations and increased cortical apoptosis (60), with similar effects on hippocampal neurogenesis (74). Furthermore, this $LPA_1$ null variant also showed behavioral deficits in exploratory and memory function (75). Thus, LPA signaling, particularly through $LPA_1$, appears to have substantially more influence - both subtle and gross - on cortical development than initially recognized.

**LPA and neurological disorders**

In addition to its role in normal cortical development, there may be an intriguing link between LPA signaling and neurological disorders (58, 76-79), particularly ones such as autism and schizophrenia that have a neurodevelopmental basis. (80). This inferred relationship is based on observed phenotypic and molecular similarities - such as craniofacial dysmorphism (58, 80, 81), defects in prepulse inhibition (80, 82), and widespread brain alterations in serotonin (5-HT) neurotransmitter levels (80, 83) – that are present in both *Lpar1*$^{-/-}$ mice and patients suffering from schizophrenia. LPA can interfere with glial cell signaling and morphology induced by the atypical antipsychotic Risperidone (84), used in the treatment of both schizophrenia and autism. Furthermore, embryonic brain exposure to LPA in the *ex vivo* murine model demonstrated altered gyrification-like changes in

the cerebral cortex (72), consistent with observations in autism (85) and schizophrenia (86).

Interestingly, some epidemiological studies link environmental perturbations such as prenatal or maternal bleeding, among other factors, to autism (87) and schizophrenia (88). Because LPA and its metabolic precursors are present in blood (89), conditions where the blood-brain barrier is compromised and/or LPA production is altered may generate abnormal LPA signaling and lead to neurological pathologies. Indeed, a pathologically high concentration of LPA (10 μM) inhibits neurogenesis in neurosphere cultures (90), suggesting that LPA exposure dosage may modulate at least one relevant parameter in brain development. Taken together, this growing body of evidence implicates LPA signaling in multiple CNS disorders, but additional mechanistic studies are needed to further understand and delineate these associations.

**Experimental approach**

Until now, LPA signaling in the nervous system and particularly the developing cerebral cortex has been studied through complementary *ex vivo* gain-of-function and *in vivo* loss-of-function approaches (58, 60, 62, 72, 74, 75). While these studies have yielded a wealth of knowledge, a major limitation has been the lack of *in vivo* gain-of-function studies in living animals, which would be valuable for examining LPA signaling in an intact physiological context at specific time periods. Therefore, a major enterprise of these studies has been the optimization of the

injection of various LPA-related ligands into the embryonic murine brain ventricles at periods of known LPA receptor expression (Figure 2.1). There are at least four advantages; this allows for the 1) delivery of ligand directly to the LPA receptors which are adjacent to the ventricles; 2) preservation of *in vivo* cortical architecture, cell cycle kinetics, and neurogenic characteristics; 3) analysis of long term pre- and postnatal cortical effects; and 4) examination of behavior in intact animals. Coupled with the ease of genetic manipulation, the mouse is an ideal system for studying how altered LPA signaling could influence the development of the cerebral cortex *in vivo*.

**References**


1. Nutton, V. (2004). Ancient medicine, (London ; New York: Routledge).

2. Baker, J.R. (1988). The cell theory : a restatement, history, and critique, (New York: Garland).

3. Mazzarello, P. (2010). Golgi : a biography of the founder of modern neuroscience, (Oxford ; New York: Oxford University Press).

4. Ramón y Cajal, S. (1988). Recollections of my life, (New York: Garland).

5. Wilt, B.A., Burns, L.D., Wei Ho, E.T., Ghosh, K.K., Mukamel, E.A., and Schnitzer, M.J. (2009). Advances in light microscopy for neuroscience. Annu Rev Neurosci *32*, 435-506.

6. Fischl, B., and Dale, A.M. (2000). Measuring the thickness of the human cerebral cortex from magnetic resonance images. Proc Natl Acad Sci U S A *97*, 11050-11055.

7. Sanes, D.H., Reh, T.A., and Harris, W.A. (2006). Development of the nervous system, 2nd Edition, (Amsterdam ; Boston: Elsevier).

8. Zelazo, P.D., Moscovitch, M., and Thompson, E. (2007). The Cambridge handbook of consciousness, (Cambridge ; New York: Cambridge University Press).

9. Wilson, S.W., and Houart, C. (2004). Early steps in the development of the forebrain. Developmental cell *6*, 167-181.

10. Liu, A., and Joyner, A.L. (2001). Early anterior/posterior patterning of the midbrain and cerebellum. Annu Rev Neurosci *24*, 869-896.

11. Angevine, J.B., Jr., and Sidman, R.L. (1961). Autoradiographic study of cell migration during histogenesis of cerebral cortex in the mouse. Nature *192*, 766-768.

12. Sidman, R.L., and Rakic, P. (1973). Neuronal migration, with special reference to developing human brain: a review. Brain Res *62*, 1-35.

13. Sauer, M.E., and Walker, B.E. (1959). Radioautographic study of interkinetic nuclear migration in the neural tube. Proc Soc Exp Biol Med *101*, 557-560.

14. Sidman, R.L., Miale, I.L., and Feder, N. (1959). Cell proliferation and migration in the primitive ependymal zone: an autoradiographic study of histogenesis in the nervous system. Exp Neurol *1*, 322-333.

15. Schenk, J., Wilsch-Brauninger, M., Calegari, F., and Huttner, W.B. (2009). Myosin II is required for interkinetic nuclear migration of neural progenitors. Proc Natl Acad Sci U S A *106*, 16487-16492.

16. Huttner, W.B., and Kosodo, Y. (2005). Symmetric versus asymmetric cell division during neurogenesis in the developing vertebrate central nervous system. Curr Opin Cell Biol *17*, 648-657.

17. Fish, J.L., Dehay, C., Kennedy, H., and Huttner, W.B. (2008). Making bigger brains-the evolution of neural-progenitor-cell division. J Cell Sci *121*, 2783-2793.

18. Farkas, L.M., and Huttner, W.B. (2008). The cell biology of neural stem and progenitor cells and its significance for their proliferation versus differentiation during mammalian brain development. Curr Opin Cell Biol *20*, 707-715.

19. Blaschke, A.J., Staley, K., and Chun, J. (1996). Widespread programmed cell death in proliferative and postmitotic regions of the fetal cerebral cortex. Development *122*, 1165-1174.

20. Rehen, S.K., McConnell, M.J., Kaushal, D., Kingsbury, M.A., Yang, A.H., and Chun, J. (2001). Chromosomal variation in neurons of the developing and adult mammalian nervous system. Proc Natl Acad Sci U S A *98*, 13361-13366.

21. Yang, A.H., Kaushal, D., Rehen, S.K., Kriedt, K., Kingsbury, M.A., McConnell, M.J., and Chun, J. (2003). Chromosome segregation defects contribute to aneuploidy in normal neural progenitor cells. J Neurosci *23*, 10454-10462.

22. Rehen, S.K., Yung, Y.C., McCreight, M.P., Kaushal, D., Yang, A.H., Almeida, B.S., Kingsbury, M.A., Cabral, K.M., McConnell, M.J., Anliker, B., et al. (2005). Constitutional aneuploidy in the normal human brain. J Neurosci *25*, 2176-2180.

23. Kingsbury, M.A., Yung, Y.C., Peterson, S.E., Westra, J.W., and Chun, J. (2006). Aneuploidy in the normal and diseased brain. Cell Mol Life Sci *63*, 2626-2641.

24. Peterson, S.E., Westra, J.W., Paczkowski, C.M., and Chun, J. (2008). Chromosomal mosaicism in neural stem cells. Methods Mol Biol *438*, 197-204.

25. Westra, J.W., Peterson, S.E., Yung, Y.C., Mutoh, T., Barral, S., and Chun, J. (2008). Aneuploid mosaicism in the developing and adult cerebellar cortex. J Comp Neurol *507*, 1944-1951.

26. Risau, W., and Flamme, I. (1995). Vasculogenesis. Annu Rev Cell Dev Biol *11*, 73-91.

27. Vasudevan, A., and Bhide, P.G. (2008). Angiogenesis in the embryonic CNS: a new twist on an old tale. Cell Adh Migr *2*, 167-169.

28. Gaiano, N., and Fishell, G. (2002). The role of notch in promoting glial and neural stem cell fates. Annu Rev Neurosci *25*, 471-490.

29. Sauvageot, C.M., and Stiles, C.D. (2002). Molecular mechanisms controlling cortical gliogenesis. Curr Opin Neurobiol *12*, 244-249.

30. Korsching, S. (1993). The neurotrophic factor concept: a reexamination. J Neurosci *13*, 2739-2748.

31. Raff, M.C., Barres, B.A., Burne, J.F., Coles, H.S., Ishizaki, Y., and Jacobson, M.D. (1993). Programmed cell death and the control of cell survival: lessons from the nervous system. Science *262*, 695-700.

32. Lowery, L.A., and Sive, H. (2009). Totally tubular: the mystery behind function and origin of the brain ventricular system. Bioessays *31*, 446-458.

33. Gutzman, J.H., and Sive, H. (2010). Epithelial relaxation mediated by the myosin phosphatase regulator Mypt1 is required for brain ventricle lumen expansion and hindbrain morphogenesis. Development *137*, 795-804.

34. Thompson, E.J. (2005). Proteins of the cerebrospinal fluid : analysis and interpretation in the diagnosis and treatment of neurological diseases, 2nd Edition, (Boston, MA: Elsevier).

35. Sarnat, H.B. (1992). Role of human fetal ependyma. Pediatr Neurol *8*, 163-178.

36. Sarnat, H.B. (1998). Histochemistry and immunocytochemistry of the developing ependyma and choroid plexus. Microsc Res Tech *41*, 14-28.

37. Spassky, N., Merkle, F.T., Flames, N., Tramontin, A.D., Garcia-Verdugo, J.M., and Alvarez-Buylla, A. (2005). Adult ependymal cells are postmitotic and are derived from radial glial cells during embryogenesis. J Neurosci *25*, 10-18.

38. Sawamoto, K., Wichterle, H., Gonzalez-Perez, O., Cholfin, J.A., Yamada, M., Spassky, N., Murcia, N.S., Garcia-Verdugo, J.M., Marin, O., Rubenstein, J.L., et al. (2006). New neurons follow the flow of cerebrospinal fluid in the adult brain. Science *311*, 629-632.

39. Miyan, J.A., Zendah, M., Mashayekhi, F., and Owen-Lynch, P.J. (2006). Cerebrospinal fluid supports viability and proliferation of cortical cells in vitro, mirroring in vivo development. Cerebrospinal Fluid Res *3*, 2.

40. Salehi, Z., and Mashayekhi, F. (2006). The role of cerebrospinal fluid on neural cell survival in the developing chick cerebral cortex: an in vivo study. Eur J Neurol *13*, 760-764.

41. Salehi, Z., Mashayekhi, F., Naji, M., and Pandamooz, S. (2009). Insulin-like growth factor-1 and insulin-like growth factor binding proteins in cerebrospinal fluid during the development of mouse embryos. J Clin Neurosci *16*, 950-953.

42. Choi, J.W., Herr, D.R., Noguchi, K., Yung, Y.C., Lee, C.W., Mutoh, T., Lin, M.E., Teo, S.T., Park, K.E., Mosley, A.N., et al. (2010). LPA receptors: subtypes and biological actions. Annu Rev Pharmacol Toxicol *50*, 157-186.

43. Yanagida, K., Masago, K., Nakanishi, H., Kihara, Y., Hamano, F., Tajima, Y., Taguchi, R., Shimizu, T., and Ishii, S. (2009). Identification and characterization of a novel lysophosphatidic acid receptor, p2y5/LPA6. J Biol Chem *284*, 17731-17741.

44. Hecht, J.H., Weiner, J.A., Post, S.R., and Chun, J. (1996). Ventricular zone gene-1 (vzg-1) encodes a lysophosphatidic acid receptor expressed in neurogenic regions of the developing cerebral cortex. J Cell Biol *135*, 1071-1083.

45. Ohuchi, H., Hamada, A., Matsuda, H., Takagi, A., Tanaka, M., Aoki, J., Arai, H., and Noji, S. (2008). Expression patterns of the lysophospholipid receptor genes during mouse early development. Dev Dyn *237*, 3280-3294.

46. Dubin, A.E., Herr, D.R., and Chun, J. (2010). Diversity of lysophosphatidic acid receptor-mediated intracellular calcium signaling in early cortical neurogenesis. J Neurosci *30*, 7300-7309.

47. Weiner, J.A., Hecht, J.H., and Chun, J. (1998). Lysophosphatidic acid receptor gene vzg-1/lpA1/edg-2 is expressed by mature oligodendrocytes during myelination in the postnatal murine brain. J Comp Neurol *398*, 587-598.

48. Weiner, J.A., and Chun, J. (1999). Schwann cell survival mediated by the signaling phospholipid lysophosphatidic acid. Proc Natl Acad Sci U S A *96*, 5233-5238.

49. Contos, J.J., and Chun, J. (2000). Genomic characterization of the lysophosphatidic acid receptor gene, lp(A2)/Edg4, and identification of a frameshift mutation in a previously characterized cDNA. Genomics *64*, 155-169.

50. Contos, J.J., Ishii, I., and Chun, J. (2000). Lysophosphatidic acid receptors. Mol Pharmacol *58*, 1188-1196.

51. McGiffert, C., Contos, J.J., Friedman, B., and Chun, J. (2002). Embryonic brain expression analysis of lysophospholipid receptor genes suggests roles for s1p(1) in neurogenesis and s1p(1-3) in angiogenesis. FEBS Lett *531*, 103-108.

52. Fukushima, N., Kimura, Y., and Chun, J. (1998). A single receptor encoded by vzg-1/lpA1/edg-2 couples to G proteins and mediates multiple cellular responses to lysophosphatidic acid. Proc Natl Acad Sci U S A *95*, 6151-6156.

53. Ishii, I., Contos, J.J., Fukushima, N., and Chun, J. (2000). Functional comparisons of the lysophosphatidic acid receptors, LP(A1)/VZG-1/EDG-2, LP(A2)/EDG-4, and LP(A3)/EDG-7 in neuronal cell lines using a retrovirus expression system. Mol Pharmacol *58*, 895-902.

54. Fukushima, N., Ishii, I., Contos, J.J., Weiner, J.A., and Chun, J. (2001). Lysophospholipid receptors. Annu Rev Pharmacol Toxicol *41*, 507-534.

55. Ishii, I., Fukushima, N., Ye, X., and Chun, J. (2004). Lysophospholipid receptors: signaling and biology. Annu Rev Biochem *73*, 321-354.

56. Choi, J.W., Lee, C.W., and Chun, J. (2008). Biological roles of lysophospholipid receptors revealed by genetic null mice: an update. Biochim Biophys Acta *1781*, 531-539.

57. Anliker, B., and Chun, J. (2004). Cell surface receptors in lysophospholipid signaling. Semin Cell Dev Biol *15*, 457-465.

58. Contos, J.J., Fukushima, N., Weiner, J.A., Kaushal, D., and Chun, J. (2000). Requirement for the lpA1 lysophosphatidic acid receptor gene in normal suckling behavior. Proc Natl Acad Sci U S A *97*, 13384-13389.

59. Weiner, J.A., Fukushima, N., Contos, J.J., Scherer, S.S., and Chun, J. (2001). Regulation of Schwann cell morphology and adhesion by receptor-mediated lysophosphatidic acid signaling. J Neurosci *21*, 7069-7078.

60. Estivill-Torrus, G., Llebrez-Zayas, P., Matas-Rico, E., Santin, L., Pedraza, C., De Diego, I., Del Arco, I., Fernandez-Llebrez, P., Chun, J., and De Fonseca, F.R. (2008). Absence of LPA1 signaling results in defective cortical development. Cereb Cortex *18*, 938-950.

61. Contos, J.J., Ishii, I., Fukushima, N., Kingsbury, M.A., Ye, X., Kawamura, S., Brown, J.H., and Chun, J. (2002). Characterization of lpa(2) (Edg4) and lpa(1)/lpa(2) (Edg2/Edg4) lysophosphatidic acid receptor knockout mice: signaling deficits without obvious phenotypic abnormality attributable to lpa(2). Mol Cell Biol *22*, 6921-6929.

62. Noguchi, K., Herr, D., Mutoh, T., and Chun, J. (2009). Lysophosphatidic acid (LPA) and its receptors. Curr Opin Pharmacol *9*, 15-23.

63. Sugiura, T., Nakane, S., Kishimoto, S., Waku, K., Yoshioka, Y., Tokumura, A., and Hanahan, D.J. (1999). Occurrence of lysophosphatidic acid and its alkyl ether-linked analog in rat brain and comparison of their biological activities toward cultured neural cells. Biochim Biophys Acta *1440*, 194-204.

64. Fukushima, N., Weiner, J.A., and Chun, J. (2000). Lysophosphatidic acid (LPA) is a novel extracellular regulator of cortical neuroblast morphology. Dev Biol *228*, 6-18.

65. Fukushima, N., Ishii, I., Habara, Y., Allen, C.B., and Chun, J. (2002). Dual regulation of actin rearrangement through lysophosphatidic acid receptor in neuroblast cell lines: actin depolymerization by Ca(2+)-alpha-actinin and polymerization by rho. Mol Biol Cell *13*, 2692-2705.

66. Fukushima, N., Weiner, J.A., Kaushal, D., Contos, J.J., Rehen, S.K., Kingsbury, M.A., Kim, K.Y., and Chun, J. (2002). Lysophosphatidic acid influences the morphology and motility of young, postmitotic cortical neurons. Mol Cell Neurosci *20*, 271-282.

67. Fukushima, N., and Morita, Y. (2006). Actomyosin-dependent microtubule rearrangement in lysophosphatidic acid-induced neurite remodeling of young cortical neurons. Brain Res *1094*, 65-75.

68. Fukushima, N., Shano, S., Moriyama, R., and Chun, J. (2007). Lysophosphatidic acid stimulates neuronal differentiation of cortical neuroblasts through the LPA1-G(i/o) pathway. Neurochem Int *50*, 302-307.

69. Svetlov, S.I., Ignatova, T.N., Wang, K.K., Hayes, R.L., English, D., and Kukekov, V.G. (2004). Lysophosphatidic acid induces clonal generation of mouse neurospheres via proliferation of Sca-1- and AC133-positive neural progenitors. Stem Cells Dev *13*, 685-693.

70. Rhee, H.J., Nam, J.S., Sun, Y., Kim, M.J., Choi, H.K., Han, D.H., Kim, N.H., and Huh, S.O. (2006). Lysophosphatidic acid stimulates cAMP accumulation and cAMP response element-binding protein phosphorylation in immortalized hippocampal progenitor cells. Neuroreport *17*, 523-526.

71. Dubin, A.E., Bahnson, T., Weiner, J.A., Fukushima, N., and Chun, J. (1999). Lysophosphatidic acid stimulates neurotransmitter-like conductance changes that precede GABA and L-glutamate in early, presumptive cortical neuroblasts. J Neurosci *19*, 1371-1381.

72. Kingsbury, M.A., Rehen, S.K., Contos, J.J., Higgins, C.M., and Chun, J. (2003). Non-proliferative effects of lysophosphatidic acid enhance cortical growth and folding. Nat Neurosci *6*, 1292-1299.

73. Rehen, S.K., Kingsbury, M.A., Almeida, B.S., Herr, D.R., Peterson, S., and Chun, J. (2006). A new method of embryonic culture for assessing global changes in brain organization. J Neurosci Methods *158*, 100-108.

74. Matas-Rico, E., Garcia-Diaz, B., Llebrez-Zayas, P., Lopez-Barroso, D., Santin, L., Pedraza, C., Smith-Fernandez, A., Fernandez-Llebrez, P., Tellez, T., Redondo, M., et al. (2008). Deletion of lysophosphatidic acid receptor LPA1 reduces neurogenesis in the mouse dentate gyrus. Mol Cell Neurosci *39*, 342-355.

75. Castilla-Ortega, E., Sanchez-Lopez, J., Hoyo-Becerra, C., Matas-Rico, E., Zambrana-Infantes, E., Chun, J., De Fonseca, F.R., Pedraza, C., Estivill-Torrus, G., and Santin, L.J. (2010). Exploratory, anxiety and spatial memory impairments are dissociated in mice lacking the LPA1 receptor. Neurobiol Learn Mem *94*, 73-82.

76. Inoue, M., Rashid, M.H., Fujita, R., Contos, J.J., Chun, J., and Ueda, H. (2004). Initiation of neuropathic pain requires lysophosphatidic acid receptor signaling. Nature medicine *10*, 712-718.

77. Inoue, M., Ma, L., Aoki, J., Chun, J., and Ueda, H. (2008). Autotaxin, a synthetic enzyme of lysophosphatidic acid (LPA), mediates the induction of nerve-injured neuropathic pain. Mol Pain *4*, 6.

78. Inoue, M., Xie, W., Matsushita, Y., Chun, J., Aoki, J., and Ueda, H. (2008). Lysophosphatidylcholine induces neuropathic pain through an action of autotaxin to generate lysophosphatidic acid. Neuroscience *152*, 296-298.

79. Ma, L., Uchida, H., Nagai, J., Inoue, M., Chun, J., Aoki, J., and Ueda, H. (2009). Lysophosphatidic acid-3 receptor-mediated feed-forward production of lysophosphatidic acid: an initiator of nerve injury-induced neuropathic pain. Mol Pain *5*, 64.

80. Harrison, S.M., Reavill, C., Brown, G., Brown, J.T., Cluderay, J.E., Crook, B., Davies, C.H., Dawson, L.A., Grau, E., Heidbreder, C., et al. (2003). LPA1 receptor-deficient mice have phenotypic changes observed in psychiatric disease. Mol Cell Neurosci *24*, 1170-1179.

81. Hennessy, R.J., Baldwin, P.A., Browne, D.J., Kinsella, A., and Waddington, J.L. (2007). Three-dimensional laser surface imaging and geometric morphometrics resolve frontonasal dysmorphology in schizophrenia. Biol Psychiatry *61*, 1187-1194.

82. Moriwaki, M., Kishi, T., Takahashi, H., Hashimoto, R., Kawashima, K., Okochi, T., Kitajima, T., Furukawa, O., Fujita, K., Takeda, M., et al. (2009). Prepulse inhibition of the startle response with chronic schizophrenia: a replication study. Neurosci Res *65*, 259-262.

83. Gonzalez-Maeso, J., and Sealfon, S.C. (2009). Psychedelics and schizophrenia. Trends Neurosci *32*, 225-232.

84. Quincozes-Santos, A., Abib, R.T., Leite, M.C., Bobermin, D., Bambini-Junior, V., Goncalves, C.A., Riesgo, R., and Gottfried, C. (2008). Effect of the atypical neuroleptic risperidone on morphology and S100B secretion in C6 astroglial lineage cells. Mol Cell Biochem *314*, 59-63.

85. Hardan, A.Y., Jou, R.J., Keshavan, M.S., Varma, R., and Minshew, N.J. (2004). Increased frontal cortical folding in autism: a preliminary MRI study. Psychiatry Res *131*, 263-268.

86. Nakamura, M., Nestor, P.G., McCarley, R.W., Levitt, J.J., Hsu, L., Kawashima, T., Niznikiewicz, M., and Shenton, M.E. (2007). Altered orbitofrontal sulcogyral pattern in schizophrenia. Brain *130*, 693-707.

87. Brimacombe, M., Ming, X., and Lamendola, M. (2007). Prenatal and birth complications in autism. Matern Child Health J *11*, 73-79.

88. Byrne, M., Agerbo, E., Bennedsen, B., Eaton, W.W., and Mortensen, P.B. (2007). Obstetric conditions and risk of first admission with schizophrenia: a Danish national register based study. Schizophr Res *97*, 51-59.

89. Aoki, J., Taira, A., Takanezawa, Y., Kishi, Y., Hama, K., Kishimoto, T., Mizuno, K., Saku, K., Taguchi, R., and Arai, H. (2002). Serum lysophosphatidic acid is produced through diverse phospholipase pathways. J Biol Chem *277*, 48737-48744.

90. Dottori, M., Leung, J., Turnley, A.M., and Pebay, A. (2008). Lysophosphatidic acid inhibits neuronal differentiation of neural stem/progenitor cells derived from human embryonic stem cells. Stem Cells *26*, 1146-1154.

# CHAPTER II

Lysophosphatidic Acid (LPA) Signaling as an Initiating Cause of Fetal Hydrocephalus

**Summary**

Congenital or fetal hydrocephalus (FH) is the most common neurological disorder of newborns, producing enlarged heads, cerebrospinal fluid (CSF) accumulation and neurological dysfunction, with therapies limited to palliative neurosurgery. Its initiating causes are unclear; however FH has been strongly associated with intracranial hemorrhage. Here we report that lysophosphatidic acid (LPA), a lipid signaling molecule, provides an etiological and mechanistic link between hemorrhage and FH. An *in vivo* model for intracranial hemorrhage in which wild type or LPA receptor-null mice were overexposed prenatally to blood fractions or LPA, consistently produced both FH and multiple associated histological defects, all of which depended predominantly on the receptor subtype $LPA_{1,}$ which is expressed on neural progenitor cells (NPCs). Administration of a short-acting $LPA_1$ antagonist prevented induced FH. These results identify LPA receptor mechanisms in FH and suggest LPA signaling pathways as attractive targets for potential therapeutic intervention.

**Introduction**

Approximately 7 of 10,000 newborns suffer from FH (1, 2), a life-threatening condition resulting from excessive accumulation of CSF within the ventricular system and associated with enlarged heads, structural brain alterations, varied neurological impairment, and death if untreated. Currently, neither preventive nor curative therapies exist. Evidence for genetic contributions to some forms of hydrocephalus have been reported (3); however, the majority of cases are sporadic, acquired disease with an unclear cellular and molecular etiology.

Intriguing observations from epidemiological studies have linked FH to prenatal bleeding events, such as intrauterine and/or intracranial hemorrhage, that could produce pathophysiological exposure to blood components or derivatives like serum (1, 2). This suggests that factors associated with blood could in some way contribute to FH. A molecular species with proven relationships to both blood and the developing cerebral cortex is LPA. It can be produced through multiple biochemical pathways (4) and has numerous biological properties that are mediated through a family of six known G protein-coupled receptors, $LPA_{1-6}$ (5, 6). LPA is also a normal component of blood and blood derivatives such as plasma and serum where it can reach reported concentrations of 20 μM (4, 7), a value that is approximately 200-300 fold over the apparent $K_d$ of its receptors (6). In the embryonic cerebral cortex, gene expression studies have identified multiple LPA receptors (8), and receptor-dependent

LPA signaling has been shown to influence a broad range of cellular effects that can alter NPC physiologies, including their electrophysiological, cytoskeletal, morphological, anti-apoptotic and proliferative properties (5). Receptor-dependent effects can also alter the overall organization of the embryonic cortex (9, 10). To assess the possible relevance of prenatal blood or LPA exposure in FH, an *in vivo* model was therefore established. This model utilized embryonic mouse brain exposure to these agents, and subsequent examination at later pre- and postnatal ages, combined with use of LPA receptor-null mutants.

## Results

### Serum or plasma exposure induces FH

Red blood cells (RBCs), plasma or serum, were delivered intraventricularly to the embryonic cerebral cortex via intracranial injection (Figure 2.1a-c) at embryonic day 13.5 (E13.5) followed by postnatal assessment. Fetal delivery of plasma or serum, but not RBCs, produced FH with postnatal animals displaying characteristic dome-shaped, enlarged heads, dilated lateral ventricles (LVs), and cortical thinning (Figure 2.1d, e, g, h). Cohorts exposed prenatally to serum or plasma developed hydrocephalus in 25-50% of animals (Figure 2.1e, h, n), whereas vehicle injection did not (Figure 2.1d, g, n; $n = 19$). In addition, early cortical disruption appeared in wildtype animals after 24 h of exposure to serum or plasma but not RBCs (Figure 2.S2). These data indicated that hydrocephalus could be initiated by hemorrhagic components, consistent with epidemiological data (1) and a published animal model of intracranial bleeding that reported the development of ventricular dilation (11), known to be associated with FH. These data also demonstrated that neither RBCs nor an acute increase in ventricular fluid volume produced by vehicle injection were

sufficient to produce ventricular dilation or hydrocephalus (Figure 2.1d, n). This supports the possibility that a serum or plasma factor or factors is capable of initiating hydrocephalus.

**LPA exposure produces FH and associated histological changes**

A bioactive factor that is present within both plasma and serum, which can alter embryonic cerebral cortical organization *ex vivo* (9), is LPA with known activities that might contribute to the induction of FH. The effects of embryonic LPA exposure were examined in wildtype embryos at E13.5, an age when NPCs respond robustly to LPA (9, 12) (Figure 2.S3), and analyzed at later developmental ages through adulthood. Strikingly, LPA-injected animals developed completely-penetrant and severe hydrocephalus (Figure 2.1f, h, n; $n = 16$) grossly visible by postnatal day 10 (P10) based on cortical thinning and ventricular dilation (Figure 2.1j). Hydrocephalus was never observed in vehicle-injected ($n = 19$) or non-injected littermates ($n = 10$) (Figure 2.1d, g, i, n). Hydrocephalic animals showed progressively increasing head width (interaural distance, Figure 2.1k), head height (mandibular-rostral distance, Figure 2.1l), and body weight loss (Figure 2.1m), although there was no statistically significant difference in the anterior-posterior dimension (fronto-occipital distance) (Figure 2.S4). In addition, these hydrocephalic animals displayed dome-shaped heads and thin, fragile skulls (Figure 2.1f), frequent intracranial hemorrhage (subdural and intraventricular), and destruction of subcortical

structures (e.g. caudate and putamen) and corpus callosum (Figure 2.1h). Hydrocephalic animals survived between 2-6 weeks after birth (Figure 2.S4).

Histological alterations common to reported mouse models and clinical cases of hydrocephalus (Table 2.1) were observed after LPA but not after control vehicle exposure. Ventricular size was bilaterally increased (Figure 2.2a-c and Figure 2.S5). In addition, the apical ventricular surface - composed of NPCs at this age - was disrupted and showed protrusions into the lateral ventricles (Figure 2.2d-f). In severely disrupted areas, rounded cell clusters appeared to detach from the ventricular surface (Figure 2.2g-i). These clusters were immunoreactive for nestin, incorporated bromodeoxyuridine (BrdU), and expressed *Lpar1* as detected by *in situ* hybridization (Figure 2.S6; *Lpar1* expression is present in the ventricular zone (VZ)), confirming their VZ origin. Furthermore, the formation of neurorosettes – abnormal, radially-oriented cells – within the VZ was observed (Figure 2.2j-l). Finally, cells from the 3rd ventricular wall protruded into the ventricle, consistent with partial 3rd ventricle occlusion (Figure 2.2m-q). This improper localization of cells is consistent with observed heterotopia formation in FH (13). One mechanism that could contribute to these diverse histological findings is altered cell adhesion that can be produced by LPA signaling (14).

**LPA exposure disrupts NPC position, adhesion, and cilia**

Cell adhesion molecules forming adherens junctions are necessary for maintaining luminal integrity of the cerebroventricular system. Knockout or

knockdown of various related components that maintain ventricular integrity such as N-cadherin (N-cad) (15, 16), Celsr 2 and 3 (17), myosin II-B (18), myosin IXa (19), Lgl1 (20), and Dlg5 (21) all produce histological features common to human hydrocephalus (Table 2.1) or frank hydrocephalus. LPA has been shown to both increase and decrease N-cad cell-cell contact in a cell-type and receptor-subtype specific manner (14, 22), suggesting that modulation of LPA signaling could similarly affect ventricular integrity. The apical surface of the lateral ventricles was examined for N-cad expression and found to be discontinuous in LPA-exposed embryos (Figure 2.3a, b). Consistent with N-cad function in maintaining proper mitotic cell attachment to the apical surface (16), LPA-injected embryos showed significantly increased mitotic displacement whereby M-phase NPCs typically found at the apical ventricular surface were instead displaced basally (Figure 2.3c, d, i; $P = 0.002$). In addition, denuded NPC spheres (Figure 2.2h, i) (29 ± 7.1 per LPA-exposed embryo) were always observed within the ventricles of LPA-treated embryos.

A cause of hydrocephalus is loss of cilia or ciliary function on ependymal cells lining the ventricular surface that is thought to reduce CSF flow (23-29). Ependymal cells arise from radial glia, differentiating during mid to late neurogenesis, and maturing by early postnatal life to form a single, multi-ciliated cell layer that can be identified by immunolabeling for acetylated α-tubulin (30). Following embryonic LPA exposure, ependymal alterations were observed by P4 whereby patchy loss of mature ependymal cells, identified by S100β immunoreactivity, was accompanied by

loss of acetylated α-tubulin immunoreactivity (Figure 2.3e, f). These results are consistent with loss of normal, ciliated ependymal cells (25, 29).

**LPA activates both Rho and Rac pathways in the embryonic cortex**

LPA receptors, particularly $LPA_1$, are powerful activators of Rho (31), as well as the closely related small GTPase, Rac (32). To determine the possible involvement of these pathways in LPA induced FH, Rho and Rac signaling were examined. Statistically significant activation of both prototypical members RhoA ($P = 0.04$) and Rac1 ($P = 0.01$) that are known to be expressed in the embryonic cortex (12) occurred rapidly following LPA stimulation (Figure 2.3j, k, and Figure 2.S7). These results confirm the activation of both Rho and Rac by LPA signaling in the embryonic cerebral cortex.

**Serum, plasma, and LPA induce FH that is LPA receptor dependent**

Several blood-related factors have been reported to be elevated in CSF from hydrocephalic individuals (33), and when administered in young mice, can cause ventricular dilation and hydrocephalus (34). This raised the possibility that factors in addition to LPA, present in serum and plasma, could be responsible for producing FH and/or associated histological changes observed in this model. To address this question, LPA receptor null mice were utilized in conjunction with serum, plasma, and

LPA injections, followed by prenatal and postnatal assessment. Based on gene expression studies, $LPA_1$ and $LPA_2$ are found in the NPC population of the VZ (Figures 2.S8 and 2.S9) and are known to couple to the same G proteins that mediate LPA signaling effects (9, 35). To minimize receptor compensation, $LPA_1$ and $LPA_2$ double null mutant mice ($LPA_1^{-/-}$ $LPA_2^{-/-}$) were examined, initially blind to genotype as compared to $LPA_2$ homozygous null/$LPA_1$ heterozygote ($LPA_1^{+/-}$ $LPA_2^{-/-}$), both of which were exposed identically to serum, plasma, or LPA. These analyses revealed that exposure to these agents in $LPA_1^{+/-}$ $LPA_2^{-/-}$ mice produced results indistinguishable from wildtype controls, indicating a primary role for $LPA_1$ in FH (Figure 2.4 and Figure 2.S10 and Table 2.S1). Both wildtype and $LPA_1^{+/-}$ $LPA_2^{-/-}$ were subsequently used as controls compared to double null mutants. Both serum and plasma induced cortical disruption that was abrogated in double-null mutants (Figure 2.S2). Critically, LPA's ability to induce FH and associated histological changes (Table 2.1 and Table 2.S1) was strongly dependent on the expression of $LPA_1$. In control animals exposed to LPA, FH showed complete penetrance ($n$ = 10, 100%). By contrast, FH was reduced to approximately 10% in double-null mutants ($n$ = 9, 11%) (Figure 2.4 and Figure 2.S10 and Table 2.S1). The rare occurrence of FH in double null mutants likely reflects contributions by one or more of the remaining four LPA receptors rescuing the double null phenotype. These data strongly suggest that induced FH, along with associated histological changes, produced by serum, plasma, and LPA exposure, are LPA receptor dependent and primarily involve $LPA_1$.

**Pharmacological $LPA_1$ blockade prevents induced FH and histological changes**

The identification of LPA receptor signaling in the initiation of FH suggested that pharmacological receptor modulation could influence the development of this disorder. A receptor antagonist Ki16425 with proven specificity against $LPA_1$ and $LPA_3$ (36) was intraventricularly injected prior to LPA exposure. Available genetic and expression data did not support a role for $LPA_3$ in LPA-induced FH (37, 38). Embryos that were treated with vehicle followed by LPA showed similar cortical defects as the LPA-only experiments (Figure 2.5a, b), while embryos treated with Ki16425 followed by LPA showed a dramatic reduction in FH and related histological changes ($n$ = 5) (Figure 2.5c, d, g-i). Treatment with Ki16425 followed by vehicle produced no such effects (Figure 2.5e-i). These data demonstrated that pharmacological intervention targeting LPA receptors, particularly $LPA_1$, could also attenuate LPA-induced FH. These data also eliminate developmental artifacts associated with constitutive receptor deletion to explain rescue of FH observed in receptor-null animals.

**Discussion**

In this study, a molecular and cellular mechanism was identified that can account for the epidemiological observations linking prenatal bleeding and FH: LPA receptor-overactivation amongst NPCs (Figure 2.S1). Moreover, LPA receptor

overactivation can explain the diverse histological presentation reported for human FH, and is further consistent with other FH-relevant animal models (Table 2.1). Based on genetic and pharmacological studies, the primary receptor mediating these effects is $LPA_1$ with comparatively minor contributions by other LPA receptor subtypes. While other contributing factors may be present in blood, genetic removal of LPA receptors prevented serum and plasma from inducing FH, supporting a primary role for LPA signaling in this process.

In addition to the direct release of LPA from blood derivatives, it is notable that both LPA precursors and the critical enzyme required for LPA production are present within the embryonic ventricles when exposed to blood and its derivatives. Thus, the LPA precursor lysophosphatidylcholine (LPC) is present within blood (39) and serum (40) where it can reach concentrations of up to 200 μM. The major LPA producing enzyme, a lysophospholipase D known as autotaxin (ATX or Enpp2), is highly expressed in the ventricular choroid plexus (41) (Figure 2.S11), where it could enzymatically convert LPC into LPA. In view of the brief half-life of LPA in biological fluids (42), its enzymatic production from highly abundant precursors – LPC approaching 10-20 fold over maximal LPA concentration in serum – could provide a more sustained overactivation of LPA signaling under pathological conditions.

A variety of genetic perturbations have been reported to result in FH. LPA signaling has been documented to interface with many if not all of these pathways. FH has been linked to cadherins (16, 21), which are altered by LPA signaling (43).

Loss of myosin IIB and IXa both result in hydrocephalus, consistent with myosin pathways in the developing CNS that are modulated by LPA signaling (44). The small GTPase Rho is activated by LPA (12, 31) and has also been linked to FH (19), and this signaling component, along with Rac, was also activated in the employed cortical model. These data support the involvement of LPA signaling that modulates multiple small GTPases in maintaining NPC and ventricular integrity through the actin cytoskeleton.

Ciliary defects have been experimentally and clinically linked to FH. Genetic deletions in cilia-related proteins, such as Polaris (Tg737), Stumpy, or Hydin (24, 26, 27) or mutations leading to primary ciliary dyskinesia (45) indicate that ciliary loss-of-function can lead to FH. The loss of cilia observed in the current study, which appears to result from NPC disruption, is consistent with these genetic data. Combined with linkage to cell signaling pathways, LPA receptor overactivation could represent a shared, proximal modulator of these molecular elements, initiated by blood or related products.

The positioning of LPA signaling as a proximal modulator is consistent with a diverse range of reported risk factors and insults that share FH as a common endpoint. Risk factors include bleeding, infection, meningitis, and brain tumors that have been associated with increased LPA signaling (46-48). The observation that a host of disparate, previously unlinked histological phenomena associated with human FH (Table 2.1) can be explained by LPA signaling supports a shared mechanism in both mice and humans. The ability to prevent FH by pharmacological antagonism of LPA

signaling provides proof-of-concept for the medical treatment of at least some forms of FH. Finally, it is notable that a host of developmentally linked disorders have also been epidemiologically associated with prenatal bleeding; these include heterotopia, cerebral palsy, schizophrenia, and autism, which could in part reflect a range of defects produced at varying developmental ages and neuroanatomical locations by altered LPA signaling.

**Material and Methods**

***Injection solutions*** 18:1 LPA (10 mM in HBSS) was prepared fresh just prior to use. Whole blood was obtained from adult mice by cardiac puncture, clotted, and spun down. The top "serum" and bottom "red blood cell" (washed and resuspended in HBSS) fractions were collected by centrifugation separation. The "plasma" fraction was obtained as previously described.(11). Ki16425 (1 mM final concentration in HBSS), ROCK inhibitor (Y-27632, 2 mM), and Rac inhibitor (NSC23766, 10 mM) were prepared for intraventricular injections. BrdU solution was prepared (10 mg/ml in HBSS, final concentration 100 mg/kg) for intraperitoneal injection.

***Injections:*** *In utero* injections of 3 μl vehicle (HBSS), serum, plasma, RBC, or LPA solutions into embryonic cortices were performed on anesthesized, timed-pregnant dams at embryonic day E13.5. Embryos were examined after 1 day (E14.5), 5 days (E18.5), or postnatally at P4, P10, P21, and 4 weeks. For postnatal assessment, since uterine positional order was lost during delivery, all embryos within each litter were injected with identical ligands. Pharmacological studies were performed using 1.5 μl of each ligand to maintain consistent injection volumes across studies.

***Histology:*** Embryos or pups were collected, dissected in cold PBS, and fixed in formalin-alcohol-acetic acid solution (FAA). Paraffinized heads were sectioned (10 μm thickness), dewaxed, and stained using hematoxylin and eosin. Only healthy embryos with observable heartbeats were analyzed (≥ 90% injected).

***Immunohistochemistry:*** Brains preserved in 4% paraformaldehyde or FAA were examined. Cryoprotected/frozen heads using 4% paraformaldehyde were sectioned, blocked with species-appropriate serum, and immunolabeled. Paraffin sections were additionally dewaxed and processed through antigen retrieval prior to antibody staining. Antibodies specific for the following antigens were used: nestin (BD Biosciences, 1:400), β-III-tubulin (Covance, 1:1000), phosphorylated histone H3 (Upstate, 1:1000), acetylated-α-tubulin (Sigma, 1:1000), N-cadherin (Calbiochem, 1:200), and BrdU (Roche, 1:50).

***Image acquisition, quantification, and statistical analysis:*** Images were acquired on a Zeiss Imager 1D microscope (Axiovision 4.7.2) using appropriate fluorescence and brightfield filters, and analyzed blindly whenever possible. Photoshop adjustments (version CS4) were strictly limited to light level and contrast enhancement for visual aesthetics which did not change data interpretation. Statistical analyses were performed using Graphpad Prism (version 5). Data were expressed as avg ± standard deviation (s.d.). T-tests (paired and unpaired) were considered significant if $P \leq 0.05$.

***Head size measurement:*** Increased head circumference, clinically used as a standard indicator of hydrocephalus, is typically measured using a cloth tape above the ears, but is not technically feasible in early postnatal mice due to small size and incomplete skull calcification. Instead, a digital caliper (C-master electronic gauge) was used to perform three uni-dimensional measurements: interaural distance (ear-to-ear), madibular-rostral distance (jaw-to-top of the head), and fronto-occipital distance (forehead-to-back of the head). Individual measurements were performed in triplicate and averaged. Measurements were performed at postnatal days 3, 6, 10, 15, 20, 25, and 30. Postnatal animals were tattooed for individual identification.

***Ventricle area measurement:*** Paraffinized embryo heads were serially sectioned and selected sections (100 μm intervals apart) were imaged. Lateral ventricles were manually traced, area sizes calculated automatically (Axiovision 4.7.2), and tabulated. At least 6 sections were measured per embryo.

***Construction and Labeling of In Situ Hybridization Probes:*** Mouse *Lpar1* Exon 3 was amplified by PCR from a BAC template using pfx 50 DNA polymerase (Invitrogen) using the following primers, A1Ex3For: 5'-TTCACAGCCATGAACGAACAAC-3' and A1Ex3Rev: 5'-ACCAAGCACAATGACCACAGTC-3', and A tailed with Taq polymerase. The 748 bp product was then isolated using the Qiaex II DNA isolation kit (Qiagen) and cloned into the pGem®-T Easy T vector (Promega), linearized with appropriate restriction

enzymes, and DIG labeled sense and antisense runoff transcripts were transcribed using DIG labeling mix (Roche) and SP6 and T7 RNA polymerases (Roche) respectively. DIG-labeled sense and antisense mouse *Lpar2* probes were prepared as previously described.(37) Mouse Enpp2 (also known as autotaxin, ATX) probe was prepared as follows: A 1.2 kb 5' DNA fragment of the mouse ATX gene was subcloned into pBluescript II SK. DIG labeled sense and antisense run off transcripts were prepared by linearization with the appropriate restriction enzymes using DIG labeling mix (Roche) and T7 and T3 RNA polymerases (Roche) respectively.

***In situ hybridization:*** Embryo heads were either snap-frozen or paraffin-embedded and examined for $LPA_1$, $LPA_2$, and Enpp2 (autotaxin) expression as previously described(12). Paraffin sections were dewaxed and rehydrated using DEPC-treated solutions prior to pretreatment and preparation for hybridization. All probes were hybridized at $65^oC$.

***RhoA and Rac1 activation ELISA assay:*** Fresh embryonic cortical hemispheres were dissected out in ice-cold serum-free Opti-MEM and matched hemispheres were cultured in media supplemented with 10 μM LPA and 0.1% fatty-acid free bovine serum albumin (FAFBSA, consistent with LPA injection concentrations noted in Figure 2.S3) or without LPA essentially as previously described(9, 49). LPA stimulation was terminated in fresh ice-cold Opti-MEM without LPA. Activation of RhoA and Rac1 levels were measured using absorbance- or chemoluminescence-based G-LISA kits, respectively, according to the manufacturer's instructions (Cytoskeleton,

Denver, CO) using a Bio-Tek EL800 microplate reader and a Bio-Tek SynergyMX luminometer (Winooski, VT). Briefly, the cortical wall overlying the lateral ventricle was quickly dissected away from the ganglionic eminences (see Figure 2.S7), triturated in lysis buffer, and snap frozen in liquid nitrogen. Antibody concentrations were optimized for machine sensitivity. Statistically significant but modest activation levels likely reflect the absence of serum starvation, used to approximate *in vivo* conditions, along with the influence of other endogenous signaling pathways that increase the basal activation of Rho and Rac.

***LPA measurements:*** The LPA extraction method was adapted from Matyash et al. 2008 with some modification.(50) Briefly, 50 μl of tissue homogenate (final concentration 200-400 mg/ml fresh tissue) was used for each sample. 187.5 μl of methanol:HCl 10:1 mixture and 625 μl of methyl-tert-butyl ether (MTBE) were added to each sample and incubated on a nutator at room temperature for one hour. 157 μl of distilled water was then added to the mixture, incubated for 10 minutes, and phase-separated by centrifugation at 13,000 rpm for 10 minutes. The initial organic phase was collected, while the aqueous phase was re-extracted with 250 μl of MTBE:methanol:$H_2O$ (10:3:2.5 ratio). Both organic phases were combined and dried using a Speedvac concentrator (Savant, New York), and resuspended in 100 μl methanol. Non-natural 17:0 LPA (Avanti Polar Lipids, Alabaster, AL) was added as an internal standard. The extracts were subjected to liquid chromatography-mass spectrometry (LC-MS) for LPA measurement at the TSRI Mass Spectrometry Core

using an Agilent 6410 triple quad mass spectrometer coupled to an Agilent 1200lc stack. Compounds were eluted with a mobile phase of $H_20$/ACN 90:10 with 10 mM $NH_4OAc$ (A) and ACN/$H_2O$ with 10mM $NH_4OAc$ (B) at 0.2 ml/min. Agilent 300SB-C8 2.1 mm x 100 mm, 3.5 μm columns were used. The gradient was t = 0, 80:20 (A:B), t=5 50:50, t=7 25:75, t=15 0:100, t=20 off. There was a 5 min re-equilibration time between samples. The source was maintained at 350$^{o}$C with a drying gas flow of 10 liters / h, and data were collected in negative ion mode. The following transition states were monitored: LPA m/z 435 -> 153, C17 m/z 423 ->153. Calibration curves were generated using 10-10,000 fmol/injection of 18:0 LPA. Peak areas of [M-H] for LPA (18:1) form were normalized to the internal standard, and normalized areas were plotted versus concentration.

**Figure 2.1: Hydrocephalus is induced by embryonic cortical exposure of plasma, serum, or LPA.** **a**, Diagram of *in utero* injections. **b, c,** Visualization (blue) of lateral, 3rd, and 4th ventricles, indicating injection diffusion. A = anterior, P = posterior. **d-f**, Mice (P30) developed macrocephalic heads after injection of plasma, serum, or LPA, but not vehicle or RBCs. **g, h** Histological examination (P30) showed grossly dilated ventricles (v) and thinned overlying cortices. **i, j** Whole-brain preparations (P10) comparing control- and LPA-injected cortex; note the increased dimensions and transparency characteristic of hydrocephalus (**j**). **k-m** Animals exposed to LPA ($n$ = 7) (red) showed significantly increased head dimensions and significantly decreased body weight compared to vehicle exposure ($n$ = 10) (blue). (mean ± s.d., unpaired t-test, see Table 2.S1 for $P$ values). **n**, Hydrocephalus penetrance was quantified for each exposure condition; numbers in parentheses represent the number of hydrocephalic animals / cohort. CC = corpus callosum, CPu = caudate and putamen. Scale bar = 0.5 cm.

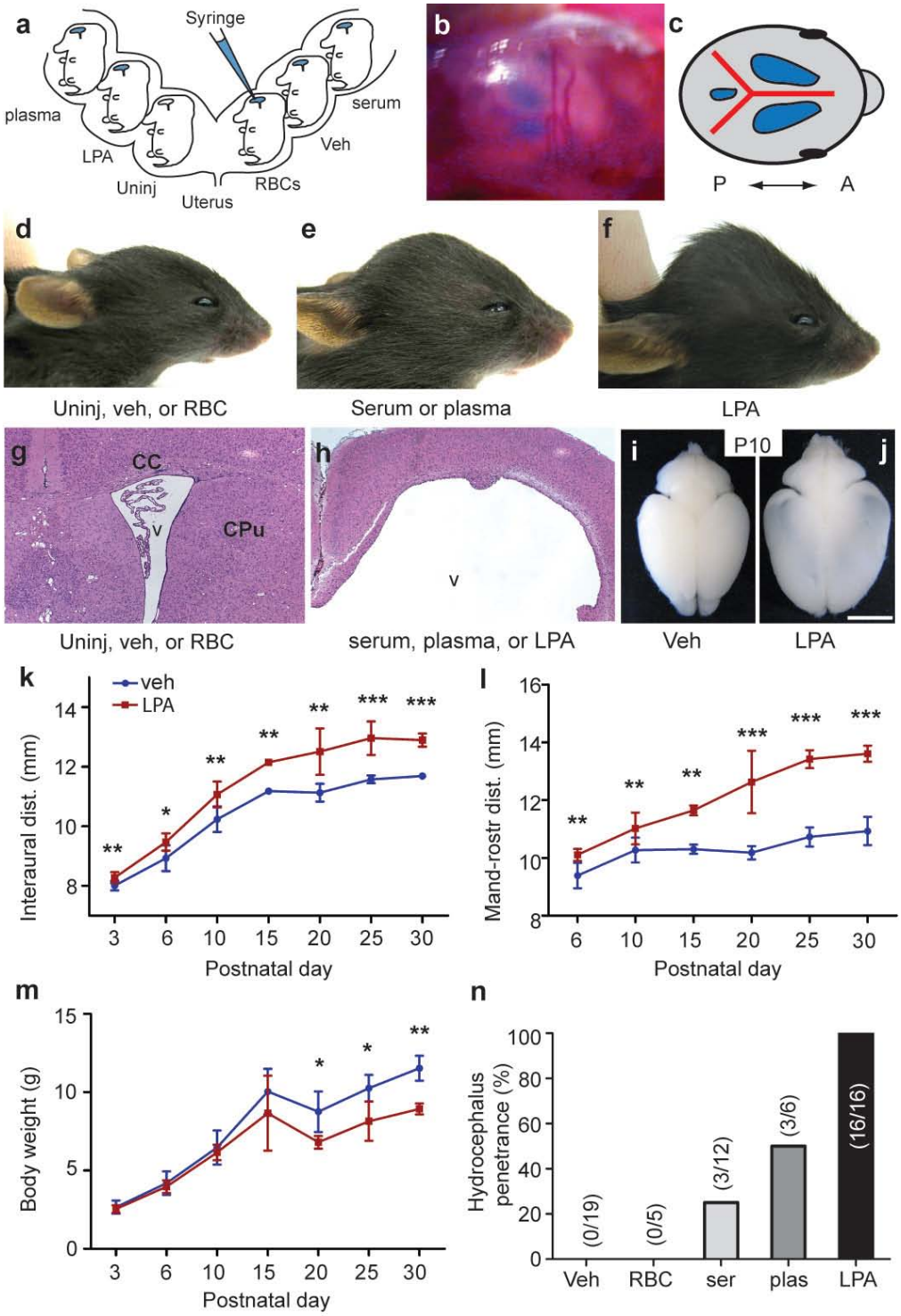
a
Syringe
plasma
serum
LPA
Veh
Uninj
RBCs
Uterus
b
c
P
A
d
e
f
Uninj, veh, or RBC
Serum or plasma
LPA
g
CC
v
CPu
h
v
i
P10
j
Uninj, veh, or RBC
serum, plasma, or LPA
Veh
LPA
k
veh
LPA
Interaural dist. (mm)
Postnatal day
l
Mand-rostr dist. (mm)
Postnatal day
m
Body weight (g)
Postnatal day
n
Hydrocephalus penetrance (%)
(0/19)
(0/5)
(3/12)
(3/6)
(16/16)
Veh
RBC
ser
plas
LPA

**Figure 2.2: Embryonic LPA exposure producing FH also produce histological features common to human FH.** Vehicle injection: a, d, g, j, m, n. LPA injection: b, e, f, h, i, k, l, o, p, q (magnified in f, i, l, q). **a-c, Ventricular dilation.** Embryos injected with LPA (analyzed at E14.5) showed lateral ventricular dilation compared to vehicle injections (dotted outlines indicate ventricles), with changes quantified in **c** (*n* = 3 embryos per condition, mean ± s.d., unpaired t-test; ipsi = ipsilateral, contra = contralateral). **d-f, Cortical disruption.** LPA exposure (analyzed at E14.5) produced cortical disruption of ventricular zone (VZ) organization and cell protrusions along the apical ventricular surface (boxed area magnified in **f**). **g-i, Neuroprogenitor cell (NPC) clusters in the lateral ventricles.** Clusters of NPCs protrude from the apical VZ surface and can be found as isolated clusters throughout the ventricle (analyzed at E18.5). **j-l**, **Neurorosettes.** These LPA-induced structures were located throughout the VZ. **m-q**, **Partial occlusion of the 3rd ventricle.** Disruption of the 3rd ventricular wall, associated with partial ventricular occlusion was frequently observed (analysed at E14.5 in **m, o**, **q**, see arrow; or E18.5 in **n, p)** v = ventricle, scale bars = 200 (**a, b, d, e, g, h, j, k, m, n, o, p**) and 50 μm (**f, i, l, q**).

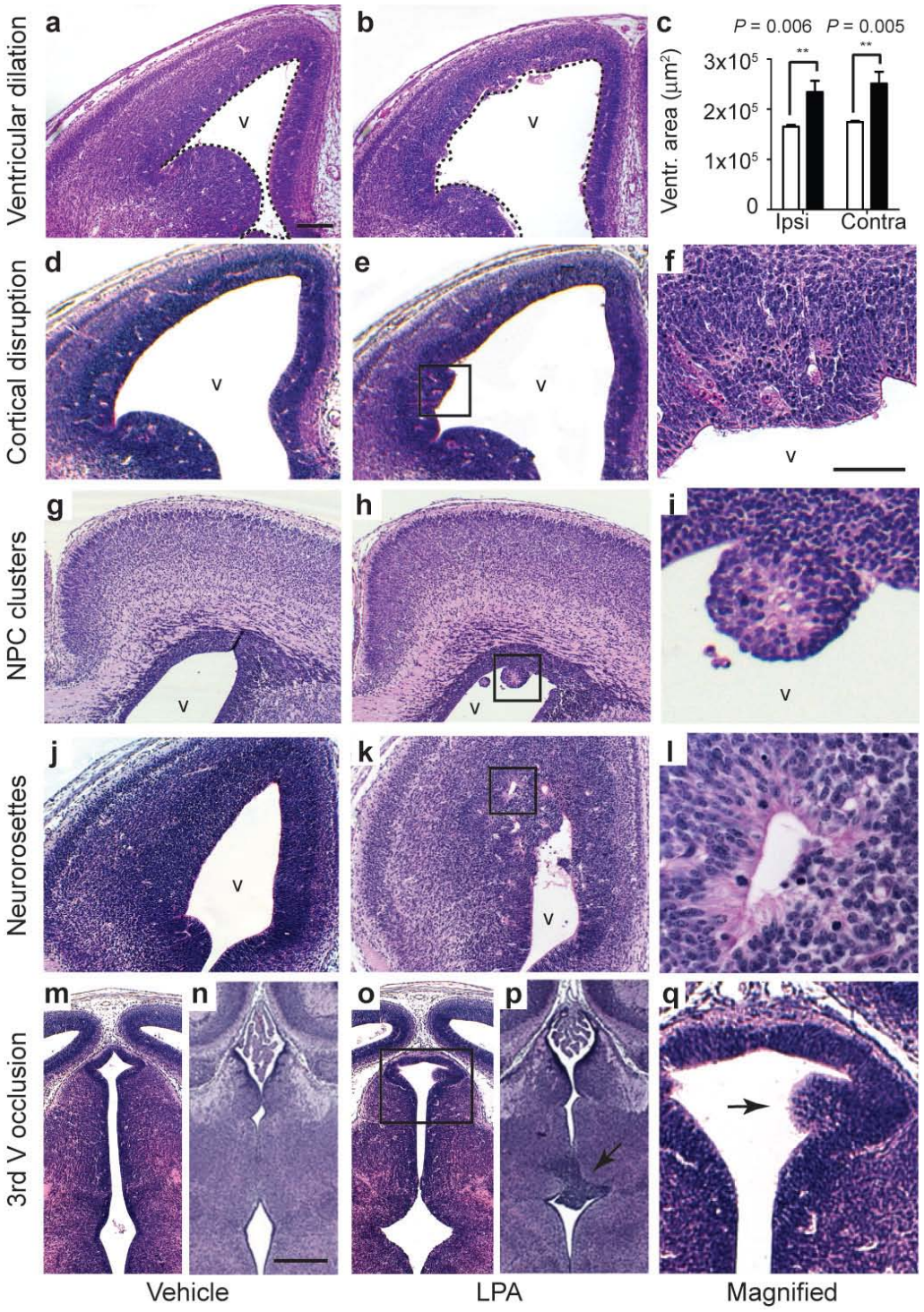
Ventricular dilation
Cortical disruption
NPC clusters
Neurorosettes
3rd V occlusion
a
b
c
d
e
f
g
h
i
j
k
l
m
n
o
p
q
V
P = 0.006
P = 0.005
**
**
Ventr. area (μm²)
3x10⁵
2x10⁵
1x10⁵
0
Ipsi
Contra
Vehicle
LPA
Magnified

**Figure 2.3: Hydrocephalus-associated LPA exposure alters NPC cell adhesion, mitotic displacement, produces heterotopia, and overactivates Rho/Rac signaling.** **a, b**, LPA exposure (analysed at E14.5) disrupted the apical ventricular surface, altering N-cadherin expression (N-cad, red, arrow, magnified in inset), in contrast to vehicle exposure. **c, d**, NPC mitotic displacement was identified by phosphorylated histone H3 (PHH3, red) immunolabeling that revealed displaced mitotic cells abnormally positioned superficially in the VZ (**d**, arrows) rather than along the ventricular surface (**c**). **e, f**, Immunolabeled ependymal cells (S100β+, red) and cilia (αAcTub+, green) were lost and altered, respectively following embryonic LPA exposure (**f**) as compared to vehicle controls (**e**) examined at P4. LPA exposure decreased the number of S100β+ cells that was associated with the loss of cilia (asterisk, **f** (arrows: in focal plane; arrowheads: out of focal plane)). **g, h**, Postmitotic neurons identified by immunolabeling with β-III-tubulin (β-III-tub+, green) indicated VZ disruption in LPA exposed cortices and the presence of heterotopic neurons (**h,** arrows) compared to vehicle exposure (**g**). **i**, Quantification of mitotically-displaced cells identified by PHH3 immunolabeling ($n$ = 5 embryos per condition, mean ± s.d., unpaired t-test, ** $P$ = 0.0022). **j, k**, Quantification of RhoA and Rac1 activation in *ex vivo* cortices following exposure to vehicle or LPA for 3 min. RhoA: $n$ = 5 pairs of matched cortical hemispheres exposed to vehicle or 10 μM LPA; mean ± s.d., $P$ = 0.0408, paired t-test. Rac1: $n$ = 6 pairs matched cortical hemispheres exposed to vehicle or 10 μM LPA, mean ± s.d., paired t-test, $P$ = 0.01. CP = cortical plate, IZ = intermediate zone, SVZ = subventricular zone, VZ = ventricular zone. Scale bars = 50 (**a-d, g-h**) and 20 μm (**e, f**).

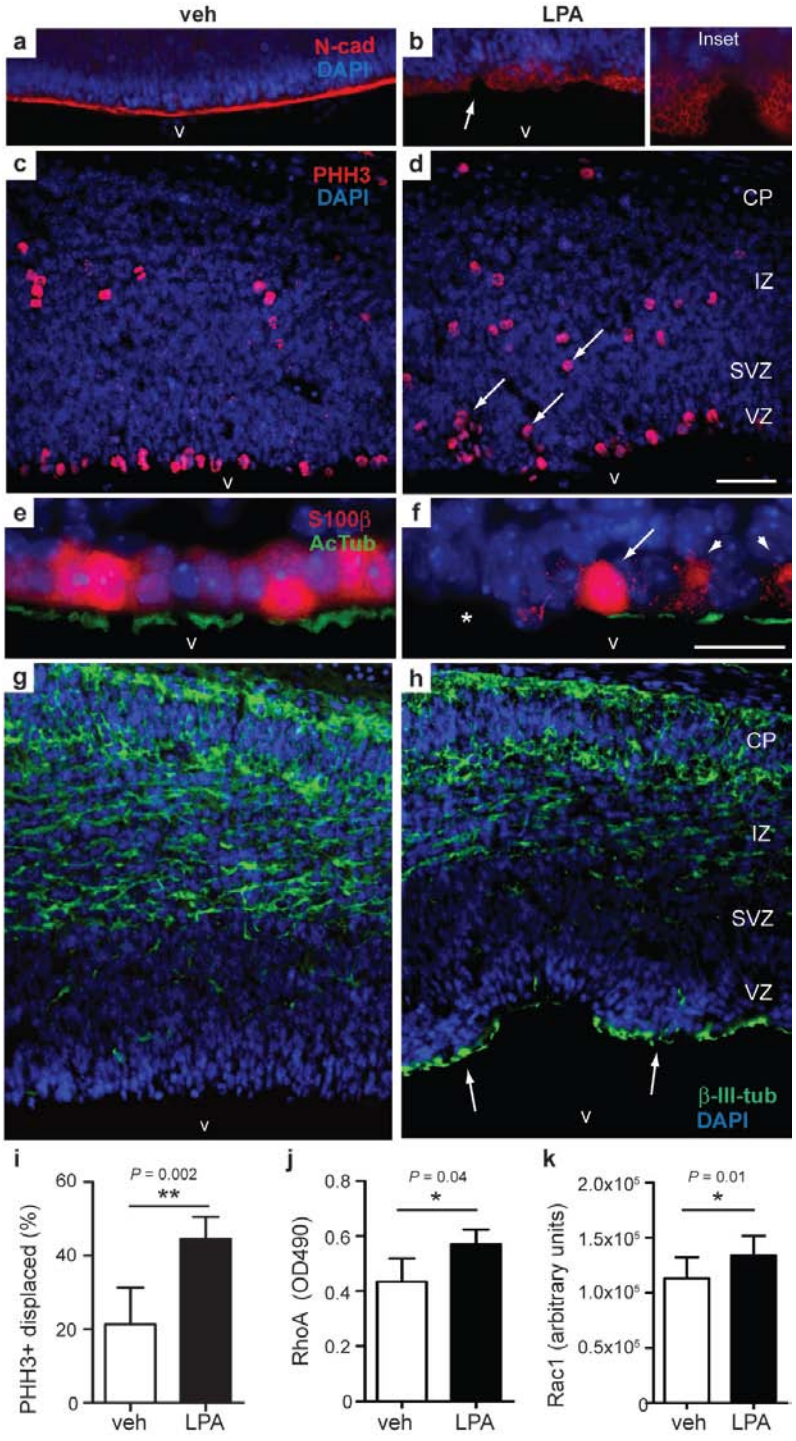
veh
LPA
a
N-cad
DAPI
b
Inset
c
PHH3
DAPI
d
CP
IZ
SVZ
VZ
e
S100β
AcTub
f
g
h
β-III-tub
DAPI
i
P = 0.002
**
PHH3+ displaced (%)
60
40
20
0
veh
LPA
j
P = 0.04
*
RhoA (OD490)
0.8
0.6
0.4
0.2
0
k
P = 0.01
*
Rac1 (arbitrary units)
2.0x10⁵
1.5x10⁵
1.0x10⁵
0.5x10⁵

**Figure 2.4: LPA-induced hydrocephalus and associated histological changes are generally absent from $LPA_1$/$LPA_2$ double-null mice. a, b**, Head dilation and hydrocephalus in postnatal animals following LPA exposure at E13.5 in control ($LPA_1^{(+/-)}$ / $LPA_2^{(-/-)}$ )(**a**) contrasted with a normal appearance and absence of hydrocephalus in the double-null mutant ($LPA_1^{(-/-)}$ / $LPA_2^{(-/-)}$) (**b**). **c-h**, LPA-injected positive controls revealed the expected presence of NPC clusters (**c**, arrows), early cortical disruption at E14.5 (**e**, arrowheads), and neurorosettes (**g**, arrows), that were generally absent (see **k**) in double-null mutants (**d, f, h**). **i, j**, LPA exposure in control mice ($n$ = 10, blue line) revealed significantly increased interaural (**i**) and mandibular-rostral distance (**j**) as early as postnatal day P3 that was attenuated in null mutants ($n$ = 9, red line) (*cf.* Figure 1, wildtype LPA exposure) ($n \geq 3$ embryos per genotype, mean ± s.d., unpaired t-test, $P < 0.05$, see Table 2.S2) **k**, Penetrance of LPA-induced hydrocephalus was quantified; numbers in parentheses represent number of hydrocephalic animals / total cohort. Scale bars = 400 (**c, d**), 200 (**e, f**) , and 50 μm (**g, h**).

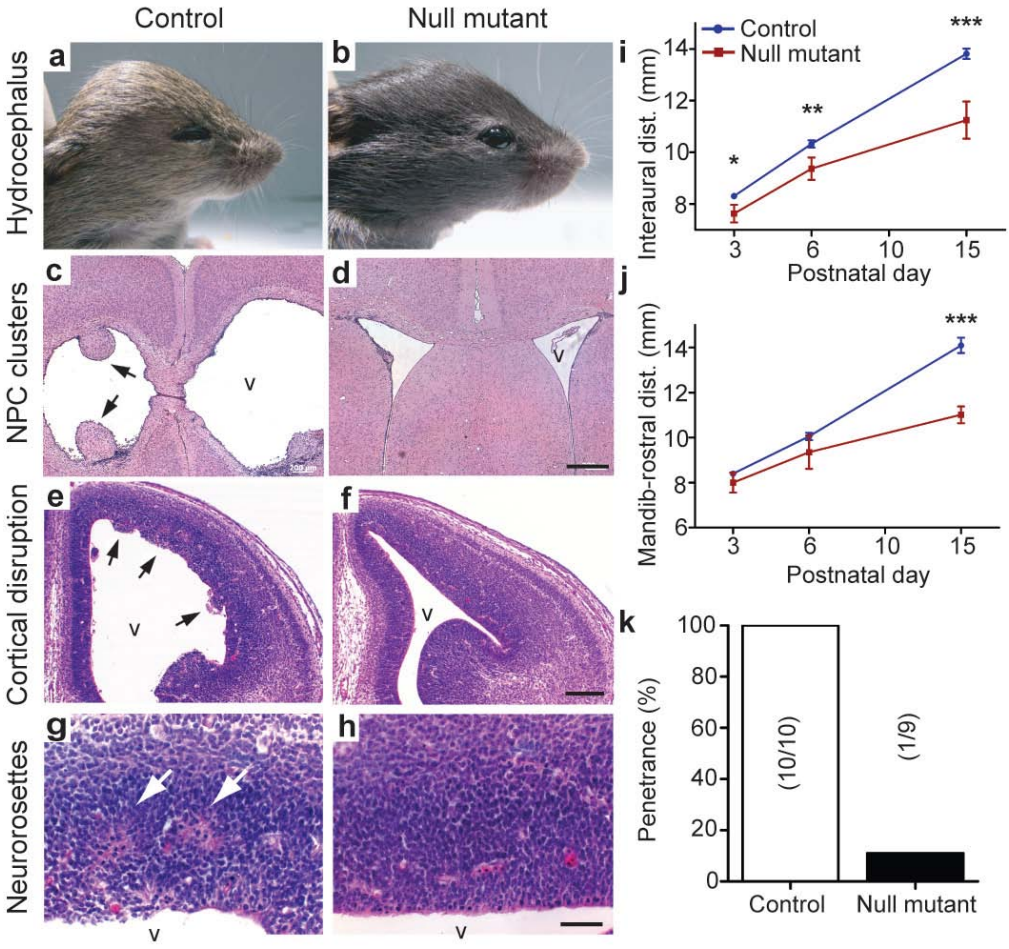
Control
Null mutant
Hydrocephalus
NPC clusters
Cortical disruption
Neurorosettes
a
b
c
d
e
f
g
h
v
i
Control
Null mutant
Interaural dist. (mm)
Postnatal day
*
**
***
j
Mandib-rostral dist. (mm)
Postnatal day
***
k
Penetrance (%)
(10/10)
(1/9)
Control
Null mutant

**Figure 2.5: Hydrocephalus can be prevented by pharmacological antagonism of $LPA_1$.** Embryos were injected sequentially with vehicle followed by LPA 10 min later at E13.5 and examined subsequently during embryonic life (**a**, E14.5) or assessed for hydrocephalus postnatally (**b**, P25). Pharmacological intervention was assessed using the same paradigm but replacing vehicle with the $LPA_{1/3}$ antagonist Ki16425 (Ki) followed by LPA, and analysed during the same embryonic (**c)** and postnatal periods **(d**). The effects of antagonist alone were similarly assessed by Ki exposure followed by veh, then further assessment (**e, f**). Apical protrusions of ventricular clusters (**a**, arrows) in vehicle-LPA injected embryos, were not observed in Ki-LPA or Ki-veh injected embryos after 24 h exposure (**c, e**). **g-i**, Quantitative assessments measured head dimensions in positive controls and antagonist-exposed animals. Positive controls using veh-LPA exposed animals produced the expected changes in head dimensions and hydrocephalus (black lines, **g-i**). In each measured head dimension, statistically significant increases were observed that contrasted with the normal head measurements obtained from antagonist-exposed brains (red and blue lines, **g-i**). No statistically significant changes were observed between Ki-veh (blue line) and Ki-LPA (red line) injected embryos ($n \geq 3$ embryos per condition, mean ± s.d., unpaired t-test, $P < 0.05$, see Table 2.S2). v = lateral ventricle. Scale bar = 100 μm.

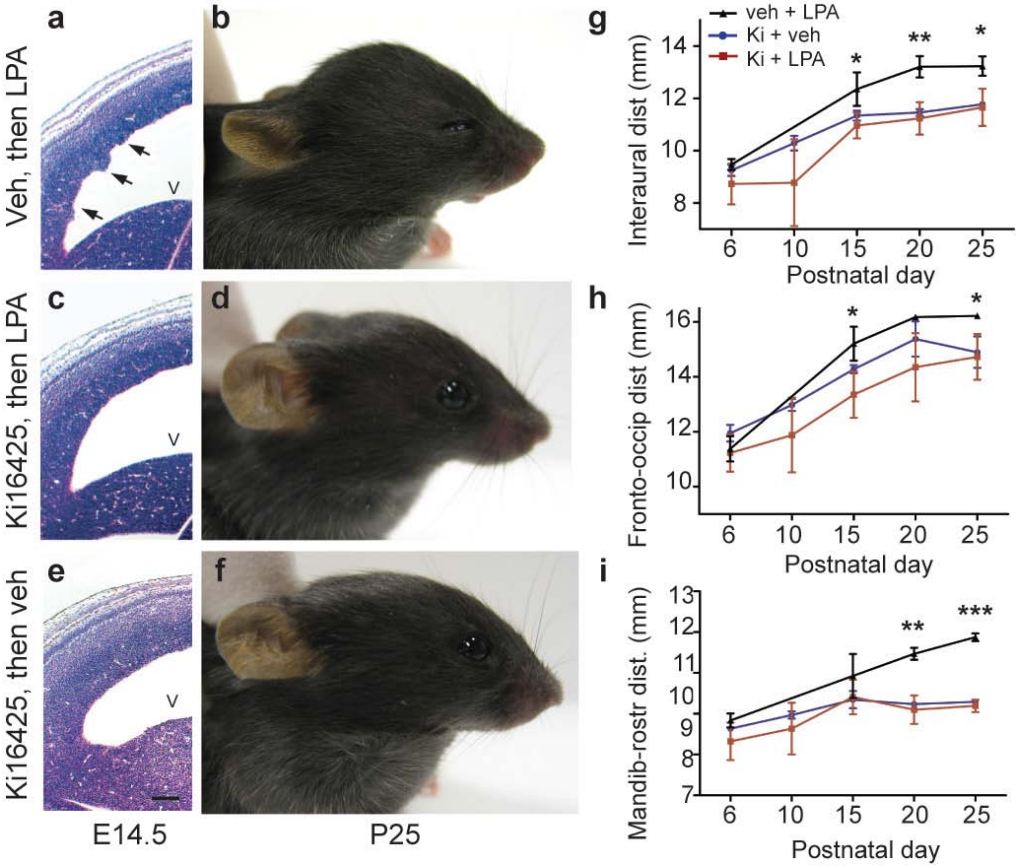
a
b
g
Veh, then LPA
V
veh + LPA
Ki + veh
Ki + LPA
Interaural dist (mm)
Postnatal day
c
d
h
Ki16425, then LPA
Fronto-occip dist (mm)
e
f
i
Ki16425, then veh
Mandib-rostr dist. (mm)
E14.5
P25

**Table 2.1: Shared histological features of hydrocephalus identified in clinical studies, other animal models, and observed following serum or LPA exposure.**

| Histological features of fetal/neonatal hydrocephalus | Clinical studies | Animal models | serum/LPA exposure |
|---|---|---|---|
| Bleeding/hemorrhage | yes[1,2,23,33] | mimicked[11,34] | mimicked |
| Ventricular dilation | yes[1-3,25,33] | yes[11,17-21,24, 26-29, 34] | yes |
| Disrupted neuroprogenitors | yes[13, 25] | yes[15,16, 20, 29] | yes |
| Loss of ependymal layer | yes[23, 25] | yes[17, 19, 21, 24, 29. 34] | yes |
| Neurorosettes found | yes[23, 25] | yes[15, 16, 20, 21, 29] | yes |
| Heterotopias found | yes[13, 23] | yes[18, 20] | yes |
| Ciliary defects | yes[25] | yes[26-28] | yes |
| 3rd ventricle occlusion and/or aqueductal stenosis | yes[23, 25, 33] | yes[18, 19, 27] | yes |

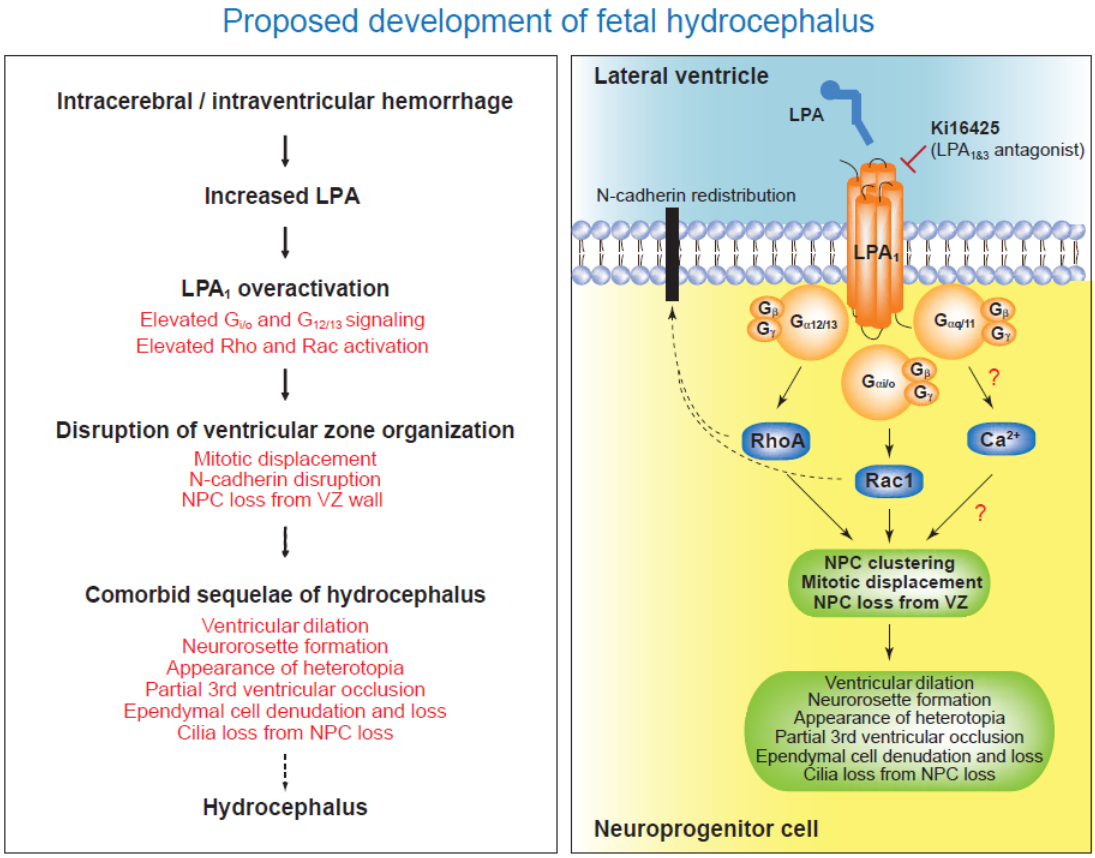


**Figure 2.S1: Proposed model of fetal hydrocephalus via $LPA_1$ overactivation.**

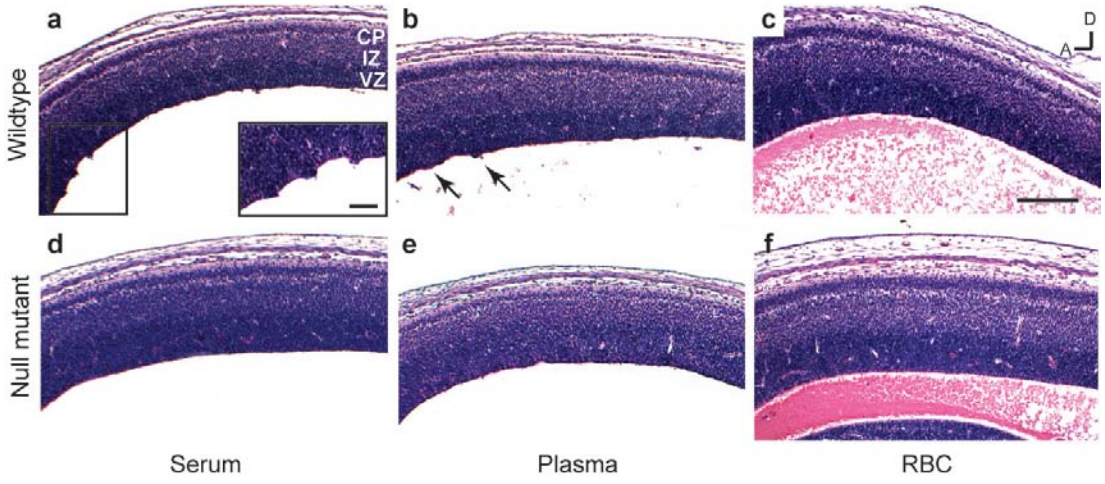


**Figure 2.S2: Serum and plasma but not RBCs produce LPA receptor dependent cortical wall disruption**. Wildtype (**a, b, and c**) or $LPA_1$ and $LPA_2$ double null mutant E13.5 embryos (**d, e, and f**) were injected with plasma, serum, or RBCs and analyzed at E14.5. **a, b**, Injection of serum or plasma produced disruptions of the apical ventricular surface (indicated by arrows and shown in the magnified boxed inset). **c**, RBC injected cortices retained a smooth apical ventricular zone. Abundant erythrocytes (pink) are seen within the lateral ventricle. **d-f**, Injection of serum, plasma, or RBCs into $LPA_1^{-/-}$ $LPA_2^{-/-}$ double null mutant embryos did not produce cortical disruption. A = anterior, D = dorsal. CP = cortical plate, IZ = intermediate zone, VZ = ventricular zone. Scale bars = 200 and 50 μm (inset).

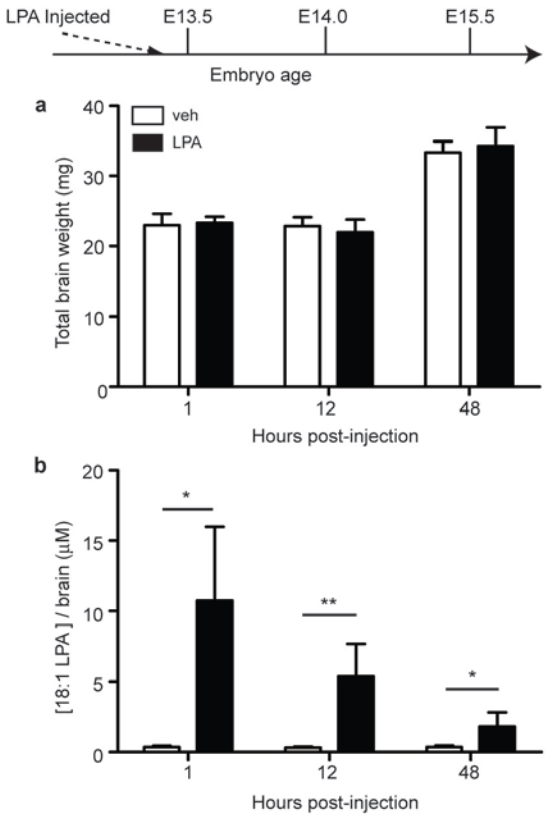


**Figure 2.S3: Experimental parameters of LPA cortical exposure model.** Embryos injected at E13.5 were examined for total brain weight and 18:1 LPA levels at E13.5 (1 h later), at E14.0 (12 h later), and E15.5 (48 h later). **a**, Total brain weights between vehicle (white bars) and LPA injected (black bars) embryos were not statistically different up to 48 hours post-exposure ($n \geq 3$ embryos per condition, mean ± s.d., unpaired t-test; 1 h, $P = 0.77$; 12 h, $P = 0.44$; 48 h, $P = 0.55$). **b**, Wildtype brain 18:1 LPA concentration remained relatively stable (between 0.32-0.35 μM ) from E13.5 to E15.5 in vehicle injected embryos (white bars). LPA cortical injection resulted in an initially elevated amount (approximately 10.75 μM 18:1 LPA) at 1 h post-exposure, declining by 48 h post-exposure to approximately 1.79 μM 18:1 LPA (black bars). Although it is unclear what fraction of total LPA is available for signaling towards the development of fetal hydrocephalus (FH) (e.g., concentration at the receptors), these levels were consistent with total LPA concentrations that could be attained under pathophysiological conditions (up to 20 μM). (1-3) ($n \geq 3$ embryos per condition, mean ± s.d., unpaired t-test; 1 h, * $P = 0.03$; 12 h, ** $P = 0.005$; 48 h, * $P = 0.01$)

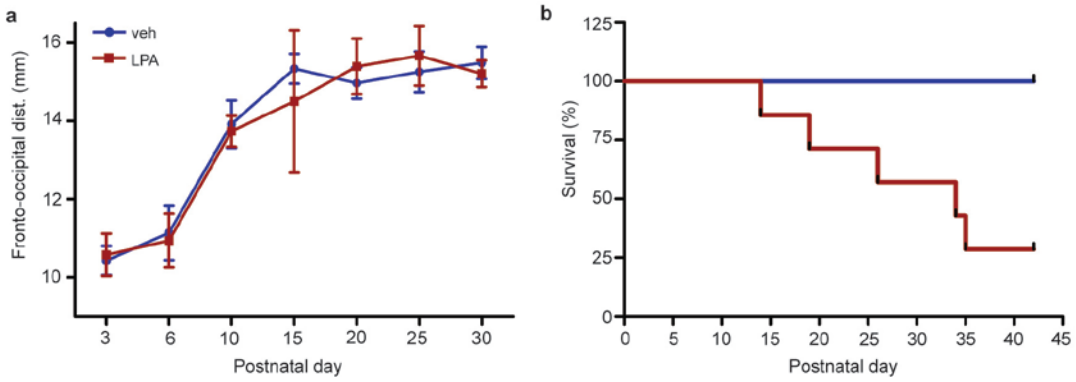


**Figure 2.S4: Lack of fronto-occipital changes and survival curve of LPA injected animals which develop hydrocephalus over time.** **a**, Embryos exposed to LPA (*n* = 7) (red lines) that develop hydrocephalus with macrocephaly and increased interaural and mandibular-rostral dimensions (Figure 1) do not display statistically different fronto-occipital distances compared with vehicle-injected embryos (*n* = 10) (blue lines) (mean ± s.d., unpaired t-test). **b**, Survival curve of postnatal animals exposed at E13.5 to vehicle (veh, blue line) or LPA (red line).

**Figure 2.S5: Bilaterally increased ventricular area and mitotic displacement following LPA exposure.** E13.5 littermates exposed to LPA for 24 h developed ventricular dilation at all levels in both left and right cortices (**b, d, f, h, j, l**), in contrast to matched vehicle exposed cortices (**a, c, e, g, i, k**). Dotted white lines indicate representative areas measured for vehicle and LPA sample cohorts. Quantification of measured ipsilateral and contralateral areas is found in Figure **2c**. Note the increased PHH3+ mitotic displacement in the LPA-exposed brains (**d**, arrows), compared with brains exposed to vehicle (**c**, arrowheads). Ctx = cortex. Dorsal is to the top of the page. Scale bar = 400 μm.

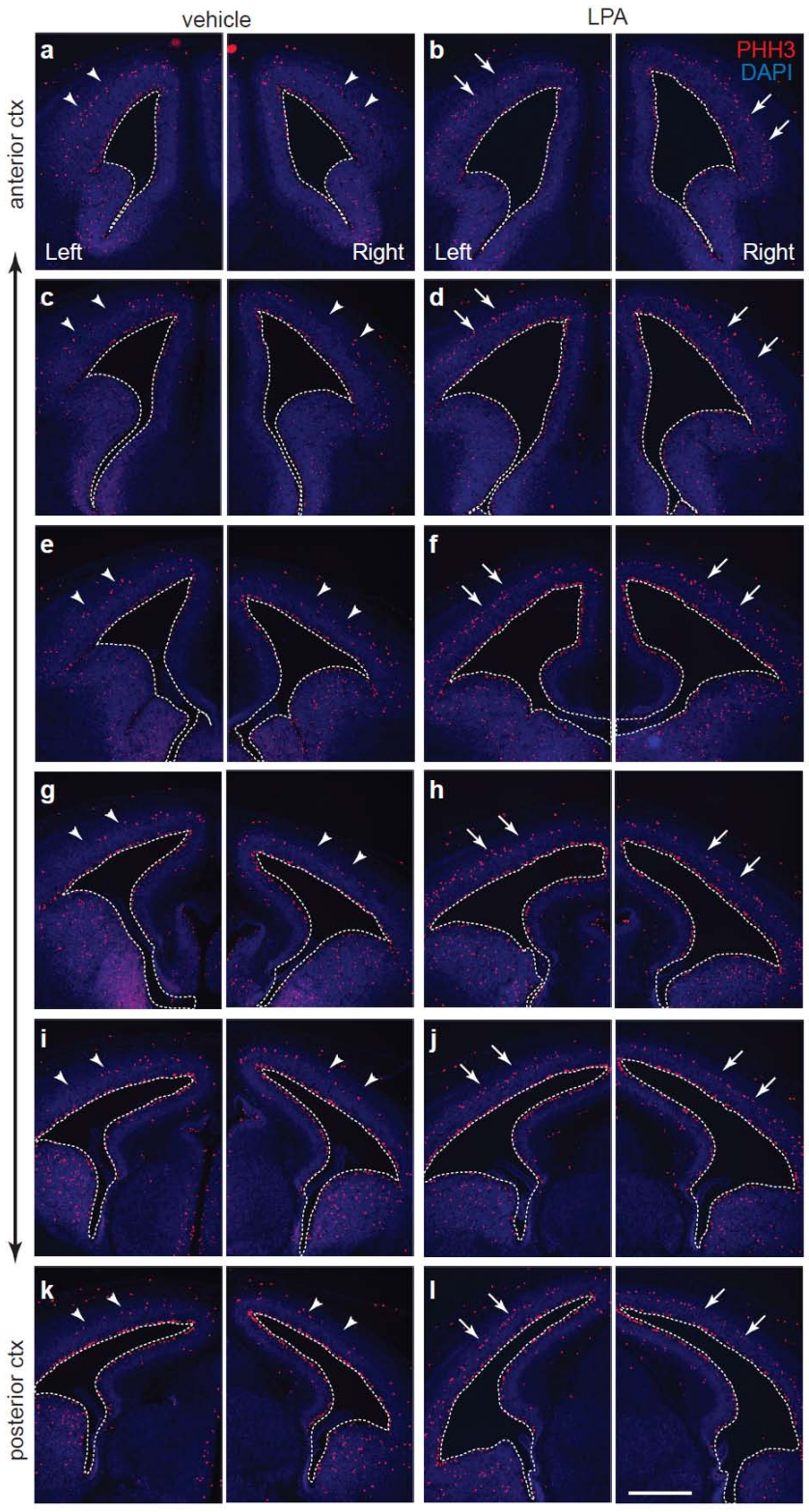
vehicle
LPA
PHH3
DAPI
anterior ctx
posterior ctx
Left
Right
Left
Right
a
b
c
d
e
f
g
h
i
j
k
l

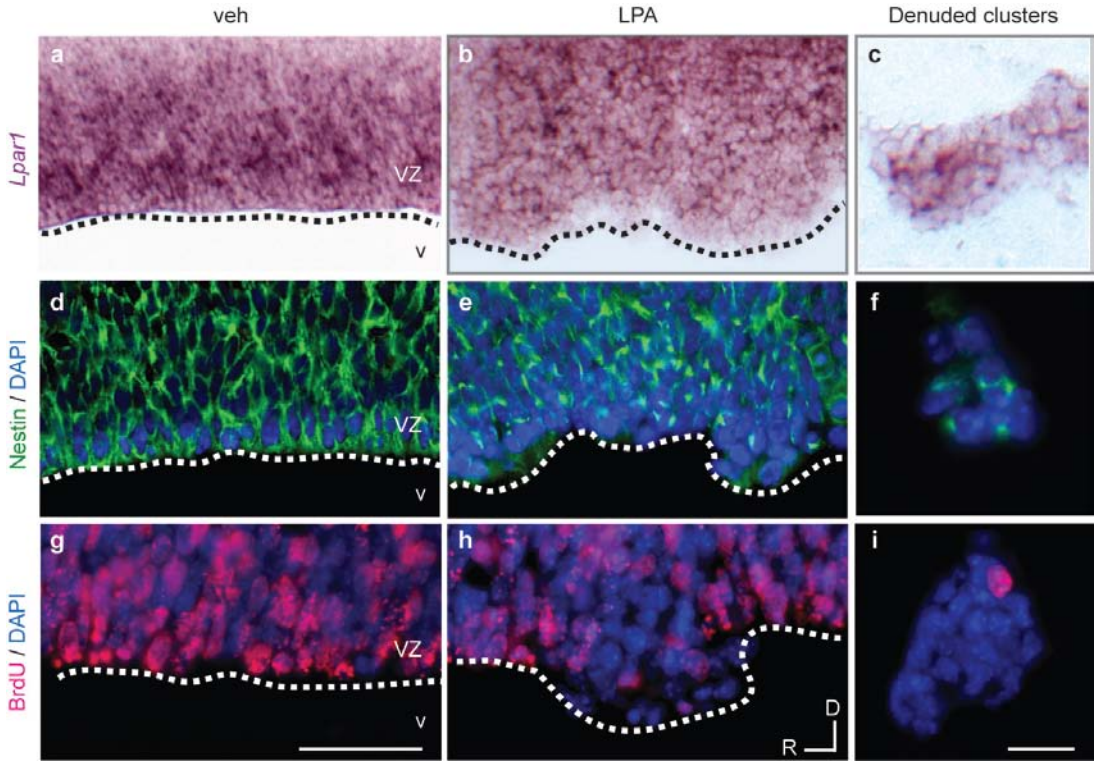


**Figure 2.S6: LPA exposure induces the formation of denuded cell clusters that originate from the ventricular zone of the developing cortex. a,b**, *In situ* hybridization with an *Lpar1* DIG labeled probe shows shows expression along the apical ventricular surface in vehicle (**a**), and LPA injected (**b**) E13.5 embryos exposed to LPA for 24 h. Note the smooth apical ventricular surface in embryos exposed to vehicle versus LPA. **d, e**, Immunohistochemistry shows nestin positive cells along the apical ventricular surface in embryos exposed to vehicle (**d**) or LPA (**e**) for 24 hours. **g, h**, BrdU staining of vehicle (**g**) and LPA (**h**) injected E13.5 embryo apical ventricle surfaces. LPA exposed cortices had undulating, disrupted apical surfaces that manifested as nodules (compare dotted outlines); in many cases, these cells appeared to detach and become free-floating cell clusters in the ventricles. **c, f, i,** These clusters were *Lpar1*$^{+}$ (**c**), nestin$^{+}$ (**f**), and BrdU$^{+}$ (**i**). R = rostral, D = dorsal, VZ = ventricular zone, v = lateral ventricle. Scale bars = 50 (**a, b, d, e, g, h**) and 20 μm (**c, f, i**).

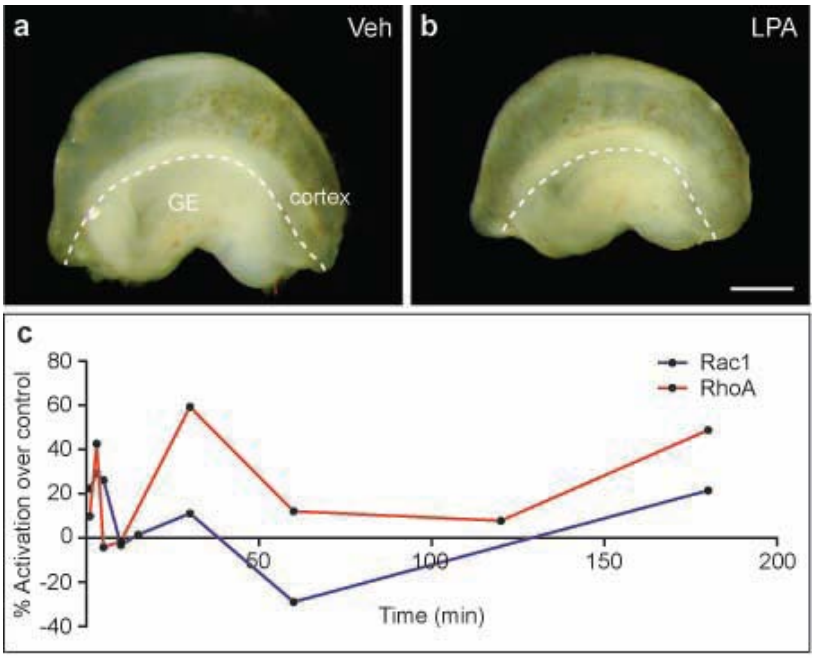


**Figure 2.S7: LPA induces RhoA and Rac1 activation. a, b**, E13.5 embryonic cortical hemispheres were exposed to vehicle (veh) alone (**a**) or LPA (**b**) for 1, 3, 5, 10 15, 30, 60, 120, or 180 minutes, then immediately microdissected on ice to remove the ganglionic eminences (GE) and enrich for the overlying cortex that is known to express $LPA_1$ receptors and which demonstrated disruption by LPA exposure (tissue region above white dotted line). **c**, Representative time courses of RhoA (red line) and Rac1 (blue line) activation upon LPA exposure by ELISA assay showed a nonlinear trend with rapid overactivation, followed by inhibition compared with control hemispheres.

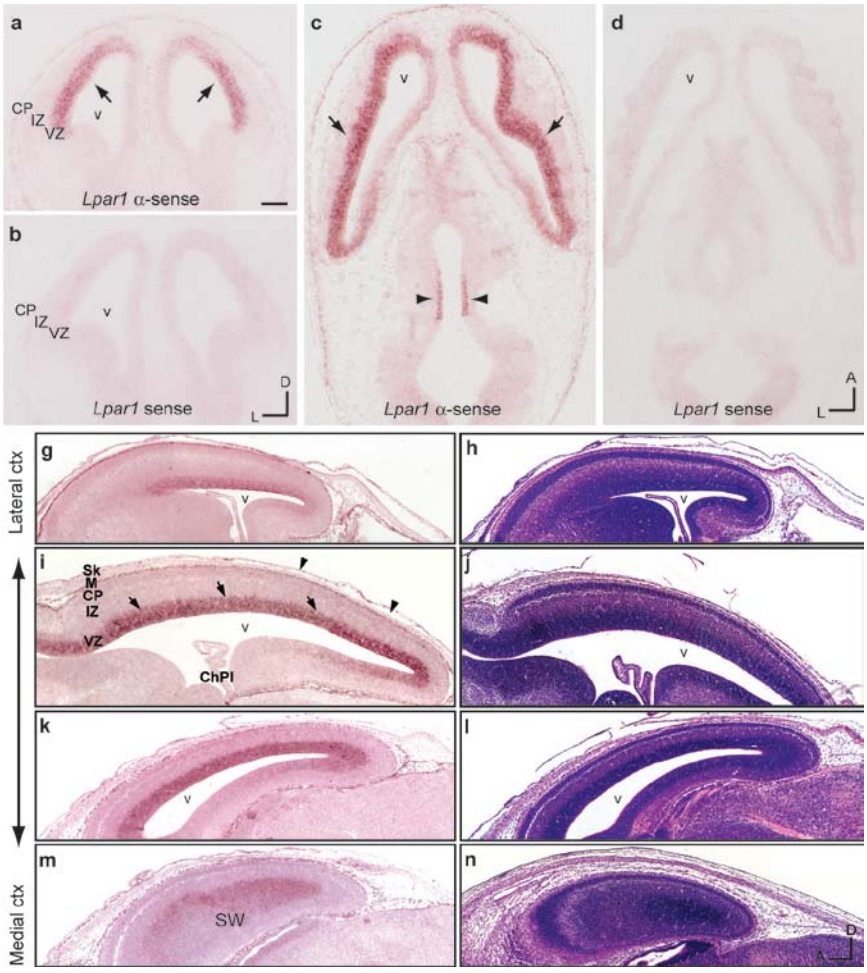


**Figure 2.S8: Expression of *Lpar1* in the developing embryonic brain at E13.5.** **a-n**, *In situ* hybridization using anti-sense and sense strand DIG-labeled probes for *Lpar1* using cryosections from freshly-frozen tissue can be seen in both the coronal view (**a, b**) and horizontal view (**c, d**). *Lpar1* was expressed in the ventricular zone (VZ) layer (**a, c,** arrows) of the lateral cortical wall at E13.5, more lightly at the medial wall, and was also present within the developing 3rd ventricle (**c**, arrowheads). The development of 3rd ventricular occlusions from LPA exposure (see also Figure 2.2) is consistent with this *Lpar1* spatiotemporal expression. **g-n**, *Lpar1 in situ* hybridization was also performed in paraffin-embedded tissue. Strong *Lpar1* expression was present in the VZ (indicated by arrows), the meninges / layer 1 of the cortex (indicated by arrowheads), and the medial septal wall (SW) between the lateral ventricles (**g, i, k, m**). Adjacent sections were stained with hematoxylin and eosin (**h, j, l, n**). v = lateral ventricle, IZ = intermediate zone, CP = cortical plate, Ctx = cortex, Sk = developing skull, ChPl = choroid plexus, D = dorsal, L = lateral, R = rostral, A = anterior. Scale bar = 200 μm.

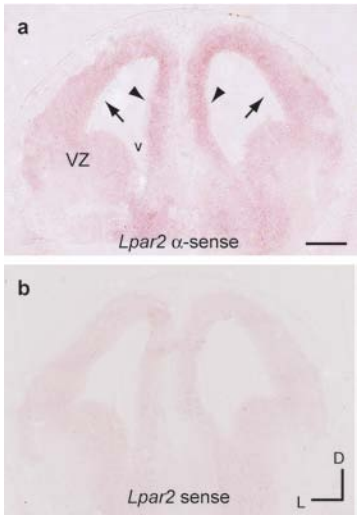


**Figure 2.S9: *Lpar2* is expressed in the developing embryonic brain at E13.5. a, b** *In situ* hybridization with DIG-labeled *Lpar2* antisense (**a**) and sense (**b**) riboprobes shows that $LPA_2$ was more diffusely expressed throughout both the medial (arrowheads) and lateral cortical wall (arrows) compared with *Lpar1*. VZ = ventricular zone, v = ventricle, D = dorsal, L = lateral. Scale bar = 200 μm.

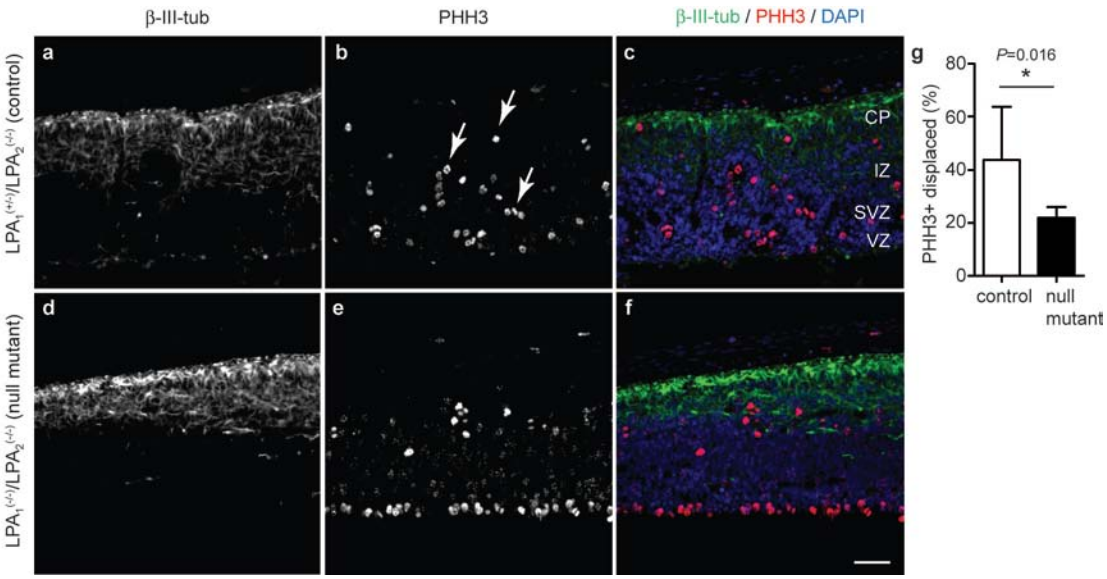


**Figure 2.S10: LPA-induced cortical disruption and mitotic displacement are abrogated in double-null mutant mice.** **a, d**, Control mice ($LPA_1^{+/-}$ $LPA_2^{-/-}$) injected with LPA showed altered β-III-tub expression, consistent with cortical disruption and heterotopia formation, in contrast to the double null mice ($LPA_1^{-/-}$ $LPA_2^{-/-}$) . **b, e**, Cortical disruption resulted in phospho-histone H3 (PHH3) positive mitotic cells moving basally away from the ventricular surface (indicated by arrows), which was not present in double null mice. **c, f**, Merged images of β-III-tub (green), PHH3 (red), and nuclear counterstaining DAPI (blue). **g**, Quantification of mitotic displacement (%) ($n \geq 4$ embryos per condition, mean ± s.d., unpaired t-test, * $P = 0.016$). Scale bar = 50 μm.

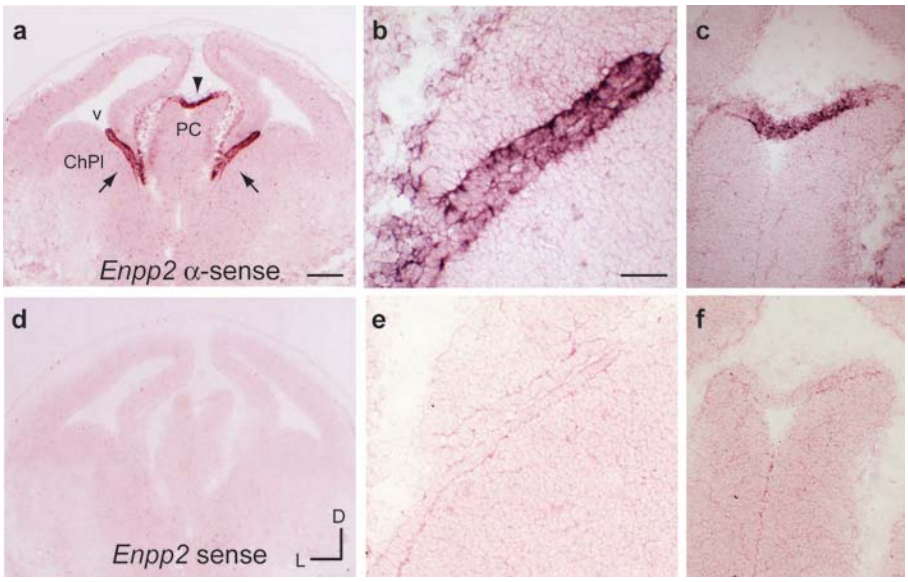


**Figure 2.S11:** ***Enpp2*** **(autotaxin) is expressed in the developing embryonic brain at E13.5.** **a-c**, *In situ* hybridization with *Enpp2* DIG labeled antisense riboprobe shows that *Enpp2* is strongly expressed in the choroid plexus (ChPl, indicated by arrows) as well as the posterior commissure (indicated by arrowhead), which are magnified in **b** (ChPl) and **c** (PC). **d-f**, DIG labeled sense strand control *in situ* hybridization of adjacent tissue sections shown in **a-c**. D = dorsal, L = lateral. Scale bar = 200 (**a, d**) and 50 μm (**b, c, e, f**).

**Table 2.S1: Histological features associated with hydrocephalus are abrogated in $LPA_1$ and $LPA_2$ double null animals.** Frank hydrocephalus was absent in ~ 90% of the double null mutants. The presence of mild histological features, markedly reduced from controls, supports the involvement of $LPA_1$ and $LPA_2$ in these histological changes, and suggest that one or more of the other 4 remaining LPA receptors may further contribute to these phenotypes.

| Histological features of fetal/neonatal hydrocephalus | LPA exposure | | serum exposure | |
|---|---|---|---|---|
| | control | null mutants | control | null mutants |
| Ventricular dilation | yes | mild | yes | mild |
| Disruption of NPCs | yes | mild | yes | mild |
| Loss of ependymal layer | yes | no | yes | no |
| Neurorosettes | yes | no | yes | no |
| Heterotopias | yes | mild | yes | mild |
| Cilia defects | yes | no | yes | no |
| 3rd ventricle occlusion | yes | no | yes | no |

**Table 2.S2: Mean ± s.d., *n*, and *P*-values of data graphed in Figures 1, 4, and 5.** *P*-values highlighted in green and red represent statistically significant ($P \leq 0.05$) and non-significant data ($P > 0.05$), respectively.

| | Figure 1k | | | | |
|---|---|---|---|---|---|
| **Age** | **Interaural distance veh (avg ± s.d.)** | ***n*** | **Interaural distance LPA (avg ± s.d.)** | ***n*** | ***P*-value** |
| P3 | 8.01 ± 0.16 | 10 | 8.28 ± 0.18 | 7 | 0.01 |
| P6 | 8.93 ± 0.43 | 10 | 9.47 ± 0.29 | 7 | 0.01 |
| P10 | 10.24 ± 0.43 | 10 | 11.07 ± 0.43 | 7 | 0.001 |
| P15 | 11.18 ± 0.10 | 10 | 12.15 ± 0.06 | 5 | 0.003 |
| P20 | 11.13 ± 0.30 | 10 | 12.51 ± 0.78 | 5 | 0.003 |
| P25 | 11.58 ± 0.13 | 10 | 12.96 ±0.56 | 4 | 0.0003 |
| P30 | 11.69 ± 0.10 | 10 | 12.9 ±0.22 | 3 | <0.0001 |

| | Figure 1l | | | | |
|---|---|---|---|---|---|
| **Age** | **Mandibular-rostral dist veh (avg ± s.d.)** | ***n*** | **Mandibular-rostral dist LPA (avg ± s.d.)** | ***n*** | ***P*-value** |
| P6 | 9.39 ± 0.44 | 10 | 10.11 ± 0.21 | 7 | 0.001 |
| P10 | 10.27 ± 0.43 | 10 | 11.02 ± 0.55 | 7 | 0.006 |
| P15 | 10.3 ± 0.16 | 10 | 11.65 ± 0.17 | 5 | 0.001 |
| P20 | 10.18 ± 0.23 | 10 | 12.63 ± 1.08 | 5 | 0.0004 |
| P25 | 10.73 ± 0.33 | 10 | 13.42 ± 0.31 | 4 | <0.0001 |
| P30 | 10.93 ± 0.49 | 10 | 13.61 ± 0.28 | 3 | <0.0001 |

| | Figure 1m | | | | |
|---|---|---|---|---|---|
| **Age** | **Body weight veh (avg ± s.d.)** | ***n*** | **Body weight LPA (avg ± s.d.)** | ***n*** | ***P*-value** |
| P3 | 2.66 ± 0.42 | 10 | 2.54 ± 0.24 | 7 | 0.49 |
| P6 | 4.2 ± 0.75 | 10 | 3.97 ± 0.40 | 7 | 0.47 |
| P10 | 6.47 ± 1.09 | 10 | 6.15 ± 0.49 | 7 | 0.48 |
| P15 | 10.04 ± 1.45 | 10 | 8.66 ± 2.39 | 5 | 0.20 |
| P20 | 8.75 ± 1.29 | 10 | 6.8 ± 0.41 | 5 | 0.01 |
| P25 | 10.25 ± 0.85 | 10 | 8.15 ± 1.26 | 4 | 0.01 |
| P30 | 11.53 ± 0.80 | 10 | 8.93 ± 0.35 | 3 | 0.001 |

| | Figure 4i | | | | |
|---|---|---|---|---|---|
| **Age** | **Interaural distance control (avg ± s.d.)** | ***n*** | **Interaural distance null mutant (avg ± s.d.)** | ***n*** | ***P*-value** |
| P3 | 8.31 ± 0.06 | 4 | 7.63 ± 0.34 | 3 | 0.01 |
| P6 | 10.33 ± 0.14 | 4 | 9.37 ± 0.43 | 3 | 0.008 |
| P15 | 13.82 ± 0.20 | 4 | 11.25 ± 0.72 | 3 | 0.001 |

| | Figure 4j | | | | |
|---|---|---|---|---|---|
| **Age** | **Mandib-rostral dist control (avg ± s.d.)** | ***n*** | **Mandib-rostral dist null mutant (avg ± s.d.)** | ***n*** | ***P*-value** |
| P3 | 8.40 ± 0.10 | 4 | 8.00 ± 0.44 | 3 | 0.13 |
| P6 | 10.05 ± 0.16 | 4 | 9.35 ± 0.74 | 3 | 0.12 |
| P15 | 14.09 ± 0.34 | 4 | 11.01 ± 0.37 | 3 | <0.0001 |

| | Figure 5g | | | | |
|---|---|---|---|---|---|
| **Age** | **Interaural distance veh + LPA (avg ± s.d.)** | ***n*** | **Interaural distance Ki+LPA (avg ± s.d.)** | ***n*** | ***P*-value** |
| P6 | 9.47 ± 0.21 | 4 | 8.73 ± 0.78 | 4 | 0.12 |
| P15 | 12.36 ± 0.64 | 3 | 10.96 ± 0.49 | 3 | 0.03 |
| P20 | 13.21 ± 0.41 | 3 | 11.24 ± 0.62 | 3 | 0.004 |
| P25 | 13.24 ± 0.37 | 3 | 11.66 ± 0.71 | 3 | 0.03 |

**Table 2.S2: Mean ± s.d., *n*, and *P*-values of data graphed in Figures 1, 4, and 5, Continued.**

**Figure 5g**

| Age | Interaural distance Ki+veh (avg ± s.d.) | *n* | Interaural distance Ki+LPA (avg ± s.d.) | *n* | *P*-value |
|---|---|---|---|---|---|
| P6 | 9.25 ± 0.21 | 3 | 8.73 ± 0.78 | 4 | 0.32 |
| P10 | 10.29 ± 0.28 | 3 | 8.78 ± 1.66 | 4 | 0.19 |
| P15 | 11.34 ± 0.19 | 3 | 10.96 ± 0.49 | 3 | 0.29 |
| P20 | 11.46 ± 0.13 | 3 | 11.24 ± 0.62 | 3 | 0.59 |
| P25 | 11.78 ± 0.09 | 3 | 11.66 ± 0.71 | 3 | 0.79 |

**Figure 5h**

| Age | Fronto-occip dist veh + LPA (avg ± s.d.) | *n* | Fronto-occip dist Ki+LPA (avg ± s.d.) | *n* | *P*-value |
|---|---|---|---|---|---|
| P6 | 11.38 ± 0.46 | 4 | 11.23 ± 0.68 | 4 | 0.72 |
| P15 | 15.21 ± 0.62 | 3 | 13.35 ± 0.84 | 3 | 0.04 |
| P20 | 16.18 ± 0.10 | 3 | 14.35 ± 1.24 | 3 | 0.06 |
| P25 | 16.22 ± 0.04 | 3 | 14.73 ± 0.83 | 3 | 0.04 |

**Figure 5h**

| Age | Fronto-occip dist Ki+veh (avg ± s.d.) | *n* | Fronto-occip dist Ki+LPA (avg ± s.d.) | *n* | *P*-value |
|---|---|---|---|---|---|
| P6 | 11.95 ± 0.30 | 3 | 11.23 ± 0.68 | 4 | 0.15 |
| P10 | 12.98 ± 0.22 | 3 | 11.88 ± 1.36 | 4 | 0.23 |
| P15 | 14.28 ± 0.15 | 3 | 13.35 ± 0.84 | 3 | 0.14 |
| P20 | 15.38 ± 0.64 | 3 | 14.35 ± 1.24 | 3 | 0.27 |
| P25 | 14.90 ± 0.57 | 3 | 14.73 ± 0.83 | 3 | 0.79 |

**Figure 5i**

| Age | Mandib-rostr dist veh + LPA (avg ± s.d.) | *n* | Mandib-rostr dist Ki+LPA (avg ± s.d.) | *n* | *P*-value |
|---|---|---|---|---|---|
| P6 | 9.67 ± 0.34 | 4 | 8.65 ± 0.92 | 4 | 0.07 |
| P15 | 11.85 ± 1.08 | 3 | 10.82 ± 0.85 | 3 | 0.26 |
| P20 | 12.94 ± 0.29 | 3 | 10.20 ± 0.70 | 3 | 0.003 |
| P25 | 13.75 ± 0.19 | 3 | 10.39 ± 0.30 | 3 | <0.0001 |

**Figure 5i**

| Age | Mandib-rostr dist Ki+veh (avg ± s.d.) | *n* | Mandib-rostr dist Ki+LPA (avg ± s.d.) | *n* | *P*-value |
|---|---|---|---|---|---|
| P6 | 9.27 ± 0.03 | 3 | 8.65 ± 0.92 | 4 | 0.31 |
| P10 | 9.94 ± 0.18 | 3 | 9.27 ± 1.27 | 4 | 0.42 |
| P15 | 10.69 ± 0.42 | 3 | 10.82 ± 0.85 | 3 | 0.82 |
| P20 | 10.47 ± 0.13 | 3 | 10.20 ± 0.70 | 3 | 0.54 |
| P25 | 10.59 ± 0.07 | 3 | 10.39 ± 0.30 | 3 | 0.31 |

**References**


1. Persson, E.K., Anderson, S., Wiklund, L.M., and Uvebrant, P. (2007). Hydrocephalus in children born in 1999-2002: epidemiology, outcome and ophthalmological findings. Childs Nerv Syst *23*, 1111-1118.

2. Moritake, K., Nagai, H., Miyazaki, T., Nagasako, N., Yamasaki, M., and Tamakoshi, A. (2007). Nationwide survey of the etiology and associated conditions of prenatally and postnatally diagnosed congenital hydrocephalus in Japan. Neurologia medico-chirurgica *47*, 448-452; discussion 452.

3. Zhang, J., Williams, M.A., and Rigamonti, D. (2006). Genetics of human hydrocephalus. Journal of neurology *253*, 1255-1266.

4. Aoki, J., Taira, A., Takanezawa, Y., Kishi, Y., Hama, K., Kishimoto, T., Mizuno, K., Saku, K., Taguchi, R., and Arai, H. (2002). Serum lysophosphatidic acid is produced through diverse phospholipase pathways. J Biol Chem *277*, 48737-48744.

5. Choi, J.W., Herr, D.R., Noguchi, K., Yung, Y.C., Lee, C.W., Mutoh, T., Lin, M.E., Teo, S.T., Park, K.E., Mosley, A.N., et al. (2010). LPA receptors: subtypes and biological actions. Annu Rev Pharmacol Toxicol *50*, 157-186.

6. Yanagida, K., Masago, K., Nakanishi, H., Kihara, Y., Hamano, F., Tajima, Y., Taguchi, R., Shimizu, T., and Ishii, S. (2009). Identification and characterization of a novel lysophosphatidic acid receptor, p2y5/LPA6. J Biol Chem *284*, 17731-17741.

7. Tokumura, A., Iimori, M., Nishioka, Y., Kitahara, M., Sakashita, M., and Tanaka, S. (1994). Lysophosphatidic acids induce proliferation of cultured vascular smooth muscle cells from rat aorta. Am J Physiol *267*, C204-210.

8. Noguchi, K., Herr, D., Mutoh, T., and Chun, J. (2009). Lysophosphatidic acid (LPA) and its receptors. Curr Opin Pharmacol *9*, 15-23.

9. Kingsbury, M.A., Rehen, S.K., Contos, J.J., Higgins, C.M., and Chun, J. (2003). Non-proliferative effects of lysophosphatidic acid enhance cortical growth and folding. Nat Neurosci *6*, 1292-1299.

10. Estivill-Torrus, G., Llebrez-Zayas, P., Matas-Rico, E., Santin, L., Pedraza, C., De Diego, I., Del Arco, I., Fernandez-Llebrez, P., Chun, J., and De Fonseca, F.R. (2008). Absence of LPA1 signaling results in defective cortical development. Cereb Cortex *18*, 938-950.

11. Cherian, S.S., Love, S., Silver, I.A., Porter, H.J., Whitelaw, A.G., and Thoresen, M. (2003). Posthemorrhagic ventricular dilation in the neonate: development and characterization of a rat model. J Neuropathol Exp Neurol *62*, 292-303.

12. Hecht, J.H., Weiner, J.A., Post, S.R., and Chun, J. (1996). Ventricular zone gene-1 (vzg-1) encodes a lysophosphatidic acid receptor expressed in neurogenic regions of the developing cerebral cortex. J Cell Biol *135*, 1071-1083.

13. Sheen, V.L., Basel-Vanagaite, L., Goodman, J.R., Scheffer, I.E., Bodell, A., Ganesh, V.S., Ravenscroft, R., Hill, R.S., Cherry, T.J., Shugart, Y.Y., et al. (2004). Etiological heterogeneity of familial periventricular heterotopia and hydrocephalus. Brain Dev *26*, 326-334.

14. Weiner, J.A., Fukushima, N., Contos, J.J., Scherer, S.S., and Chun, J. (2001). Regulation of Schwann cell morphology and adhesion by receptor-mediated lysophosphatidic acid signaling. J Neurosci *21*, 7069-7078.

15. Ganzler-Odenthal, S.I., and Redies, C. (1998). Blocking N-cadherin function disrupts the epithelial structure of differentiating neural tissue in the embryonic chicken brain. J Neurosci *18*, 5415-5425.

16. Kadowaki, M., Nakamura, S., Machon, O., Krauss, S., Radice, G.L., and Takeichi, M. (2007). N-cadherin mediates cortical organization in the mouse brain. Dev Biol *304*, 22-33.

17. Tissir, F., Qu, Y., Montcouquiol, M., Zhou, L., Komatsu, K., Shi, D., Fujimori, T., Labeau, J., Tyteca, D., Courtoy, P., et al. (2010). Lack of cadherins Celsr2 and Celsr3 impairs ependymal ciliogenesis, leading to fatal hydrocephalus. Nat Neurosci *13*, 700-707.

18. Ma, X., Bao, J., and Adelstein, R.S. (2007). Loss of cell adhesion causes hydrocephalus in nonmuscle myosin II-B-ablated and mutated mice. Mol Biol Cell *18*, 2305-2312.

19. Abouhamed, M., Grobe, K., Leefa Chong San, I.V., Thelen, S., Honnert, U., Balda, M.S., Matter, K., and Bahler, M. (2009). Myosin IXa Regulates Epithelial Differentiation and Its Deficiency Results in Hydrocephalus. Mol Biol Cell.

20. Klezovitch, O., Fernandez, T.E., Tapscott, S.J., and Vasioukhin, V. (2004). Loss of cell polarity causes severe brain dysplasia in Lgl1 knockout mice. Genes & development *18*, 559-571.

21. Nechiporuk, T., Fernandez, T.E., and Vasioukhin, V. (2007). Failure of epithelial tube maintenance causes hydrocephalus and renal cysts in Dlg5-/- mice. Developmental cell *13*, 338-350.

22. Yanagida, K., Ishii, S., Hamano, F., Noguchi, K., and Shimizu, T. (2007). LPA4/p2y9/GPR23 mediates rho-dependent morphological changes in a rat neuronal cell line. J Biol Chem *282*, 5814-5824.

23. Fukumizu, M., Takashima, S., and Becker, L.E. (1995). Neonatal posthemorrhagic hydrocephalus: neuropathologic and immunohistochemical studies. Pediatr Neurol *13*, 230-234.

24. Banizs, B., Pike, M.M., Millican, C.L., Ferguson, W.B., Komlosi, P., Sheetz, J., Bell, P.D., Schwiebert, E.M., and Yoder, B.K. (2005). Dysfunctional cilia lead to altered ependyma and choroid plexus function, and result in the formation of hydrocephalus. Development *132*, 5329-5339.

25. Dominguez-Pinos, M.D., Paez, P., Jimenez, A.J., Weil, B., Arraez, M.A., Perez-Figares, J.M., and Rodriguez, E.M. (2005). Ependymal denudation and alterations of the subventricular zone occur in human fetuses with a moderate communicating hydrocephalus. J Neuropathol Exp Neurol *64*, 595-604.

26. Dawe, H.R., Shaw, M.K., Farr, H., and Gull, K. (2007). The hydrocephalus inducing gene product, Hydin, positions axonemal central pair microtubules. BMC biology *5*, 33.

27. Town, T., Breunig, J.J., Sarkisian, M.R., Spilianakis, C., Ayoub, A.E., Liu, X., Ferrandino, A.F., Gallagher, A.R., Li, M.O., Rakic, P., et al. (2008). The stumpy gene is required for mammalian ciliogenesis. Proc Natl Acad Sci U S A *105*, 2853-2858.

28. Wodarczyk, C., Rowe, I., Chiaravalli, M., Pema, M., Qian, F., and Boletta, A. (2009). A novel mouse model reveals that polycystin-1 deficiency in ependyma and choroid plexus results in dysfunctional cilia and hydrocephalus. PLoS One *4*, e7137.

29. Paez, P., Batiz, L.F., Roales-Bujan, R., Rodriguez-Perez, L.M., Rodriguez, S., Jimenez, A.J., Rodriguez, E.M., and Perez-Figares, J.M. (2007). Patterned neuropathologic events occurring in hyh congenital hydrocephalic mutant mice. J Neuropathol Exp Neurol *66*, 1082-1092.

30. Spassky, N., Merkle, F.T., Flames, N., Tramontin, A.D., Garcia-Verdugo, J.M., and Alvarez-Buylla, A. (2005). Adult ependymal cells are postmitotic and are derived from radial glial cells during embryogenesis. J Neurosci *25*, 10-18.

31. Ridley, A.J., and Hall, A. (1992). The small GTP-binding protein rho regulates the assembly of focal adhesions and actin stress fibers in response to growth factors. Cell *70*, 389-399.

32. Van Leeuwen, F.N., Olivo, C., Grivell, S., Giepmans, B.N., Collard, J.G., and Moolenaar, W.H. (2003). Rac activation by lysophosphatidic acid LPA1 receptors through the guanine nucleotide exchange factor Tiam1. J Biol Chem *278*, 400-406.

33. Heep, A., Stoffel-Wagner, B., Bartmann, P., Benseler, S., Schaller, C., Groneck, P., Obladen, M., and Felderhoff-Mueser, U. (2004). Vascular endothelial growth factor and transforming growth factor-beta1 are highly expressed in the cerebrospinal fluid of premature infants with posthemorrhagic hydrocephalus. Pediatr Res *56*, 768-774.

34. Cherian, S., Thoresen, M., Silver, I.A., Whitelaw, A., and Love, S. (2004). Transforming growth factor-betas in a rat model of neonatal posthaemorrhagic hydrocephalus. Neuropathol Appl Neurobiol *30*, 585-600.

35. Ishii, I., Contos, J.J., Fukushima, N., and Chun, J. (2000). Functional comparisons of the lysophosphatidic acid receptors, LP(A1)/VZG-1/EDG-2, LP(A2)/EDG-4, and LP(A3)/EDG-7 in neuronal cell lines using a retrovirus expression system. Mol Pharmacol *58*, 895-902.

36. Ohta, H., Sato, K., Murata, N., Damirin, A., Malchinkhuu, E., Kon, J., Kimura, T., Tobo, M., Yamazaki, Y., Watanabe, T., et al. (2003). Ki16425, a subtype-selective antagonist for EDG-family lysophosphatidic acid receptors. Mol Pharmacol *64*, 994-1005.

37. McGiffert, C., Contos, J.J., Friedman, B., and Chun, J. (2002). Embryonic brain expression analysis of lysophospholipid receptor genes suggests roles for s1p(1) in neurogenesis and s1p(1-3) in angiogenesis. FEBS Lett *531*, 103-108.

38. Dubin, A.E., Herr, D.R., and Chun, J. (2010). Diversity of lysophosphatidic acid receptor-mediated intracellular calcium signaling in early cortical neurogenesis. J Neurosci *30*, 7300-7309.

39. Gauster, M., Rechberger, G., Sovic, A., Horl, G., Steyrer, E., Sattler, W., and Frank, S. (2005). Endothelial lipase releases saturated and unsaturated fatty acids of high density lipoprotein phosphatidylcholine. J Lipid Res *46*, 1517-1525.

40. Nakamura, K., Kishimoto, T., Ohkawa, R., Okubo, S., Tozuka, M., Yokota, H., Ikeda, H., Ohshima, N., Mizuno, K., and Yatomi, Y. (2007). Suppression of lysophosphatidic acid and lysophosphatidylcholine formation in the plasma in vitro: proposal of a plasma sample preparation method for laboratory testing of these lipids. Anal Biochem *367*, 20-27.

41. Bachner, D., Ahrens, M., Betat, N., Schroder, D., and Gross, G. (1999). Developmental expression analysis of murine autotaxin (ATX). Mech Dev *84*, 121-125.

42. Albers, H.M., Dong, A., van Meeteren, L.A., Egan, D.A., Sunkara, M., van Tilburg, E.W., Schuurman, K., van Tellingen, O., Morris, A.J., Smyth, S.S., et al. (2010). Boronic acid-based inhibitor of autotaxin reveals rapid turnover of LPA in the circulation. Proc Natl Acad Sci U S A *107*, 7257-7262.

43. Jourquin, J., Yang, N., Kam, Y., Guess, C., and Quaranta, V. (2006). Dispersal of epithelial cancer cell colonies by lysophosphatidic acid (LPA). J Cell Physiol *206*, 337-346.

44. Fukushima, N., and Morita, Y. (2006). Actomyosin-dependent microtubule rearrangement in lysophosphatidic acid-induced neurite remodeling of young cortical neurons. Brain Res *1094*, 65-75.

45. Ibanez-Tallon, I., Pagenstecher, A., Fliegauf, M., Olbrich, H., Kispert, A., Ketelsen, U.P., North, A., Heintz, N., and Omran, H. (2004). Dysfunction of axonemal dynein heavy chain Mdnah5 inhibits ependymal flow and reveals a novel mechanism for hydrocephalus formation. Hum Mol Genet *13*, 2133-2141.

46. Wikoff, W.R., Pendyala, G., Siuzdak, G., and Fox, H.S. (2008). Metabolomic analysis of the cerebrospinal fluid reveals changes in phospholipase expression in the CNS of SIV-infected macaques. J Clin Invest *118*, 2661-2669.

47. Baumforth, K.R., Flavell, J.R., Reynolds, G.M., Davies, G., Pettit, T.R., Wei, W., Morgan, S., Stankovic, T., Kishi, Y., Arai, H., et al. (2005). Induction of autotaxin by the Epstein-Barr virus promotes the growth and survival of Hodgkin lymphoma cells. Blood *106*, 2138-2146.

48. Kishi, Y., Okudaira, S., Tanaka, M., Hama, K., Shida, D., Kitayama, J., Yamori, T., Aoki, J., Fujimaki, T., and Arai, H. (2006). Autotaxin is overexpressed in glioblastoma multiforme and contributes to cell motility of glioblastoma by converting lysophosphatidylcholine to lysophosphatidic acid. J Biol Chem *281*, 17492-17500.

49. Rehen, S.K., Kingsbury, M.A., Almeida, B.S., Herr, D.R., Peterson, S., and Chun, J. (2006). A new method of embryonic culture for assessing global changes in brain organization. J Neurosci Methods *158*, 100-108.

50. Matyash, V., Liebisch, G., Kurzchalia, T.V., Shevchenko, A., and Schwudke, D. (2008). Lipid extraction by methyl-tert-butyl ether for high-throughput lipidomics. J Lipid Res *49*, 1137-1146.

# CHAPTER III

## Concluding Remarks and Future Directions

**Initiation and development of FH**

A large body of clinical observations have shed light on important aspects of FH, including epidemiology (1, 2), presentation (3), histological heterogeneity (4), and associated comorbidities (5). An important advance has been the refined visualization and monitoring of early *in utero* antenatal changes, such as ventriculomegaly, that can lead to FH (6-8), made possible by innovations in sonography (e.g., ultrasound imaging) (9) and MRI (magnetic resonance imaging) (10).

Ventricular dilation, detectable as early as 16 weeks of gestational age, can precede frank hydrocephalus by many weeks (11-13). In addition, postmortem analysis of fetuses at various ages, including gestational week 16, revealed disruption of the neuroepithelial/ependymal lining of the aqueduct and telencephalon (14, 15) and the presence of neuroprogenitor cells within the CSF (16). Thus, pathological neuroarchitectural and cellular changes can occur early during fetal development, even within the first trimester (17). These clinical findings are consistent with the experimental observations reported in chapter II, in which a single, initiating event at E13.5 in mice (approximately equivalent to gestational week 7, Figure 3.1) can produce most of the histological sequelae associated with FH and frank hydrocephalus at perinatal ages.

Bleeding in the fetal brain - variably described as intracranial, intraventricular, or germinal matrix hemorrhage - have all been reported to be major risk factors for the development of FH (18). Blood associated factors such as TGF-β (transforming

**Figure 3.1: Neural developmental timeline in mouse, macaque, and man.** **S**pecific cellular layers and anatomical components of the developing brain form within stereotyped time periods of varying lengths in 3 species: mouse, macaque monkey, and man. The known period of $LPA_1$ expression in the ventricular zone of the mouse cerebral cortex (light blue) extends from post-conception or embryonic day 12 to birth; this expression is extrapolated in macaque and man, based on a comparison of brain developmental maturity. LPA injections, as performed in studies described in chapter II, occur on E13.5 (arrow). Corpus callo = corpus callosum, ctx = cortex, ant comm = anterior commissure, Ent = entorhinal, SN = septal nuclei, E = embryonic day, P = postnatal day.

## Neural Developmental Timeline in Mouse, Macaque, and Man

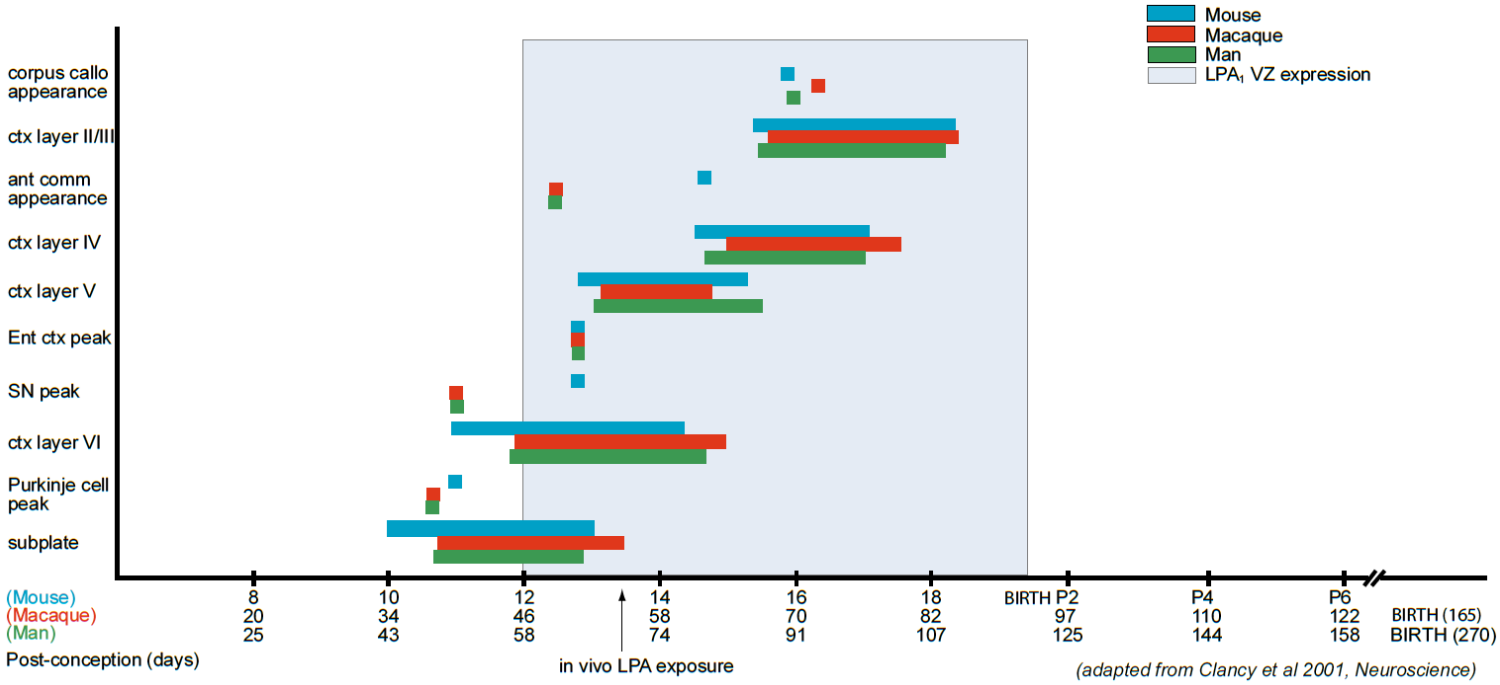


*(adapted from Clancy et al 2001, Neuroscience)*

growth factor beta) and VEGF (vascular endothelial growth factor), when injected into neonatal mouse or rat brains, have been reported to cause ventricular dilation and hydrocephalus (19-21). Furthermore, elevated levels of these factors have been found in preterm infants with germinal matrix hemorrhage and hydrocephalus (22, 23). However, it is notable that LPA appears to be the chief early initiator in the development of FH, since deletion of $LPA_1$ is sufficient to nearly prevent the development of FH due to serum or plasma exposure. There is evidence of cross-talk and cross-regulation between LPA, its receptors, and these factors (24-26), but their relationship is likely more complex than currently appreciated and warrants further investigation. Importantly, these observations can help direct future clinical and experimental approaches towards the study of FH.

**Current therapies**

Fetal brain hemorrhage is a well-known risk factor for multiple neurological disorders, particularly in the development of ventricular dilation and FH. The observation of pooling or residual blood within the ventricles, hemosiderin deposits proximal to the ventricular lining (27, 28), and stenosing clots within the aqueduct (29) have galvanized numerous clinical therapeutic approaches - including lumbar puctures, brain lavage, diuretic drugs, and fibrolytic therapy - to remove old blood, decrease bulk CSF volume, and to dissolve blockages (30, 31). However, despite the logical soundness of these interventions, they have not been successful in the

prevention of subsequent surgical shunt placement (32). Moreover, the unexpected development of secondary hemorrhagic events nullified any modest benefits from these physical interventions (32).

Additional studies that identified elevation of TGF-β and VEGF in the CSF of post-hemorrhagic infants (22, 23) suggested a more targeted approach using pharmacological inhibitors. In a study of intracranial hemorrhage and ventricular dilation in rat pups, animals were treated with perfenidone and losartan, two drugs that lower TGB-β levels. Unexpectedly, however, there was no significant reduction of ventricular dilation (33). Currently, no VEGF inhibition studies have been carried out in either clinical or experimental settings. Thus, the pathological significance and contribution to FH of these two factors, among many, remains unclear and merits further investigation.

**A fresh understanding of FH**

Rapid advances in whole genome sequencing and embryonic stem cell targeting technologies have allowed the independent generation of genetic null mutant mice with relative ease. Many of these animals develop similar and overlapping histological changes, ventricular dilation, and FH (Table 3.1 and Table 2.1), suggesting that multiple genetic changes can result in FH in mice, with corroborating studies needed in humans (34). Whether environmental insults, as postulated for acquired hydrocephalus, proceed through similar genetic pathways had been a difficult

**Table 3.1: Genetic perturbations in mice that result in histological alterations found in FH or result in frank hydrocephalus.**

| Affected structure | Gene | Functional effects | References |
|---|---|---|---|
| **Cilia** | Mdnah5 | A component of the axonemal structure; null mice lack cilia beating and develop hydrocephalus | (35) |
| | Spag6 | A component of the axonemal structure; null mice lack cilia beating and develop hydrocephalus | (36) |
| | Polaris (Ift88) | Concentrated near apical membrane of basal bodies and is involved in left-right axis patterning and tissue planar polarity; mutations cause immotile cilia/sperm and hydrocephalus (among other pathologies) | (37) |
| | Stumpy | Required for axonemal extension; null mice have deformed or absent cilia, impaired CSF, and hydrocephalus | (38) |
| | Celsr 2 and 3 | Mammalian ortholog of drosophila *Flamingo* (also known as *Starry Night*), which are among the planar cell polarity core proteins; Celsr 2 and 3 double null mice have defects in ciliogenesis and develop hydrocephalus | (39) |
| **Ependyma** | Hyh (Napa) | Napa gene in alpha SNAP and SNARE-mediated vesicle fusion; natural mutation results in ependymal denudation and subsequent hydrocephalus | (40-47) |
| | RFX3 | Transcription factor that regulates ciliated ependymal cell differentiation; gene deletion results in hydrocephalus | (48) |
| **Cell adhesion / polarity / intracellular signaling** | N-cadherin | A cell adhesion molecule highly expressed at the apical ventricular surface and embryonic cerebral cortex; conditional null deletion or neutralizing antibody *in vivo* caused histological features of hydrocephalus | (49-52) |
| | Dlg5 | Functions in plasma membrane delivery of cadherin via t-SNARE complex; null mice have fully penetrant hydrocephalus | (53) |
| | Lgl1 | Thought to function in maintaining cell polarity; null mice are unable to asymmetrically localize Numb and develop hydrocephalus | (54) |
| | PTEN | Conditional deletion in mice in the midbrain result in enlargement of midbrain and hydrocephalus | (55) |
| | β-catenin | Conditional deletion in mice in the midbrain result in enlargement of midbrain and hydrocephalus | (55) |

**Table 3.1: Genetic perturbations in mice that result in histological alterations found in FH or result in frank hydrocephalus, Continued.**

| Affected structure | Gene | Functional effects | References |
|---|---|---|---|
| **G-protein coupled receptors** | PAC1 | Human GPCR; transgenic expression in mouse brain leads to enlarged lateral ventricle, ependymal cilia disruption, and hydrocephalus | (56) |
| | $G\alpha_i$ RASSL | $G\alpha i$-coupled GPCR is activated by a synthetic ligand; when transgenically expressed by astrocytes *in vivo*, causes ependymal denudation and hydrocephalus | (57) |
| | $G\alpha_{2i}$ | $G\alpha$ subunit with restricted expression in the VZ, ependyma, and cilia; *in vivo* oligonucleotide knockdown in mice results in immotile cilia and ventricular dilatation/hydrocephalus | (58) |

question to answer. A hemorrhage animal model using injections TGF-β produced hydrocephalus with incomplete penetrance and variable severity (21) and moderate histological alteration, though injection of blood and blood derivatives seem to increase the phenotype, both grossly and histologically (59). Correlates such as neuroprogenitor disruption, heterotopia formation, and ependymal loss were reported in the latter model (59). LPA is the first known hemorrhage-derived factor that can produce FH with all of the seemingly unrelated histological changes observed clinically and in genetic animal models, including ventricular dilation, NPC disruption and denudation, neurorosette formation, mitotic displacement, 3rd ventricular occlusion, loss of cilia, and heterotopia formation. Observed differences in the severity and timing of these disturbances likely result from spatiotemporal differences and degree of LPA exposure. Overall, however, these results help link a diverse array of genetic disturbances to fetal intracranial hemorrhage that result in FH and create a broad working scaffold for future studies.

**Conclusion**

The work presented here demonstrates a causative relationship between hemorrhage, exposure to blood derivatives, and the initiation of FH *in vivo* through the overactivation of $LPA_1$. Prevention of FH by a $LPA_1$ antagonist provides proof-of-concept towards potential treatment of at least some forms of this disorder. The ultimate goal of these studies is to enable the future development of effective therapies of FH through the understanding of the biology of this disorder *in vivo*.

**References**


1. Persson, E.K., Hagberg, G., and Uvebrant, P. (2005). Hydrocephalus prevalence and outcome in a population-based cohort of children born in 1989-1998. Acta Paediatr *94*, 726-732.

2. Persson, E.K., Anderson, S., Wiklund, L.M., and Uvebrant, P. (2007). Hydrocephalus in children born in 1999-2002: epidemiology, outcome and ophthalmological findings. Childs Nerv Syst *23*, 1111-1118.

3. Volpe, J.J. (2008). Neurology of the newborn, 5th Edition, (Philadelphia: Saunders/Elsevier).

4. Humphreys, P., Muzumdar, D.P., Sly, L.E., and Michaud, J. (2007). Focal cerebral mantle disruption in fetal hydrocephalus. Pediatr Neurol *36*, 236-243.

5. Moritake, K., Nagai, H., Miyazaki, T., Nagasako, N., Yamasaki, M., and Tamakoshi, A. (2007). Nationwide survey of the etiology and associated conditions of prenatally and postnatally diagnosed congenital hydrocephalus in Japan. Neurologia medico-chirurgica *47*, 448-452; discussion 452.

6. Reece, E.A., and Goldstein, I. (1997). Early prenatal diagnosis of hydrocephalus. Am J Perinatol *14*, 69-73.

7. Aubry, M.C., Aubry, J.P., and Dommergues, M. (2003). Sonographic prenatal diagnosis of central nervous system abnormalities. Childs Nerv Syst *19*, 391-402.

8. Goldstein, I., Copel, J.A., and Makhoul, I.R. (2005). Mild cerebral ventriculomegaly in fetuses: characteristics and outcome. Fetal Diagn Ther *20*, 281-284.

9. Guillerman, R.P. (2010). Infant craniospinal ultrasonography: beyond hemorrhage and hydrocephalus. Semin Ultrasound CT MR *31*, 71-85.

10. Glenn, O.A., and Coakley, F.V. (2009). MRI of the fetal central nervous system and body. Clin Perinatol *36*, 273-300, viii.

11. Volpe, J.J., Pasternak, J.F., and Allan, W.C. (1977). Ventricular dilation preceding rapid head growth following neonatal intracranial hemorrhage. Am J Dis Child *131*, 1212-1215.

12. Horbar, J.D., Walters, C.L., Philip, A.G., and Lucey, J.F. (1980). Ultrasound detection of changing ventricular size in posthemorrhagic hydrocephalus. Pediatrics *66*, 674-678.

13. Benacerraf, B.R., and Birnholz, J.C. (1987). The diagnosis of fetal hydrocephalus prior to 22 weeks. J Clin Ultrasound *15*, 531-536.

14. de Wit, O.A., den Dunnen, W.F., Sollie, K.M., Munoz, R.I., Meiners, L.C., Brouwer, O.F., Rodriguez, E.M., and Sival, D.A. (2008). Pathogenesis of cerebral malformations in human fetuses with meningomyelocele. Cerebrospinal Fluid Res *5*, 4.

15. Dominguez-Pinos, M.D., Paez, P., Jimenez, A.J., Weil, B., Arraez, M.A., Perez-Figares, J.M., and Rodriguez, E.M. (2005). Ependymal denudation and alterations of the subventricular zone occur in human fetuses with a moderate communicating hydrocephalus. J Neuropathol Exp Neurol *64*, 595-604.

16. Krueger, R.C., Jr., Wu, H., Zandian, M., Danielpour, M., Kabos, P., Yu, J.S., and Sun, Y.E. (2006). Neural progenitors populate the cerebrospinal fluid of preterm patients with hydrocephalus. J Pediatr *148*, 337-340.

17. Senat, M.V., Bernard, J.P., Delezoide, A., Saugier-Veber, P., Hillion, Y., Roume, J., and Ville, Y. (2001). Prenatal diagnosis of hydrocephalus-stenosis of the aqueduct of Sylvius by ultrasound in the first trimester of pregnancy. Report of two cases. Prenat Diagn *21*, 1129-1132.

18. Whitelaw, A. (2001). Intraventricular haemorrhage and posthaemorrhagic hydrocephalus: pathogenesis, prevention and future interventions. Semin Neonatol *6*, 135-146.

19. Tada, T., Kanaji, M., and Kobayashi, S. (1994). Induction of communicating hydrocephalus in mice by intrathecal injection of human recombinant transforming growth factor-beta 1. J Neuroimmunol *50*, 153-158.

20. Kanaji, M., Tada, T., and Kobayashi, S. (1997). A murine model of communicating hydrocephalus: Role of TGF-beta1. J Clin Neurosci *4*, 51-56.

21. Cherian, S., Thoresen, M., Silver, I.A., Whitelaw, A., and Love, S. (2004). Transforming growth factor-betas in a rat model of neonatal posthaemorrhagic hydrocephalus. Neuropathol Appl Neurobiol *30*, 585-600.

22. Kitazawa, K., and Tada, T. (1994). Elevation of transforming growth factor-beta 1 level in cerebrospinal fluid of patients with communicating hydrocephalus after subarachnoid hemorrhage. Stroke *25*, 1400-1404.

23. Heep, A., Stoffel-Wagner, B., Bartmann, P., Benseler, S., Schaller, C., Groneck, P., Obladen, M., and Felderhoff-Mueser, U. (2004). Vascular endothelial growth factor and transforming growth factor-beta1 are highly expressed in the cerebrospinal fluid of premature infants with posthemorrhagic hydrocephalus. Pediatr Res *56*, 768-774.

24. Jeon, E.S., Heo, S.C., Lee, I.H., Choi, Y.J., Park, J.H., Choi, K.U., Park do, Y., Suh, D.S., Yoon, M.S., and Kim, J.H. (2010). Ovarian cancer-derived lysophosphatidic acid stimulates secretion of VEGF and stromal cell-derived factor-1 alpha from human mesenchymal stem cells. Exp Mol Med *42*, 280-293.

25. Ptaszynska, M.M., Pendrak, M.L., Stracke, M.L., and Roberts, D.D. (2010). Autotaxin signaling via lysophosphatidic acid receptors contributes to vascular endothelial growth factor-induced endothelial cell migration. Mol Cancer Res *8*, 309-321.

26. Xu, M.Y., Porte, J., Knox, A.J., Weinreb, P.H., Maher, T.M., Violette, S.M., McAnulty, R.J., Sheppard, D., and Jenkins, G. (2009). Lysophosphatidic acid induces alphavbeta6 integrin-mediated TGF-beta activation via the LPA2 receptor and the small G protein G alpha(q). Am J Pathol *174*, 1264-1279.

27. Fukumizu, M., Takashima, S., and Becker, L.E. (1995). Neonatal posthemorrhagic hydrocephalus: neuropathologic and immunohistochemical studies. Pediatr Neurol *13*, 230-234.

28. Lategan, B., Chodirker, B.N., and Del Bigio, M.R. (2010). Fetal hydrocephalus caused by cryptic intraventricular hemorrhage. Brain Pathol *20*, 391-398.

29. Whitelaw, A. (2001). Intraventricular streptokinase after intraventricular hemorrhage in newborn infants. Cochrane Database Syst Rev, CD000498.

30. Shooman, D., Portess, H., and Sparrow, O. (2009). A review of the current treatment methods for posthaemorrhagic hydrocephalus of infants. Cerebrospinal Fluid Res *6*, 1.

31. Poca, M.A., and Sahuquillo, J. (2005). Short-term medical management of hydrocephalus. Expert Opin Pharmacother *6*, 1525-1538.

32. Whitelaw, A., Evans, D., Carter, M., Thoresen, M., Wroblewska, J., Mandera, M., Swietlinski, J., Simpson, J., Hajivassiliou, C., Hunt, L.P., et al. (2007). Randomized clinical trial of prevention of hydrocephalus after intraventricular hemorrhage in preterm infants: brain-washing versus tapping fluid. Pediatrics *119*, e1071-1078.

33. Aquilina, K., Hobbs, C., Tucker, A., Whitelaw, A., and Thoresen, M. (2008). Do drugs that block transforming growth factor beta reduce posthaemorrhagic ventricular dilatation in a neonatal rat model? Acta Paediatr *97*, 1181-1186.

34. Zhang, J., Williams, M.A., and Rigamonti, D. (2006). Genetics of human hydrocephalus. Journal of neurology *253*, 1255-1266.

35. Ibanez-Tallon, I., Pagenstecher, A., Fliegauf, M., Olbrich, H., Kispert, A., Ketelsen, U.P., North, A., Heintz, N., and Omran, H. (2004). Dysfunction of axonemal dynein heavy chain Mdnah5 inhibits ependymal flow and reveals a novel mechanism for hydrocephalus formation. Hum Mol Genet *13*, 2133-2141.

36. Sapiro, R., Kostetskii, I., Olds-Clarke, P., Gerton, G.L., Radice, G.L., and Strauss, I.J. (2002). Male infertility, impaired sperm motility, and hydrocephalus in mice deficient in sperm-associated antigen 6. Mol Cell Biol *22*, 6298-6305.

37. Taulman, P.D., Haycraft, C.J., Balkovetz, D.F., and Yoder, B.K. (2001). Polaris, a protein involved in left-right axis patterning, localizes to basal bodies and cilia. Mol Biol Cell *12*, 589-599.

38. Town, T., Breunig, J.J., Sarkisian, M.R., Spilianakis, C., Ayoub, A.E., Liu, X., Ferrandino, A.F., Gallagher, A.R., Li, M.O., Rakic, P., et al. (2008). The stumpy gene is required for mammalian ciliogenesis. Proc Natl Acad Sci U S A *105*, 2853-2858.

39. Tissir, F., Qu, Y., Montcouquiol, M., Zhou, L., Komatsu, K., Shi, D., Fujimori, T., Labeau, J., Tyteca, D., Courtoy, P., et al. (2010). Lack of cadherins Celsr2 and Celsr3 impairs ependymal ciliogenesis, leading to fatal hydrocephalus. Nat Neurosci *13*, 700-707.

40. Bronson, R.T., and Lane, P.W. (1990). Hydrocephalus with hop gait (hyh): a new mutation on chromosome 7 in the mouse. Brain Res Dev Brain Res *54*, 131-136.

41. Perez-Figares, J.M., Jimenez, A.J., Perez-Martin, M., Fernandez-Llebrez, P., Cifuentes, M., Riera, P., Rodriguez, S., and Rodriguez, E.M. (1998). Spontaneous congenital hydrocephalus in the mutant mouse hyh. Changes in the ventricular system and the subcommissural organ. J Neuropathol Exp Neurol *57*, 188-202.

42. Jimenez, A.J., Tome, M., Paez, P., Wagner, C., Rodriguez, S., Fernandez-Llebrez, P., Rodriguez, E.M., and Perez-Figares, J.M. (2001). A programmed ependymal denudation precedes congenital hydrocephalus in the hyh mutant mouse. J Neuropathol Exp Neurol *60*, 1105-1119.

43. Perez-Figares, J.M., Jimenez, A.J., and Rodriguez, E.M. (2001). Subcommissural organ, cerebrospinal fluid circulation, and hydrocephalus. Microsc Res Tech *52*, 591-607.

44. Wagner, C., Batiz, L.F., Rodriguez, S., Jimenez, A.J., Paez, P., Tome, M., Perez-Figares, J.M., and Rodriguez, E.M. (2003). Cellular mechanisms involved in the stenosis and obliteration of the cerebral aqueduct of hyh mutant mice developing congenital hydrocephalus. J Neuropathol Exp Neurol *62*, 1019-1040.

45. Batiz, L.F., Paez, P., Jimenez, A.J., Rodriguez, S., Wagner, C., Perez-Figares, J.M., and Rodriguez, E.M. (2006). Heterogeneous expression of hydrocephalic phenotype in the hyh mice carrying a point mutation in alpha-SNAP. Neurobiol Dis *23*, 152-168.

46. Paez, P., Batiz, L.F., Roales-Bujan, R., Rodriguez-Perez, L.M., Rodriguez, S., Jimenez, A.J., Rodriguez, E.M., and Perez-Figares, J.M. (2007). Patterned neuropathologic events occurring in hyh congenital hydrocephalic mutant mice. J Neuropathol Exp Neurol *66*, 1082-1092.

47. Chae, T.H., Kim, S., Marz, K.E., Hanson, P.I., and Walsh, C.A. (2004). The hyh mutation uncovers roles for alpha Snap in apical protein localization and control of neural cell fate. Nat Genet *36*, 264-270.

48. Baas, D., Meiniel, A., Benadiba, C., Bonnafe, E., Meiniel, O., Reith, W., and Durand, B. (2006). A deficiency in RFX3 causes hydrocephalus associated with abnormal differentiation of ependymal cells. Eur J Neurosci *24*, 1020-1030.

49. Bronner-Fraser, M., Wolf, J.J., and Murray, B.A. (1992). Effects of antibodies against N-cadherin and N-CAM on the cranial neural crest and neural tube. Dev Biol *153*, 291-301.

50. Radice, G.L., Rayburn, H., Matsunami, H., Knudsen, K.A., Takeichi, M., and Hynes, R.O. (1997). Developmental defects in mouse embryos lacking N-cadherin. Dev Biol *181*, 64-78.

51. Ganzler-Odenthal, S.I., and Redies, C. (1998). Blocking N-cadherin function disrupts the epithelial structure of differentiating neural tissue in the embryonic chicken brain. J Neurosci *18*, 5415-5425.

52. Kadowaki, M., Nakamura, S., Machon, O., Krauss, S., Radice, G.L., and Takeichi, M. (2007). N-cadherin mediates cortical organization in the mouse brain. Dev Biol *304*, 22-33.

53. Nechiporuk, T., Fernandez, T.E., and Vasioukhin, V. (2007). Failure of epithelial tube maintenance causes hydrocephalus and renal cysts in Dlg5-/- mice. Developmental cell *13*, 338-350.

54. Klezovitch, O., Fernandez, T.E., Tapscott, S.J., and Vasioukhin, V. (2004). Loss of cell polarity causes severe brain dysplasia in Lgl1 knockout mice. Genes & development *18*, 559-571.

55. Ohtoshi, A. (2008). Hydrocephalus caused by conditional ablation of the Pten and beta-catenin gene. Cerebrospinal Fluid Res *5*, 16.

56. Lang, B., Song, B., Davidson, W., MacKenzie, A., Smith, N., McCaig, C.D., Harmar, A.J., and Shen, S. (2006). Expression of the human PAC1 receptor leads to dose-dependent hydrocephalus-related abnormalities in mice. J Clin Invest *116*, 1924-1934.

57. Sweger, E.J., Casper, K.B., Scearce-Levie, K., Conklin, B.R., and McCarthy, K.D. (2007). Development of hydrocephalus in mice expressing the G(i)-coupled GPCR Ro1 RASSL receptor in astrocytes. J Neurosci *27*, 2309-2317.

58. Monkkonen, K.S., Hakumaki, J.M., Hirst, R.A., Miettinen, R.A., O'Callaghan, C., Mannisto, P.T., and Laitinen, J.T. (2007). Intracerebroventricular antisense knockdown of G alpha i2 results in ciliary stasis and ventricular dilatation in the rat. BMC Neurosci *8*, 26.

59. Cherian, S.S., Love, S., Silver, I.A., Porter, H.J., Whitelaw, A.G., and Thoresen, M. (2003). Posthemorrhagic ventricular dilation in the neonate: development and characterization of a rat model. J Neuropathol Exp Neurol *62*, 292-303.

# APPENDIX A

## CONSTITUTIONAL ANEUPLOIDY IN THE NORMAL HUMAN BRAIN

Journal of Neuroscience, **25**(9): 2176-80 (2005).

**A word about aneuploidy**

Aneuploidy is defined as the gain or loss of chromosomes to produce a numerical deviation from multiples of the haploid chromosome complement (1). Well-known examples include the systemic gain of an extra copy of chromosome 21 that produces Down's syndrome (also known as trisomy 21) (2) or the abnormal, varied chromosome complements in cancers (3-5). However, recent evidence has suggested that another form of aneuploidy also exists, particularly in the brain (6). Nondiseased murine brains contain post-mitotic cells which have sporadic gains or losses of single copies of chromosomes, which form a constitutive mosaic of aneuploid, functional cells within the circuitry and architecture of the brain (7, 8). Moreover, dividing neuroprogenitor cells also exhibit a wide variety of aneuploidy, as determined by karyotype analysis (9, 10). Such aneuploidy likely has consequences that may range from the normal production of genetic diversity among individuals to relevance in neurological and neuropsychiatric disorders (11).

Therefore, I and others undertook studies to examine the chromosome complement in murine and human brains specifically in the cerebral cortex and cerebellum, areas that, in part, mediate cognition and motor activity. Using a variety of detailed and high-throughput independent methods, including fluorescence in situ hybridization (FISH), spectral karyotyping (SK), and fluorescence-activated cell sorting (FACS), we find that aneuploidy variations exist across cell type, brain region, and species (12-14). Other groups have validated and complemented these studies in

both scope and direction (15-18). This body of work provides a continuing chain of observations that shed light on constitutional aneuploidy as a novel biological phenomenon.

2176 • The Journal of Neuroscience, March 2, 2005 • 25(9):2176–2180

Brief Communication

# Constitutional Aneuploidy in the Normal Human Brain

**Stevens K. Rehen, Yun C. Yung, Matthew P. McCreight, Dhruv Kaushal, Amy H. Yang, Beatriz S. V. Almeida, Marcy A. Kingsbury, Kátia M. S. Cabral, Michael J. McConnell, Brigitte Anliker, Marisa Fontanoz, and Jerold Chun**
Helen L. Dorris Child and Adolescent Neuropsychiatric Disorder Institute, The Scripps Research Institute, La Jolla, California 92037

**The mouse brain contains genetically distinct cells that differ with respect to chromosome number manifested as aneuploidy (Rehen et al., 2001); however, the relevance to humans is not known. Here, using double-label fluorescence *in situ* hybridization for the autosome chromosome 21 (chromosome 21 point probes combined with chromosome 21 "paint" probes), along with immunocytochemistry and cell sorting, we present evidence for chromosome gain and loss in the human brain. Chromosome 21 aneuploid cells constitute ~4% of the estimated one trillion cells in the human brain and include non-neuronal cells and postmitotic neurons identified by the neuron-specific nuclear protein marker. In comparison, human interphase lymphocytes present chromosome 21 aneuploidy rates of 0.6%. Together, these data demonstrate that human brain cells (both neurons and non-neuronal cells) can be aneuploid and that the resulting genetic mosaicism is a normal feature of the human CNS.**

*Key words:* **cerebral cortex; chromosome variation; mosaicism; histochemistry; hybridization; trisomy 21**

## Introduction

Aneuploidy is defined as the loss and/or gain of chromosomes to produce a numerical deviation from multiples of the haploid chromosomal complement (King and Stansfield, 1990). It exists in cells of the developing and adult mouse brain (Rehen et al., 2001). Aneuploidy in these cells arises at least in part via chromosome missegregation mechanisms during mitosis (Yang et al., 2003). The existence of aneuploid cells in normal humans is unknown; however, human genetic diseases that produce systemic aneuploidy can affect morphogenesis (Kalousek, 2000) and correlate with the severity of several neurogenetic disorders such as Down's syndrome (Modi et al., 2003), Turner syndrome (Nazarenko et al., 1999), and mosaic variegated aneuploidy syndrome (MVA) (Bitoun et al., 1994). Toward determining the presence of constitutional aneuploidy in the human brain, we report here an analysis of the frequency of chromosome 21 gain and loss among neurons and non-neuronal cells isolated from the cerebral cortex and hippocampus of normal individuals ranging from 2 to 86 years of age. Chromosome 21 was chosen for examination because of the availability of trisomy 21 cells (Bhattacharyya and Svendsen, 2003) that could serve as a positive control for fluorescence *in situ* hybridization (FISH).

Received Nov. 5, 2004; revised Dec. 21, 2004; accepted Jan. 13, 2005.

This work was supported by the National Institute of Mental Health (J.C.), postdoctoral funding from the Pew Foundation (S.K.R.), predoctoral funding from the Pharmaceutical Research and Manufacturers of America foundation (D.K.), the National Institute of General Medical Sciences (M.J.M., A.H.Y.), and postdoctoral funding from the Swiss National Science Foundation (B.A.). We thank Grace Kennedy for technical help, Cheryl Silao and Alan Saluk from the Scripps Flow Cytometry Core Facility for cell-sorting assistance, and Drs. Anita Bhattacharyya and Clive Svendsen for providing trisomy 21 cells. We declare that we have no competing financial interests.

S.K.R. and Y.C.Y. contributed equally to this work.

Correspondence should be addressed to Dr. Jerold Chun, Department of Molecular Biology, The Scripps Research Institute, 10550 Torrey Pines Road, Institute for Childhood and Neglected Diseases-118, La Jolla, CA 92037. E-mail: jchun@scripps.edu.

DOI:10.1523/JNEUROSCI.4560-04.2005

 0270-6474/05/252176-05$15.00/0

## Materials and Methods

*Tissue collection.* Fresh-frozen samples of postmortem brain tissue from normal cerebral cortices and hippocampi were obtained from the Harvard Brain Bank (United States Public Health Service MH/NS 31862) and from the University of Miami/University of Maryland Brain and Tissue Bank (National Institute of Child Health and Human Development NO1-HD-8-3284). Samples were thawed before mincing and incubated in $Ca^{2+}/Mg^{2+}$-free PBS supplemented with 2 mM EGTA for 30–60 min at 4°C. After incubation, samples were triturated with a series of 1 ml pipette tips of decreasing diameter, filtered with a 40 $\mu$m cell filter (BD Biosciences, Bedford, MA), and centrifuged at 500 × *g* for 5 min. After centrifugation, the supernatant was discarded, and the cell pellet was resuspended in a small volume of PBS. Nuclei were isolated by detergent lysis as described previously and fixed briefly for 15 min in ice-cold 1% paraformaldehyde (Ausubel et al., 1994; Rehen et al., 2001). As a control, metaphase spreads and nuclei from human lymphocytes isolated from a normal 33-year-old male were prepared and analyzed according to standard techniques (Barch et al., 1997). To demonstrate the specificity of the FISH probes with regard to detecting numerical abnormalities of chromosome 21, neural progenitor cells derived from Down's syndrome fetuses (Svendsen et al., 1998; Bhattacharyya and Svendsen, 2003), kindly provided by Dr. Clive N. Svendsen (Waisman Center, University of Wisconsin, Madison, WI), were also analyzed.

*FISH probes.* FISH "paint" probes against the whole q arm of chromosome 21 and a point probe against a region on the q arm of 21 (21q22.13–q22.2) were obtained from Vysis (Downer's Grove, IL). Fluorescence images were captured using a Zeiss Axioskop microscope and Axiocam CCD camera (Carl Zeiss, Thornwood, NY).

*Cell sorting and immunocytochemistry.* Isolated nuclei from brain samples were blocked for 30 min in PBS and 2.5% BSA, washed, and then incubated for 1 h at room temperature with primary mouse antibody against neuron-specific nuclear protein (NeuN) (1:100; monoclonal antibody 377; Chemicon, Temecula, CA), a known nuclear antigen in neurons (Mullen et al., 1992). Subsequently, NeuN-labeled cells were detected using an Alexa Fluor 488-labeled donkey anti-mouse secondary antibody (1:500; Molecular Probes, Eugene, OR). Nuclei were sorted using the Becton Dickinson (Mountain View, CA) FACSAria system, and the purity of sorted nuclei was confirmed by direct microscope observa-

tion. FISH was performed as described previously (Rehen et al., 2001; Kaushal et al., 2003).

*Data analysis.* Between 500 and 1500 cells per human brain sample, as compared with lymphocytes, were hybridized using dual-color FISH, counted by two blinded individuals, and analyzed using Microsoft (Seattle, WA) Excel. To assess the specificity of the FISH probes with regard to detecting numerical abnormalities of chromosome 21, 150 neural progenitor cells derived from Down's syndrome fetuses (Svendsen et al., 1998; Bhattacharyya and Svendsen, 2003) were also counted.

## Results

### Chromosome 21 aneuploidy is observed among cells isolated from the normal human brain

FISH was used to examine chromosome number in individual cells in interphase (i.e., cells without condensed chromosomes), as reported previously for brain tissue sections of mouse (Rehen et al., 2001) and diseased human brain (Yang et al., 2001). However, the use of brain sections has the disadvantage of producing partial nuclei or closely apposed nuclei that can result in chromosome loss or gain artifacts, respectively (Rehen et al., 2001; Yang et al., 2001). To eliminate sectioning artifacts, individual brain cell nuclei were isolated for FISH. This population of nuclei consisted of both neural cells (i.e., neurons and glia) and non-neural cells (e.g., endothelial cells and microglia). To identify neuronal nuclei, immunolabeling for NeuN was combined with FISH.

To increase the specificity of chromosome 21 FISH, two distinct kinds of nucleotide probes using different colors were used whereby isolated nuclei were hybridized with a chromosome 21 paint (a mixture of probes specifically against the whole q arm of chromosome 21) and double-labeled with a different-colored probe for 21q22.13–q22.2. Only double-labeled chromosomes were quantified, to reduce the possibility of false-positive and false-negative hybridization signals (Fig. 1*A*,*C*).

Control FISH counts on ~1500 human lymphocyte interphase nuclei (Fig. 1*B*) identified rates of aneuploidy of 0.6% (Table 1), consistent with previously published data in humans (Leach et al., 2004). In addition, FISH specificity for detecting chromosome 21 gain in neural cells derived from Down's syndrome fetuses (Fig. 1*C*,*D*, Table 1) validated our enumeration criteria for examining chromosome 21 aneuploidy in the CNS. These control data were analyzed in parallel with ~9000 interphase nuclei isolated from the cerebral cortex and hippocampus of six normal individuals, which were hybridized and counted using the same protocol applied to control cells (i.e., human lymphocytes and Down's syndrome neural cells). On average, ~93% of the cells isolated from the brains of individuals ranging from 2 to 86 years of age were disomic for chromosome 21, whereas 4% of these cells had gained or lost one copy of chromosome 21 (Table 1). Monosomic, trisomic, and even tetrasomic chromosome 21 cells were present in every brain examined (Fig. 1*E*–*H*). Cells missing both copies or harboring more than four copies of chromosome 21 were not observed in this population. It is noteworthy that the mean copy numbers of chromosome 21 in brain cells and lymphocytes were 2.05 and 2.00, respectively (Table 1), corresponding to a ploidy difference that is likely undetectable by classical methods (Podlisny et al., 1987). This extent of aneuploidy was also observed in preliminary analyses using sex chromosomes and two other autosomes (data not shown). Together, these data demonstrate that millions of aneuploid cells, defined by even a single chromosome, are present in the human brain, regardless of age and in the absence of any documented neurological condition or preexisting disease.

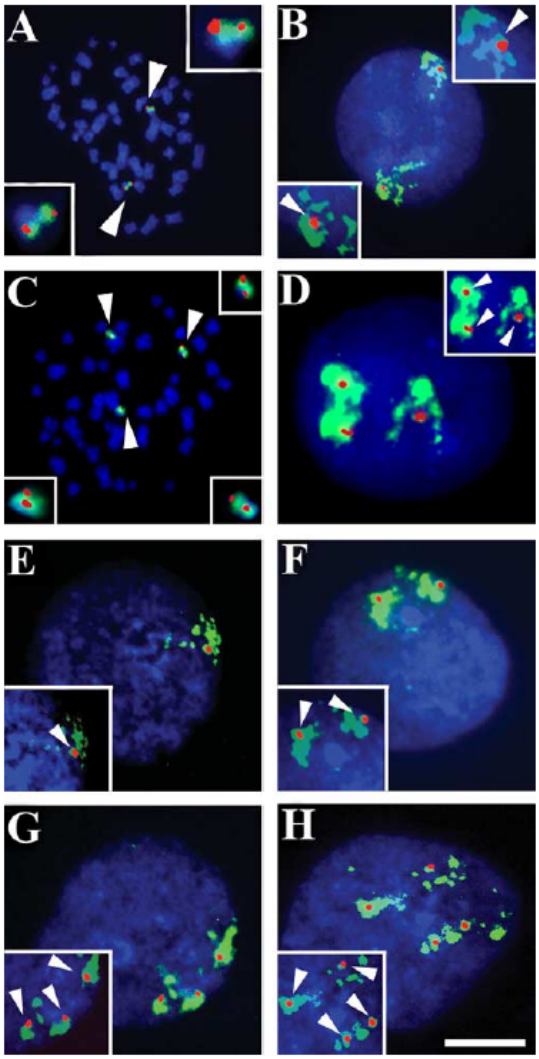


**Figure 1.** Chromosome 21 gain and loss is observed in cells isolated from the normal human brain. Human lymphocyte labeling demonstrates the specificity of the paint and point probes in metaphase spreads (***A***) and interphase nuclei (***B***). Neural progenitor cells from a Down's syndrome fetus have three copies of chromosome 21, as seen in a metaphase chromosome spread (***C***) and in an interphase nucleus (***D***), demonstrating the sensitivity of the FISH probes with regard to detecting numerical abnormalities of chromosome 21. ***E–H***, Nuclei isolated from the brains of different patients containing one (***E***), two (***F***), three (***G***), or four (***H***) copies of chromosome 21. Blue indicates 4′,6-diamidino-2-phenylindole, whole-chromosome paint is shown in green, and the chromosome 21 point probe is shown in red. There is complete overlap between the paint and the point probe, as seen at higher magnification in the insets. Arrowheads indicate the numbers of chromosome 21 per cell. Scale bar, 5 μm.

### Both postmitotic neurons and non-neuronal cells are aneuploid in the human brain

Glial cells, which represent the majority of brain cells (Pakkenberg et al., 2003), are able to proliferate in some pathological circumstances in the adult brain, whereas postmitotic neurons cannot reenter the cell cycle to proliferate. To determine whether chromosome 21 aneuploidy was present in both postmitotic neu-

**Table 1. Percentages of whole chromosome 21 gain and loss in the brain vary within and among individuals**

| | | | | Aneuploid karyotype | | | |
|---|---|---|---|---|---|---|---|
| Age (years) | Cell type | % Disomy | % Tetrasomy | % Monosomy | % Trisomy | % Aneuploidy | Mean chromosome number |
| 2 | Frontal cortex cells | 94.3 | 2.5 | 1.7 | 1.5 | 3.2 | 2.05 |
| 15 | Occipital cortex cells | 93.8 | 2.4 | 2.2 | 1.6 | 3.8 | 2.04 |
| 35 | Frontal cortex cells | 93.9 | 2.4 | 1.8 | 1.8 | 3.6 | 2.05 |
| 48 | Frontal cortex cells | 93.8 | 2.6 | 1.6 | 2.0 | 3.6 | 2.06 |
| 77 | Hippocampal cells | 91.5 | 3.8 | 2.6 | 2.3 | 4.8 | 2.07 |
| 86 | Hippocampal cells | 92.4 | 2.4 | 3.0 | 2.2 | 5.2 | 2.04 |
| Average | Brain cells | 93.3 | 2.7 | 2.1 | 1.9 | 4.0 | 2.05 |
| 33 | Lymphocytes | 99.8 | 0.2 | 0.4 | 0.2 | 0.6 | 2.00 |
| <0 | Down's syndrome neural cells | 7.1 | 3.6 | 0 | 89.3 | 89.3 | 2.96 |

Lymphocytes and Down's syndrome cells were used to validate the counting criteria using chromosome 21 FISH probes.

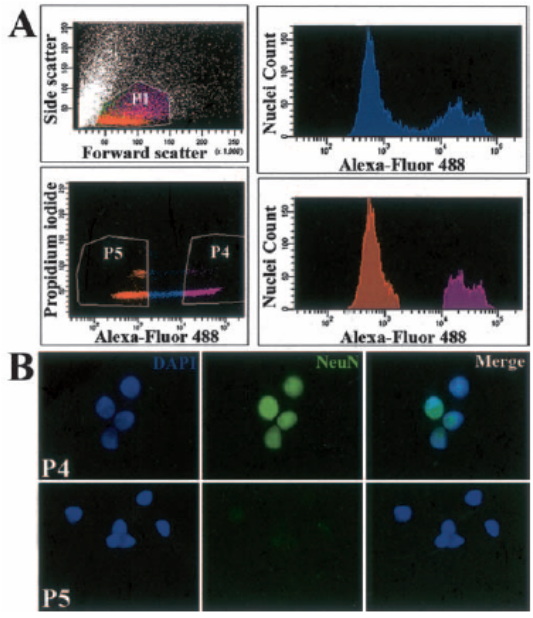


**Figure 2.** NeuN immunolabeling and cell sorting. ***A***, Isolated normal human brain nuclei populations (P1) were gated based on forward scatter and side scatter and gated into NeuN+ (P4) and NeuN− (P5) sort populations based on Alexa Fluor 488 signal. The NeuN+ population is generally composed of larger nuclei than NeuN− nuclei based on forward scatter, although there is a significant size overlap. ***B***, A representative preparation of sorted nuclei demonstrating >99.5% purity of separation between NeuN+ (P4) and NeuN− (P5) populations.

rons and non-neuronal cells in the normal human brain, nuclei isolated from one infant and two adult individuals were incubated with an antibody against NeuN, a known nuclear antigen specific for neurons (Mullen et al., 1992). NeuN-labeled nuclei were then sorted by fluorescence-activated cell sorting (FACS) (Fig. 2*A*) to produce >99.5% enrichment of NeuN-positive nuclei (Fig. 2*B*). These purified populations were then examined by chromosome 21 FISH. From analyses of FACS-purified nuclei, both neurons and non-neuronal cells accounted for the aneuploid population present in the human brain (Table 2), indicating that the mechanisms able to generate chromosome gain and loss may be similar for both cell types (Yang et al., 2003). In summary, these results demonstrate that neurons as well as non-neuronal cells constitute the aneuploid population present in the human brain.

## Discussion

Based on a strategy that combines nuclear isolation, multiprobe FISH, immunocytochemistry, and FACS, the rates of chromosome 21 gain and loss were determined in cells isolated from the brains of normal human individuals. Significant levels of gain and loss were detected, demonstrating that the normal human nervous system contains aneuploid cells. Furthermore, the observation of chromosome 21 gain and loss in NeuN-positive cells supports the view that aneuploid postmitotic neurons may participate in the cortical circuitry of the human brain (Rehen et al., 2001; Kaushal et al., 2003; Yang et al., 2003).

Previous studies of normal murine embryonic brain demonstrated the existence of neural aneuploid cells (Rehen et al., 2001; Kaushal et al., 2003) generated at least in part by chromosomal missegregation mechanisms during mitosis (Yang et al., 2003). The observation of both monosomy and trisomy for chromosome 21 suggests that nondisjunction may account for the generation of aneuploid neurons in the human brain as well.

In view of the existence of aneuploidy in the mouse and human brain, the role or roles of this genome-altering change remain to be determined. It is notable that the 4% rate of aneuploidy described here is based only on analysis of a single autosome, and in theory, if the loss and gain of whole chromosomes are similar and unbiased for other chromosomes, the overall percentage of aneuploid neurons and aneuploidy in the human brain will be much higher. One hypothetical function of aneuploidy is as a mechanism for generating cellular diversity through chromosomal variation. This is consistent in concept with a recent report describing large-scale copy-number polymorphisms among individuals as a new factor in understanding genomic diversity and disease susceptibilities (Sebat et al., 2004). Our results demonstrate that chromosome copy-number differences produced by aneuploidy can also vary within neuronal populations from single individuals and among individuals, suggesting another layer of systemic genetic complexity. It may also provide a link between aneuploidy and human brain diseases (Heston and Mastri, 1977; Schweber, 1985; Potter, 1991; Yurov et al., 2001), including cases in which certain non-neuronal aneuploid cells in the brains of normal patients may, under appropriate conditions, contribute to brain tumorigenesis (Lengauer et al., 1998).

Constitutive aneuploidy was found at all ages, from infants (age 2, 3.2% aneuploidy) to young adults (age 15, 3.8% aneuploidy), through middle age (ages 35 and 48, 3.6% aneuploidy), and in geriatric samples (ages 77 and 86, 4.8% and 5.2% aneuploidy, respectively). These data do not rigorously address potential quantitative changes that might occur with age, which would require much larger sample sizes, and do not address the possibility of neuroanatomical differences in aneuploidy rates. By vir-

**Table 2. Percentages of whole chromosome 21 gain and loss in neurons and non-neuronal cells isolated from the brains of three different individuals and sorted by FACS**

| | | | | Aneuploid karyotype | | | |
|---|---|---|---|---|---|---|---|
| Age (years) | Cell type | % Disomy | % Tetrasomy | % Monosomy | % Trisomy | % Aneuploidy | Mean chromosome number |
| 2 | Neurons | 95.4 | 1.2 | 2.0 | 1.4 | 3.4 | 2.02 |
| 2 | Non-neuronal cells | 95.8 | 0.9 | 2.5 | 0.8 | 3.3 | 2.00 |
| 35 | Neurons | 96.4 | 0.8 | 1.8 | 1.0 | 2.8 | 2.01 |
| 35 | Non-neuronal cells | 95.0 | 1.6 | 2.5 | 0.9 | 3.4 | 2.02 |
| 48 | Neurons | 96.5 | 1.3 | 1.5 | 0.8 | 2.3 | 2.02 |
| 48 | Non-neuronal cells | 94.7 | 1.4 | 3.1 | 0.8 | 3.9 | 2.01 |
| Average | Neurons | 96.1 | 1.1 | 1.8 | 1.1 | 2.8 | 2.0 |
| Average | Non-neuronal cells | 95.2 | 1.3 | 2.7 | 0.8 | 3.5 | 2.0 |

tue of using FISH probes against chromosome 21, our data can be compared with previous studies of Alzheimer's disease (AD) brains (Herrup and Yang, 2001; Yang et al., 2001) and hypotheses on a relationship between Down's syndrome and AD (Heston and Mastri, 1977; Schweber, 1985; Potter, 1991). As reported for AD, tetrasomic cells could involve cell-cycle re-entering processes associated with neuronal death and would not fit the definition of aneuploidy (Herrup and Yang, 2001; Yang et al., 2001; Herrup and Arendt, 2002; Herrup et al., 2004). The existence of tetrasomic as well as aneuploid cells in normal human brain reported here was not observed previously in normal controls (Yang et al., 2001; Yurov et al., 2001), which likely reflects increased sensitivity of FISH on isolated nuclei used here and/or use of multiple loci probes for a single chromosome. The hypothesis that AD may involve trisomy 21 is intriguing albeit controversial (Heston and Mastri, 1977; St George-Hyslop et al., 1987) and based primarily on non-neuronal trisomic 21 cells from AD patients (Geller and Potter, 1999). The finding here that trisomic 21 neurons exist in the normal brain, without an obvious relationship to AD, suggests that a basal level of trisomy is not correlated with AD, even in an 86-year-old individual. However, we speculate that a combination of factors, including age [a hint of increased trisomic 21 cells is present in our samples (Table 1)] might increase the relative population of trisomic 21 cells toward approximating a Down's syndrome-like condition that contributes to AD. Future studies using AD brains could assess this possibility.

Increased rates of constitutive aneuploidy in humans could contribute to disruption of normal brain development and/or function. Down's syndrome represents a special case in which chromosome 21 trisomy produces clear CNS defects. A disease producing more pervasive increases in constitutive aneuploidy is MVA, a genetic recessive disorder characterized in part by mosaic aneuploidies, predominantly trisomies and monosomies, and cancer predisposition (Kawame et al., 1999). A recent report (Hanks et al., 2004) identified mutations in the mitotic spindle checkpoint protein, BUBR1, in five MVA families, which indicated a causal link between gain and loss of whole chromosomes and cancer. Coincidentally, MVA is also associated with mental retardation, severe brain anomalies, and microcephaly (Bitoun et al., 1994), and the exacerbation of normal aneuploidy levels may lead to a variety of neural sequelas, including increased neural cell death and/or aborted neurogenesis, which could account for the observed microcephaly. Furthermore, locus triplication of α-synuclein is linked to Parkinson's disease (Singleton et al., 2003) that could hypothetically be produced by a chromosome 4 trisomy. The relationship between constitutive aneuploidy and increased non-neural cancer predisposition combined with deleterious neural sequelas likely extends to other genes affecting ploidy, as reported for Ataxia-Telangiectasia mutated (McConnell et al., 2004). We speculate that a range of normal-through-diseased neural functions reflect a continuum of quantitative and qualitative aneuploidy differences in the CNS.

## References


Ausubel FM, Brent R, Kingston RE, Moore DD, Seidman JG, Smith JA, Struhl K (1994) Current protocols in molecular biology. New York: Wiley.

Barch MJ, Knutsen T, Spurbeck JL (1997) The AGT cytogenetics laboratory manual. Philadelphia: Lippincott.

Bhattacharyya A, Svendsen CN (2003) Human neural stem cells: a new tool for studying cortical development in Down's syndrome. Genes Brain Behav 2:179–186.

Bitoun P, Martin-Pont B, Tamboise E, Gaudelus J (1994) Optic atrophy, microcephaly, mental retardation and mosaic variegated aneuploidy: a human mitotic mutation. Ann Genet 37:75–77.

Geller LN, Potter H (1999) Chromosome missegregation and trisomy 21 mosaicism in Alzheimer's disease. Neurobiol Dis 6:167–179.

Hanks S, Coleman K, Reid S, Plaja A, Firth H, Fitzpatrick D, Kidd A, Mehes K, Nash R, Robin N, Shannon N, Tolmie J, Swansbury J, Irrthum A, Douglas J, Rahman N (2004) Constitutional aneuploidy and cancer predisposition caused by biallelic mutations in BUB1B. Nat Genet 36:1159–1161.

Herrup K, Arendt T (2002) Re-expression of cell cycle proteins induces neuronal cell death during Alzheimer's disease. J Alzheimers Dis 4:243–247.

Herrup K, Yang Y (2001) Pictures in molecular medicine: contemplating Alzheimer's disease as cancer: a loss of cell-cycle control. Trends Mol Med 7:527.

Herrup K, Neve R, Ackerman SL, Copani A (2004) Divide and die: cell-cycle events as triggers of nerve cell death. J Neurosci 24:9232–9239.

Heston LL, Mastri AR (1977) The genetics of Alzheimer's disease: associations with hematologic malignancy and Down's syndrome. Arch Gen Psychiatry 34:976–981.

Kalousek DK (2000) Pathogenesis of chromosomal mosaicism and its effect on early human development. Am J Med Genet 91:39–45.

Kaushal D, Contos JJ, Treuner K, Yang AH, Kingsbury MA, Rehen SK, McConnell MJ, Okabe M, Barlow C, Chun J (2003) Alteration of gene expression by chromosome loss in the postnatal mouse brain. J Neurosci 23:5599–5606.

Kawame H, Sugio Y, Fuyama Y, Hayashi Y, Suzuki H, Kurosawa K, Maekawa K (1999) Syndrome of microcephaly, Dandy–Walker malformation, and Wilms tumor caused by mosaic variegated aneuploidy with premature centromere division (PCD): report of a new case and review of the literature. J Hum Genet 44:219–224.

King RC, Stansfield WD (1990) A dictionary of genetics, Ed 4. New York: Oxford UP.

Leach NT, Rehder C, Jensen K, Holt S, Jackson-Cook C (2004) Human chromosomes with shorter telomeres and large heterochromatin regions have a higher frequency of acquired somatic cell aneuploidy. Mech Ageing Dev 125:563–573.

Lengauer C, Kinzler KW, Vogelstein B (1998) Genetic instabilities in human cancers. Nature 396:643–649.

McConnell MJ, Kaushal D, Yang AH, Kingsbury MA, Rehen SK, Treuner K, Helton R, Annas EG, Chun J, Barlow C (2004) Failed clearance of aneuploid embryonic neural progenitor cells leads to excess aneuploidy in the *Atm*-deficient but not the Trp53-deficient adult cerebral cortex. J Neurosci 24:8090–8096.

Modi D, Berde P, Bhartiya D (2003) Down syndrome: a study of chromosomal mosaicism. Reprod Biomed Online 6:499–503.

Mullen RJ, Buck CR, Smith AM (1992) NeuN, a neuronal specific nuclear protein in vertebrates. Development 116:201–211.

Nazarenko SA, Timoshevsky VA, Sukhanova NN (1999) High frequency of tissue-specific mosaicism in Turner syndrome patients. Clin Genet 56:59–65.

Pakkenberg B, Pelvig D, Marner L, Bundgaard MJ, Gundersen HJ, Nyengaard JR, Regeur L (2003) Aging and the human neocortex. Exp Gerontol 38:95–99.

Podlisny MB, Lee G, Selkoe DJ (1987) Gene dosage of the amyloid $\beta$ precursor protein in Alzheimer's disease. Science 238:669–671.

Potter H (1991) Review and hypothesis: Alzheimer disease and Down syndrome–chromosome 21 nondisjunction may underlie both disorders. Am J Hum Genet 48:1192–1200.

Rehen SK, McConnell MJ, Kaushal D, Kingsbury MA, Yang AH, Chun J (2001) Chromosomal variation in neurons of the developing and adult mammalian nervous system. Proc Natl Acad Sci USA 98:13361–13366.

Schweber M (1985) A possible unitary genetic hypothesis for Alzheimer's disease and Down syndrome. Ann NY Acad Sci 450:223–238.

Sebat J, Lakshmi B, Troge J, Alexander J, Young J, Lundin P, Maner S, Massa H, Walker M, Chi M, Navin N, Lucito R, Healy J, Hicks J, Ye K, Reiner A, Gilliam TC, Trask B, Patterson N, Zetterberg A, et al. (2004) Large-scale copy number polymorphism in the human genome. Science 305:525–528.

Singleton AB, Farrer M, Johnson J, Singleton A, Hague S, Kachergus J, Hulihan M, Peuralinna T, Dutra A, Nussbaum R, Lincoln S, Crawley A, Hanson M, Maraganore D, Adler C, Cookson MR, Muenter M, Baptista M, Miller D, Blancato J, et al. (2003) $\alpha$-Synuclein locus triplication causes Parkinson's disease. Science 302:841.

St George-Hyslop PH, Tanzi RE, Polinsky RJ, Neve RL, Pollen D, Drachman D, Growdon J, Cupples LA, Nee L, Myers RH, O'Sullivan D, Watkins PC, Amos JA, Deutsch CK, Bodfish JW, Kinsbourne M, Feldman RG, Bruni A, Amaducci L, Foncin J-F, et al. (1987) Absence of duplication of chromosome 21 genes in familial and sporadic Alzheimer's disease. Science 238:664–666.

Svendsen CN, ter Borg MG, Armstrong RJ, Rosser AE, Chandran S, Ostenfeld T, Caldwell MA (1998) A new method for the rapid and long-term growth of human neural precursor cells. J Neurosci Methods 85:141–152.

Yang AH, Kaushal D, Rehen SK, Kriedt K, Kingsbury MA, McConnell MJ, Chun J (2003) Chromosome segregation defects contribute to aneuploidy in normal neural progenitor cells. J Neurosci 23:10454–10462.

Yang Y, Geldmacher DS, Herrup K (2001) DNA replication precedes neuronal cell death in Alzheimer's disease. J Neurosci 21:2661–2668.

Yurov YB, Vostrikov VM, Vorsanova SG, Monakhov VV, Iourov IY (2001) Multicolor fluorescent in situ hybridization on post-mortem brain in schizophrenia as an approach for identification of low-level chromosomal aneuploidy in neuropsychiatric diseases. Brain Dev 23 [Suppl 1]:S186–S190.

The text of Appendix A is, in full, a reprint of material as it appears in the Journal of Neuroscience. The dissertation author was a primary researcher and co-author of this work, and Dr. Jerold Chun supervised the research that forms the basis of this chapter. Appendix A is reprinted here with full permission of all the authors, and of the journal, as per its published copyright transfer agreement.

**References**


1. King, R.C., and Stansfield, W.D. (2002). A dictionary of genetics, 6th Edition, (New York: Oxford University Press).

2. Dierssen, M., Herault, Y., and Estivill, X. (2009). Aneuploidy: from a physiological mechanism of variance to Down syndrome. Physiol Rev *89*, 887-920.

3. Pellman, D. (2007). Cell biology: aneuploidy and cancer. Nature *446*, 38-39.

4. Bannon, J.H., and Mc Gee, M.M. (2009). Understanding the role of aneuploidy in tumorigenesis. Biochem Soc Trans *37*, 910-913.

5. Thompson, S.L., Bakhoum, S.F., and Compton, D.A. (2010). Mechanisms of chromosomal instability. Curr Biol *20*, R285-295.

6. Rehen, S.K., McConnell, M.J., Kaushal, D., Kingsbury, M.A., Yang, A.H., and Chun, J. (2001). Chromosomal variation in neurons of the developing and adult mammalian nervous system. Proc Natl Acad Sci U S A *98*, 13361-13366.

7. Kaushal, D., Contos, J.J., Treuner, K., Yang, A.H., Kingsbury, M.A., Rehen, S.K., McConnell, M.J., Okabe, M., Barlow, C., and Chun, J. (2003). Alteration of gene expression by chromosome loss in the postnatal mouse brain. J Neurosci *23*, 5599-5606.

8. Kingsbury, M.A., Friedman, B., McConnell, M.J., Rehen, S.K., Yang, A.H., Kaushal, D., and Chun, J. (2005). Aneuploid neurons are functionally active and integrated into brain circuitry. Proc Natl Acad Sci U S A *102*, 6143-6147.

9. Yang, A.H., Kaushal, D., Rehen, S.K., Kriedt, K., Kingsbury, M.A., McConnell, M.J., and Chun, J. (2003). Chromosome segregation defects contribute to aneuploidy in normal neural progenitor cells. J Neurosci *23*, 10454-10462.

10. Peterson, S.E., Westra, J.W., Paczkowski, C.M., and Chun, J. (2008). Chromosomal mosaicism in neural stem cells. Methods Mol Biol *438*, 197-204.

11. Kingsbury, M.A., Yung, Y.C., Peterson, S.E., Westra, J.W., and Chun, J. (2006). Aneuploidy in the normal and diseased brain. Cell Mol Life Sci *63*, 2626-2641.

12. Rehen, S.K., Yung, Y.C., McCreight, M.P., Kaushal, D., Yang, A.H., Almeida, B.S., Kingsbury, M.A., Cabral, K.M., McConnell, M.J., Anliker, B., et al. (2005). Constitutional aneuploidy in the normal human brain. J Neurosci *25*, 2176-2180.

13. Westra, J.W., Peterson, S.E., Yung, Y.C., Mutoh, T., Barral, S., and Chun, J. (2008). Aneuploid mosaicism in the developing and adult cerebellar cortex. J Comp Neurol *507*, 1944-1951.

14. Westra, J.W., Rivera, R.R., Bushman, D.M., Yung, Y.C., Peterson, S.E., Barral, S., and Chun, J. (2010). Neuronal DNA content variation (DCV) with regional and individual differences in the human brain. J Comp Neurol *518*, 3981-4000.

15. Yurov, Y.B., Iourov, I.Y., Monakhov, V.V., Soloviev, I.V., Vostrikov, V.M., and Vorsanova, S.G. (2005). The variation of aneuploidy frequency in the developing and adult human brain revealed by an interphase FISH study. J Histochem Cytochem *53*, 385-390.

16. Yurov, Y.B., Iourov, I.Y., Vorsanova, S.G., Liehr, T., Kolotii, A.D., Kutsev, S.I., Pellestor, F., Beresheva, A.K., Demidova, I.A., Kravets, V.S., et al. (2007). Aneuploidy and confined chromosomal mosaicism in the developing human brain. PLoS One *2*, e558.

17. Yurov, Y.B., Vorsanova, S.G., Iourov, I.Y., Demidova, I.A., Beresheva, A.K., Kravetz, V.S., Monakhov, V.V., Kolotii, A.D., Voinova-Ulas, V.Y., and Gorbachevskaya, N.L. (2007). Unexplained autism is frequently associated with low-level mosaic aneuploidy. J Med Genet *44*, 521-525.

18. Iourov, I.Y., Vorsanova, S.G., Liehr, T., and Yurov, Y.B. (2009). Aneuploidy in the normal, Alzheimer's disease and ataxia-telangiectasia brain: differential expression and pathological meaning. Neurobiol Dis *34*, 212-220.

## APPENDIX B

## IDENTIFICATION OF NEURAL PROGRAMMED CELL DEATH THROUGH THE DETECTION OF DNA FRAGMENTATION IN SITU AND BY PCR

Current Protocols in Neuroscience, Chapter 3: Unit 3.8 (2009).

**A word about cell death during brain development**

The nervous system is shaped through a continuous sequence of formative events, among them a balance between cell proliferation and death (1, 2). Programmed cell death (PCD) is the physiological elimination of cells (3-5), apoptosis being the most common form, and characterized by DNA fragmentation, blebbing of the cell membrane, and chromatin condensation (6-8). In the developing cerebral cortex, as neurons migrate and grow into their targets, they establish functional connections or die by apoptosis. Signaling by neurotrophic factors from target cells is, at least in part, responsible for prevention of this cell death (9, 10).

PCD also occurs at an earlier neurodevelopmental period during which dividing progenitor cells increase overall cell number through rapid division. This death is termed **proliferative cell death**, and such dying cells can be detected by the methods described in this appendix (11). During this neuroproliferative phase, an average of 50% of cells are dying at any given point within the developing cerebral cortex (12) and neuraxis (13). Multiple independent studies using genetic deletion of pro-apoptotic (14-17) and pro-cell death proteins (18-21) have found prominent hyperplasia of embryonic brain cells during this proliferative period, consistent with at least partial rescue of proliferative cell death. Furthermore, deletion of anti-cell death genes resulted in smaller brains or progenitor pools (22-24). These studies support the concept that regressive events like proliferative cell death are essential for normal cortical brain development.

While the molecular determinants of proliferative cell death are currently being identified, recent studies in axon guidance molecules (reviewed in (25)) such as netrins (26-28), semaphorins (29), and ephrins (30) provide insight into their unanticipated influence in proliferative cell death. Conversely, signaling molecules with influences on cell death or survival (31, 32) may equally function in neuronal axon guidance and connectivity. These studies contribute to identification of a growing body molecular factors with pleiotropic and unifying functions in the proper formation of the cerebral cortex.

# Identification of Neural Programmed Cell Death Through the Detection of DNA Fragmentation In Situ and by PCR

**Yun C. Yung,[1,2] Grace Kennedy,[1] and Jerold Chun[1]**

[1]Helen L. Dorris Child and Adolescent Neuropsychiatric Disorder Institute, The Scripps Research Institute, La Jolla, California
[2]University of California, San Diego School of Medicine, San Diego, California

## ABSTRACT

Programmed cell death is a fundamental process for the development and somatic maintenance of organisms. This unit describes methods for visualizing both dying cells in situ and for detection of nucleosomal ladders. A description of various current detection strategies is provided, as well as support protocols for preparing positive and negative controls and for preparing genomic DNA. *Curr. Protoc. Neurosci.* 48:3.8.1-3.8.24. © 2009 by John Wiley & Sons, Inc.

Keywords: cell death • apoptosis • ISEL • TUNEL • nucleosomal ladder

## INTRODUCTION

A universal feature in the development of multicellular organisms is a physiological form of cell death termed programmed cell death (PCD). A subset of PCD is apoptosis, which is defined by characteristic cellular morphological changes and genomic DNA fragmentation producing nucleosomal ladders. To understand how PCD operates in a developing tissue or in a tissue following an experimental procedure, dying cells must be identified in relation to their surviving neighbors. One way to accomplish this is to visualize fragmented DNA in situ, in combination with independent approaches such as gel electrophoresis of isolated DNA to visualize the nucleosomal ladders associated with apoptosis.

Two protocols for assessing apoptosis are presented in this unit. In situ end-labeling plus (ISEL+), a technique that originated from studies of central nervous system (CNS) tissue, identifies dying cells in tissue sections or cell culture (optimized for embryonic samples; see Basic Protocol 1). Ligation-mediated polymerase chain reaction (LMPCR) identifies nucleosomal ladders from intact tissues (see Basic Protocol 2). Also included are protocols for preparing thymocyte cell cultures for use as controls in the ISEL+ procedure (see Support Protocol 1) and for isolating genomic DNA for LMPCR (see Support Protocol 2).

*NOTE:* All protocols using live animals must be reviewed and approved by an Institutional Animal Care and Use Committee (IACUC) and must follow officially approved procedures for the care and use of laboratory animals.

*NOTE:* Use of human tissues requires appropriate IRB approval. Possible biosafety and biohazardous materials must also be similarly considered by the appropriate oversight committee.

## STRATEGIC PLANNING

Table 3.8.1 gives an overview of the features of different methods currently used to visualize cell death in histological sections. ISEL+ is currently the most sensitive method for

*Current Protocols in Neuroscience* 3.8.1-3.8.24, July 2009
Published online July 2009 in Wiley Interscience (www.interscience.wiley.com).
DOI: 10.1002/0471142301.ns0308s48

**Table 3.8.1** Comparison of ISEL+, TUNEL (As Originally Reported), and Hybrid Techniques

| | ISEL+ | TUNEL | Hybrid (ISEL) |
|---|---|---|---|
| Tissue Isolation | Snap-freeze | Fixation | Fixation |
| Sectioning | Frozen and vacuum baked | Paraffin embedded | Frozen or paraffin embedded |
| Fixation | Post-sectioning 4% paraformaldehyde (fresh) | Pre-sectioning 4% paraformaldehyde or formalin 1-7 days | Pre-sectioning 4% paraformaldehyde or formalin |
| Post-fixation | Triton X-100 permeabilization Dehydration | De-paraffinization Proteinase K digestion Peroxidase treatment | De-paraffinization, Sodium citrate antigen retrieval, Proteinase K digestion |
| Hapten | Digoxigenin | Biotin | Digoxigenin |
| Visualization | Alkaline phosphatase, fluorescence | Peroxidase | Alkaline phosphatase, fluorescence |
| Relative sensitivity | 10× (thousands of ends) | 1× | Intermediate |

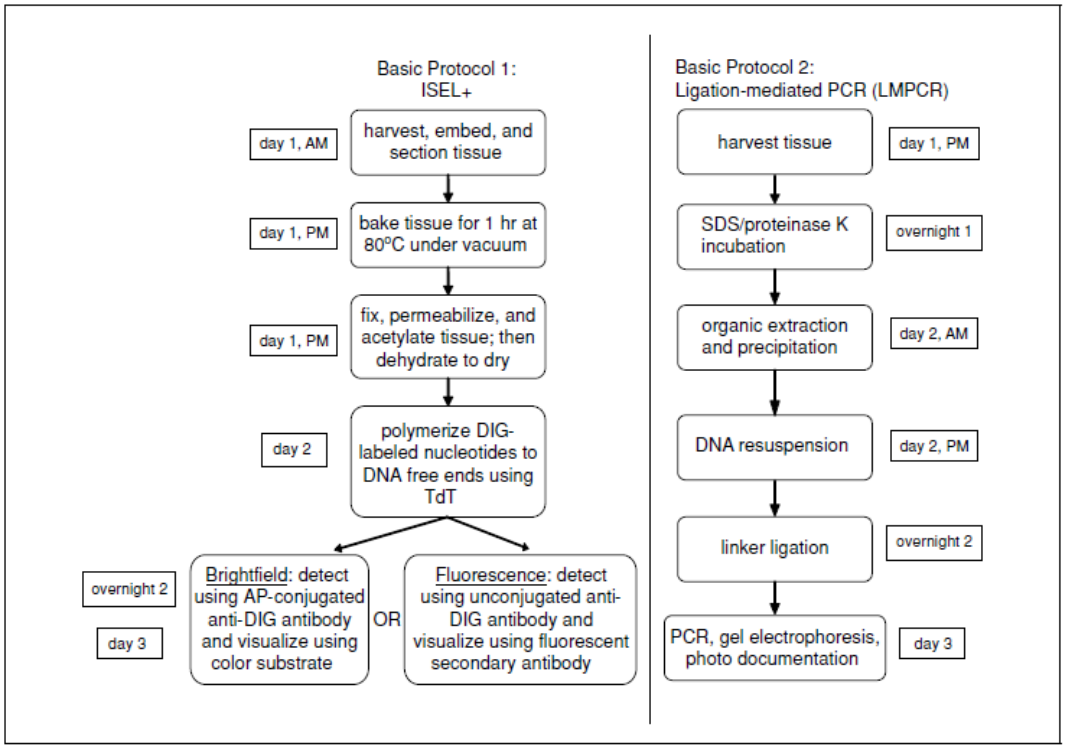


**Figure 3.8.1** Diagram of workflow for Basic Protocol 1 and Basic Protocol 2 and time requirements.

detecting dying cells, up to 10× more sensitive than TUNEL, as originally reported. Over the past decade, hybrid protocols (generally still referred to as TUNEL or ISEL) offer a combination of flexibility and convenience for sample preparation and visualization. Figure 3.8.1 is a flow chart outlining the major steps of Basic Protocol 1 and Basic Protocol 2 and their time requirements.

## DETECTION OF PROGRAMMED CELL DEATH BY IN SITU END-LABELING PLUS (ISEL+)

*BASIC PROTOCOL 1*

Tissue is rapidly and carefully dissected, frozen, and sectioned by cryostat. Sections are quickly thawed onto charged glass slides, air dried, then baked in a vacuum oven, fixed in paraformaldehyde, permeabilized in Triton X-100, acetylated, dehydrated through graded concentrations of ethanol, dried, and either stored desiccated at −80°C or used immediately. Slides to be processed further are end-labeled with terminal deoxynucleotidyl transferase (TdT) in the presence of labeled nucleotides, and the polymerized label is visualized by immunohistochemistry. Modifications for use of ISEL+ with cells in culture are also noted. The protocol is optimized for mouse tissues.

### *Materials*

Pregnant mice *or* tissue culture cells grown on 12-mm glass coverslips coated with an appropriate adhesive (e.g., poly-L-lysine, *APPENDIX 2A*, or Cell-Tak from Becton Dickinson)
DMEM or other dissection medium, 4°C
OCT compound (e.g., Tissue-Tek II from Sakura) or other water-soluble embedding medium, 4°C
Appropriate controls (see step 1 annotation)
Liquefied Histo-Freeze (Fisher Sci), CryoKwik (Damon), *or* liquid nitrogen
Dry ice, finely crushed (optional)
Fixative (see recipe)
2× SSPE (*APPENDIX 2A*)
2× SSPE/0.6% Triton X-100 (see recipe)
0.1 M triethanolamine (TEA; see recipe)
Acetic anhydride (Sigma, cat. no. 91204)
DNase-free water
30%, 50%, 70%, 95%, and 100% ethanol, prepared with DNase-free water
ISEL+ TdT solution (see recipe)
Parafilm
MABS buffer (see recipe)
Blocking buffer (see recipe)
AP-conjugated sheep anti-DIG antibody (Roche, cat. no. 11093274910)
Alkaline phosphate buffer (see recipe)
Alkaline phosphatase color substrate buffer (see recipe)
Nuclear fast red solution (see recipe)
Permanent mounting medium (e.g., Crystal Mount from Biomeda and DPX from Fluka)
Unconjugated sheep anti-DIG antibody (Roche, cat. no. 11333089001)
Phosphate-buffered saline (*APPENDIX 2A*)
Fluorescent tagged anti-sheep antibody (e.g., AlexaFluor 488 tagged; Invitrogen, cat. no. A-11015)
4′,6-diamidino-2-phenylindole (DAPI; Sigma, cat. no. D9542)
Fluorescence mounting medium (e.g., Vectashield from Vector Labs)

Dissecting instruments including:
Fine forceps
Fine scissors
Blunt forceps and spatula
Freezing molds (Fisher Scientific, optional)
Cryostat
Superfrost Plus glass slides (Fisher Scientific)
Slide-warmer (Barnstead Thermolyne), 50°C
Slide-processing holders and vessels
80°C vacuum oven with house vacuum/pump
24-well microtiter plates (if using coverslip-mounted cells as controls)
Airtight containers for slide storage with desiccant (Tupperware)
Humidified chamber for microscope slides
Coverslips
Microscope, preferably equipped for brightfield, DIC, and/or fluorescence

*CAUTION:* Paraformaldehyde, triethanolamine, acetic anhydride, and potassium cacodylate (in the TdT buffer) are toxic and must be used in accordance with safety standards.

***Prepare tissue***

1. Harvest embryos (or other tissues) using fine scissors and forceps by laparotomy, uterine exposure, and careful incision of the uterus. Remove one embryo at a time, taking care not to rupture the amniotic sacs or transect the umbilical cords (and umbilical arteries/veins) of other embryos, so as to keep individual embryos blood-perfused as long as possible. For tissues requiring dissection, place tissue in ice-cold DMEM (or similar dissection medium). Rapidly isolate the tissue (within minutes, faster is better) and place it in ice-cold embedding medium preferably in a freezing mold using blunt forceps and/or spatula; embryos too small to dissect easily can be placed directly into embedding medium.

   *Care and speed are essential in isolating tissues. As with lengthy post-mortem intervals, physical damage to tissues may create detectable artifacts associated with induced cell death.*

   *Positive and negative controls, particularly internal controls processed on the same slide as the experimental tissues, are useful in establishing this procedure or in troubleshooting. For a positive control in tissue sections, use developing thymus (4 weeks postnatal) or adult small intestine; these tissues contain many dying cells and will produce a robust and unambiguous signal (see Commentary). In a pinch, thymocytes in culture (see below) may be used instead. For negative controls, showing relatively little PCD, use adult (>4 months) neocortex, embryonic day 10 (E10) cerebral cortex, or adult liver (liver may produce increased background because of cytosolic alkaline phosphatase labeling, but this can be distinguished from true positive nuclear labeling; it can be reduced or eliminated by improved fixation and vacuum baking).*

   *For positive controls in tissue culture, use a primary thymocyte culture treated with dexamethasone, where a marked increase in cell death is observed, beginning at step 5 below. For a negative control in cell cultures, use any healthy cell line (e.g., 3T3 fibroblast or undifferentiated P19 cells). Some cell death is always observed in culture (typically up to a few percent of total cells), but this is easily distinguished from the >80% of thymocytes induced to die by dexamethasone exposure. Untreated thymocytes can also be used in conjunction with dexamethasone-treated thymocytes. However, the large number of normally dying cells in the untreated thymus results in a substantial level of dying cells in controls, which should be expected.*

2. Position the tissue by floating it in either a drop of ice-cold embedding medium or, optionally, in a rectangular plastic mold. Freeze the sample in liquefied Histo-freeze, CryoKwik, or a liquid nitrogen bath; powdered dry ice may also be used for small

samples. If possible, include positive and negative controls in the same mold so that they appear on the same slide as the tissue in question.

*When using dry ice as an alternative method, crush the dry ice blocks into a fine powder to expedite cooling (a hammer is often used for this). During the isolation procedure, the tissue should be kept as cool as possible; the entire procedure, from harvesting to freezing, should take no more than 5 min, preferably less. Rapid freezing is essential, to avoid artifacts associated with cell death during isolation procedures through the freezing step.*

*Once frozen, blocks of embedded tissue can be stored up to several weeks at −80°C, preferably in an airtight container.*

3. Cut sections using a cryostat with a sharp blade to produce 10-µm-thick sections (see *UNIT 1.1*).

*Substandard cutting blades can result in artifacts produced by tissue damage.*

4. After cutting, position the slide carefully over the section, thaw in place, and place on the 50°C slide warmer until ready for the next section. When all the slides have been collected, place slides in a slide rack and bake them in a preheated vacuum oven for 1 hr at 80°C under house vacuum.

*Initial drying of slides at 50°C inhibits nucleases that may otherwise produce detectable, artifactual DNA damage. Further drying in a vacuum oven ensures complete dehydration, particularly important in humid climates. Coverslip-mounted culture cells used as controls (see Support Protocol 1) do not have to be baked.*

***Fix, permeabilize, and acetylate tissue sections***

5. Incubate slide-mounted tissue sections in slide-processing vessels containing *fresh* fixative for 5 min at room temperature. If using dexamethasone-treated primary thymocyte cultures as controls, process the coverslip-mounted cells in parallel with the experimental slides from this point on.

*Typically, 24 slides per rack are processed; coverslips are processed in the wells of a 24-well microtiter plate. Use fresh solutions whenever possible.*

6. Wash twice in 2× SSPE, 5 min each time, at room temperature.

7. Permeabilize in 2× SSPE/0.6% Triton X-100 for 30 min at room temperature.

8. Wash slides twice in 2× SSPE, 5 min each time, at room temperature. During this wash step, prepare for acetylation by combining 300 ml of 0.1 M TEA with 750 µl acetic anhydride while stirring until acetic anhydride globules have dissolved. Submerge slide rack immediately in TEA/acetic anhydride and incubate slides 10 min at room temperature.

*Cultures do not need to be acetylated. Acetylation decreases nonspecific background, which is more problematic with tissue sections, particularly from embryonic brain.*

9. Wash in 2× SSPE for 5 min followed by a wash in $dH_2O$ for 5 min, both at room temperature. Dehydrate through graded ethanol solutions diluted in $dH_2O$ where needed: 30%, 50%, 70%, 95%, 100%, 100% (v/v), 2 min each.

*It is vital to ensure that no TEA or SSPE remains in the tissue section, as TdT is inhibited by $Na^+$, $NH_4^+$, Tris buffer, and metal chelators such as EDTA. Phosphates can cause precipitation of the cobalt in the TdT buffer.*

10. Dry slides 20 min at 50°C. (*Optional:* Dry in vacuum oven 20 min at 50°C under house vacuum).

*Slides and cultures can now be stained immediately or stored in well-sealed slide containers with desiccant for up to 6 months at −80°C.*

***Polymerize digoxigenin-labeled nucleotides to free DNA ends***

11. To each slide, without prewetting, add 50 µl ISEL+ TdT solution. Overlay sections gently with precut Parafilm and incubate in a humidified chamber 1 hr at 37°C.

    *For coverslip-mounted cultures, add ISEL+ TdT solution directly to wells of 24-well microtiter plate and incubate as for slides. The Triton X-100 in the TdT solution and Parafilm allow for even distribution of a minimum volume of buffer. Incubate on a level surface, free from falling debris or other objects. Keep free of bubbles.*

12. To terminate the reaction, remove Parafilm and wash with 2× SSPE for 5 min, then wash twice in MABS buffer for 5 min each.

    *MABS is a transition buffer that washes out phosphate from the previous SSPE buffer.*

***Detect labeled nucleotides/AP activity for brightfield visualization***

13a. Incubate in blocking buffer 1 hr at room temperature in a humidified chamber.

    *Typical volumes are ~500 µl per microscope slide and 300 µl per coverslip-mounted culture.*

14a. Replace blocking solution with sheep (or other species) anti-DIG/AP diluted 1:2000 in blocking buffer and incubate overnight at 4°C in a humidified chamber.

15a. Wash twice in MABS and three times in alkaline phosphate buffer, 5 min each at room temperature.

16a. Replace buffer with alkaline phosphatase color substrate buffer. Allow color (bluish precipitate) to develop for 1 to 2 hr, up to overnight, in darkness for maximum labeling, and terminate the reaction by transferring slides into $dH_2O$. Monitor color reaction every 15 min until complete.

    *Typical volume of color substrate buffer for both slides and cultures is ~500 µl.*

    *Nuclei of cells in culture appear to provide a much more accessible target for TdT and subsequent immunological and enzymatic amplification steps (somewhat analogous to amounts of antibody required for immunoblots versus immunohistochemistry). Because of this, the reaction times are often much shorter (e.g., several minutes to completion), and the investigator should initially monitor the reaction using appropriate controls.*

17a. Repeat $dH_2O$ wash three times, 10 min each.

18a. Lightly counterstain nuclei (if desired) using nuclear fast red solution for 5 min, then wash slides in running tap water for 2 min.

19a. Dehydrate sections in 70%, 95%, 95%, 100%, 100% (v/v) ethanol, 2 min each, and dry at 50°C for 2 min.

20a. Overlay sections with a thin film of permanent mounting medium (e.g., Crystal Mount), spread gently using a piece of clean Parafilm, dry at 50°C for 5 min, then coverslip using DPX and appropriate coverslip. View samples under a light microscope.

    *Crystal Mount creates a strong permanent seal for the sections and further mounting with DPX and coverslip allows for oil-immersion microscopy. Slides prepared in this manner will last for years.*

***Detect labeled nucleotides/DIG label for fluorescence visualization***

13b. Incubate in blocking buffer 1 hr at room temperature in a humidified chamber.

14b. Replace blocking solution with polyclonal sheep (or other) anti-DIG antibody diluted 1:500 in PBS and incubate overnight at 4°C in a humidified chamber.

15b. Wash three times, 5 min each, in PBS at room temperature.

16b. Add AlexaFluor 488 donkey anti-sheep antibody (or other immunofluorescent component of choice) diluted 1:500 (or appropriate dilution) in PBS for 1 hr at room temperature. Wash three times, 5 min each, in PBS at room temperature.

17b. Counterstain nuclei with 0.3 μg/ml DAPI in $dH_2O$ and coverslip using fluorescence mounting medium (e.g., Vectashield). View samples under a fluorescence microscope with appropriate filters.

*Glycerol-based mounted samples (e.g., Vectashield) are less permanent than brightfield preparations. Samples are typically stored for up to 1 month at −20°C before discarding. Longer storage may result in fungal-contaminated slides or fading of fluorescence signals.*

## PREPARATION OF THYMOCYTE CELL CULTURES FOR ISEL+

***SUPPORT PROTOCOL 1***

To obtain primary thymocyte cultures, thymus cells are grown on 12-mm round glass coverslips (coated with a desired adhesive, e.g., poly-L-lysine or Cell-Tak). The cultures are then treated with dexamethasone to induce apoptosis. They can then be used as a positive control and compared with untreated thymocyte cultures being assessed for programmed cell death (see Basic Protocol 1).

### *Materials*

4-week-old mice
DMEM/F-12 (*APPENDIX 2A*), containing 0.0025% trypsin
DMEM/F-12/5% FBS (*APPENDIX 2A*)
12-mm diameter round glass coverslips coated with poly-L-lysine (*APPENDIX 2A*) or Cell-Tak (Collaborative Research)
Dexamethasone stock solution: 2 mM dexamethasone in 100% ethanol

Long-nose Pasteur pipet, flame polished
24-well microtiter dishes

Additional reagents and equipment for tissue culture (for cultured cells; see *APPENDIX 3B*)

1. Harvest thymi from appropriately anesthetized 4-week-old mice. Isolate and mince thymi in DMEM/F-12 containing 0.0025% trypsin, and then triturate with a flame-polished long-nose Pasteur pipet.

   *A single mouse thymus is sufficient, but several can be combined if desired.*

2. Centrifuge cells 5 min at 800 × *g*, room temperature, remove trypsin medium, and resuspend resulting pellet in 2 ml DMEM/F-12/5% FBS.

3. Count cells (*APPENDIX 3B*), adjust concentration to $2 \times 10^6$ cells per well, and plate cells on coated 12-mm coverslips placed in 24-well microtiter dishes.

4. Add 1 μM dexamethasone (from 2 mM stock in ethanol) and incubate 4 hr in a humidified 37°C, 5% $CO_2$ incubator.

5. Use coverslip-plated cells as positive controls for the assessment of PCD in tissue sections (see Basic Protocol 1, steps 5 to 20).

   *The coverslip-plated cells are fixed and processed like the slides containing the sections being analyzed, with the exception that acetylation and baking are not required (since the cell monolayers are rapidly and thoroughly fixed on the coverslip).*

   *Coverslip-plated cells may be stored at −80°C for later use, but it is preferable to use them within 24 hr.*

*BASIC PROTOCOL 2*

## DETECTION OF NUCLEOSOMAL LADDERS ASSOCIATED WITH PROGRAMMED CELL DEATH BY LIGATION-MEDIATED POLYMERASE CHAIN REACTION (LMPCR)

DNA ladders with nucleosomal-sized rungs are a hallmark of apoptosis, but ladders can be difficult to visualize in tissues where apoptosis is nonsynchronous, such as in developing tissues. In addition, a significant amount of starting tissue is generally required to isolate enough DNA for precise analyses. Most ladder rungs appear to be blunt ended and 5′-phosphorylated on each end, allowing their identification by ligation of artificial, dephosphorylated linkers followed by amplification using the polymerase chain reaction (PCR). The resulting amplified DNA is visualized by agarose gel electrophoresis and ethidium bromide staining.

### *Materials*

Isolated and quantified genomic DNA (see Support Protocol 2)
Oligonucleotides for ligation, unphosphorylated:
12-bp: 5′-TGCGGTGAGAGG-3′
24-bp: 5′-AGCACTCTCGAGCCTCTCACCGCA-3′
10× T4 DNA ligase buffer (prepared fresh; see recipe)
T4 DNA ligase (Roche; store up to 1 month at −20°C)
DNase-free water
PCR buffer (see recipe)
Oligonucleotides for single-copy-gene PCR controls: e.g., for mouse *engrailed*:
5′-AGGACAAGCGGCCTCGCACA-3′
5′-CGGTGTCCGACTTGCCCTC-3′
*Taq* DNA polymerase
Agarose gels, analytical grade (see *APPENDIX 1N*), prepared in TBE buffer (*APPENDIX 2A*)
Ethidium bromide staining solution (*APPENDIX 2A*)

0.5-ml microcentrifuge tubes
Thermal cycler
Gel photographic setup

Additional reagents and equipment for agarose gel electrophoresis (*APPENDIX 1N*)

*CAUTION:* Ethidium bromide is a mutagen and should be handled, stored, and disposed of with appropriate care.

### *Ligate linkers*

1. Combine in a 0.5-ml microcentrifuge tube:

   ≤2.5 µg genomic DNA
   ≤1 nmol 12-bp unphosphorylated oligonucleotide
   ≤1 nmol 24-bp unphosphorylated oligonucleotide
   6 µl 10× T4 DNA ligase buffer
   $dH_2O$ to 60 µl.

   Mix thoroughly.

   *Very small amounts of genomic DNA (≤1 ng) can also be used, depending on the extent of apoptosis in the tissue. Be sure that the T4 DNA ligase and ATP-containing T4 ligase buffer are fresh, and that salt concentrations are sufficiently low to allow ligation. Note that the 12- and 24-bp oligonucleotides must be equimolar.*

2. Anneal oligonucleotides by heating ligation mixture 5 min at 55°C in thermal cycler.

3. Gently mix contents by flicking tube.

   *Never vortex DNA at this stage.*

4. Heat mixture 5 min more at 55°C in the thermal cycler.
5. Slowly cool mixture to 10°C over a 55-min period, and incubate at least 10 min at 10°C.

   *Heating and cooling can be programmed into the thermal cycler.*

6. Add 3 U T4 DNA ligase, mix, and briefly centrifuge contents to the bottom of the tube. Incubate 12 to 16 hr (i.e., overnight) at 16°C.

   *Be certain ligase is well mixed into the ligation solution.*

7. Dilute reactions with DNase-free water to attain a final concentration of 2.5 to 5 ng genomic DNA/µl.

   *Samples can be stored at −20°C indefinitely, provided they are not contaminated with DNases, before analysis by PCR.*

***Analyze DNA by PCR***

8. Set up PCR reaction for experimental samples at room temperature:

   150 ng ligated DNA
   124 pmol 24-bp linker (as primer)
   10 µl PCR buffer
   $H_2O$ to 100 µl.
   Mix thoroughly.

   *Smaller amounts of ligated DNA can also be used, and this step can be optimized by varying the amount of input DNA.*

9. Set up PCR reaction for controls at room temperature:

   150 ng ligated DNA
   100 pmol oligonucleotides for single-copy gene of choice PCR controls [e.g., *engrailed* as originally used in Staley et al. (1997)]
   10 µl PCR buffer
   $H_2O$ to 100 µl.
   Mix thoroughly.

10. Heat tubes 3 min at 72°C in thermal cycler. Add 5 U *Taq* DNA polymerase to each reaction tube and incubate an additional 5 min at 72°C.

    *The 3-min, 72°C heating step eliminates the 12-bp fragment, which can no longer hybridize to its now ligated partner, while the addition of Taq DNA polymerase allows the filling in of the resulting single-stranded, 5′-protruding ends of the ligated adapters during the 5-min step.*

11. Amplify experimental samples using the following cycling conditions:

| | | |
|---|---|---|
| 20 to 30 cycles: | 1 min | 94°C |
| | 3 min | 72°C. |

12. Amplify controls using the following cycling conditions:

| | | |
|---|---|---|
| 25 to 30 cycles: | 1 min | 94°C |
| | 1 min | 70°C |
| | 1 min | 72°C. |

*This will produce a single-band control (e.g., using engrailed primers, a 270-bp PCR product clearly visible upon ethidium bromide staining of the agarose gel). This control is to ensure loading of equal amounts of ligated DNA, making LMPCR semiquantitative. See Staley et al. (1997) for more information.*

13. Analyze 15 µl of each PCR product by electrophoresis through 1.2% agarose/TBE buffer gel (*APPENDIX 1N*). Stain with ethidium bromide and record photographically.

    *Using control tissue like the unmanipulated thymus, obvious ladders consisting of five to seven rungs should be observable after <30 cycles; test aliquots in 2-cycle increments.*

***SUPPORT PROTOCOL 2***

## ISOLATION OF GENOMIC DNA FROM TISSUES AND CULTURES

Analysis of DNA by LMPCR requires its isolation from intact tissues or cells in culture. Tissues are rapidly frozen in liquid nitrogen and pulverized using a liquid nitrogen–cooled mortar and pestle; then the cells are lysed in warmed SDS/proteinase K buffer. Cultured cells are not frozen; instead they are immediately lysed in SDS/proteinase K buffer, and the resulting slurry is incubated overnight and processed like tissues. In both cases, after an overnight incubation with agitation, the DNA solution is extracted with phenol/chloroform, precipitated, washed, resuspended, quantified, and used for LMPCR in Basic Protocol 2.

### *Materials*

Mice *or* tissue culture cells (see *APPENDIX 3B*) grown on 12-mm glass coverslips coated with an appropriate adhesive (e.g., poly-L-lysine, *APPENDIX 2A*, or Cell-Tak, Collaborative Research)
Sodium dodecyl sulfate (SDS)/proteinase K buffer (see recipe)
Molecular biology–grade 25:24:1 (v/v/v) phenol/chloroform/isoamyl alcohol equilibrated with Tris·Cl, pH 8.0 (*APPENDIX 2A*)
24:1 (v/v) chloroform/isoamyl alcohol
3 M sodium acetate, pH 5.0 (*APPENDIX 2A*)
100% ethanol, −20°C
70% ethanol
TE buffer, pH 8.0 (*APPENDIX 2A*)
RNase A solution, DNase-free (*APPENDIX 2A*; optional)

Ceramic mortar and pestle, precooled with liquid nitrogen
15- and 50-ml polypropylene tubes with caps
50°C oven with rocker platform
Fluorometer or spectrophotometer

Additional reagents and equipment for DNA quantitation using a spectrophotometer (see *APPENDIX 1K*)

1. Harvest tissue from the anesthetized mouse. Rapidly dissect tissue and immediately freeze in liquid nitrogen.

   *Where multiple samples are to be combined, homemade foil cups partially submerged in liquid nitrogen can be used to accumulate samples. Keep the size of the tissue as small as possible before freezing (large pieces are difficult to crush).*

   *When working with tissue culture cells, proceed directly to step 3.*

2. Grind frozen tissue into a fine powder with mortar and pestle.

   *Be sure to precool both mortar and pestle with liquid nitrogen, and then add small volumes of the liquid nitrogen during the crushing process. Wear eye protection and laboratory coat when grinding.*

3. Transfer powdered, frozen tissue to a 15-ml polypropylene tube containing 5 ml SDS/proteinase K digestion buffer per gram or less of tissue. For tissue culture cells, spin down cells and resuspend in 5 ml digestion buffer per 15-cm plate. Incubate 12 to 16 hr at 50°C with gentle agitation (e.g., using a rocker platform).

*The tissue powder is most easily transferred as liquid nitrogen slurry (use a minimal amount of nitrogen; see caution below). Preheat buffer to 50°C before adding tissue powder. SDS will form a white precipitate if the solution is too cold; however, this is reversible upon heating.*

CAUTION: *Be sure to warm tissue/buffer slurry to at least 37°C before sealing the top, as remaining liquid nitrogen, once vaporized, can cause the sealed tube to explode.*

4. Using 50-ml polypropylene tubes, extract twice with one volume of 25:24:1 (v/v/v) phenol/chloroform/isoamyl alcohol and then once with one volume of 24:1 (v/v) chloroform/isoamyl alcohol.

5. Precipitate DNA with 1/10 vol of 3 M sodium acetate, pH 5.0, and 2.5 vol precooled 100% ethanol. Centrifuge 15 min at 1500 × *g*, 4°C. Decant, wash pellet with 70% ethanol, and centrifuge as before. Decant solution, dry pellet, and resuspend in sterile water if examining them immediately. Resuspend in TE buffer for prolonged storage.

   *Other precipitation methods are acceptable, including standard spooling procedures, as long as they result in a final DNA product that is of sufficiently low salt concentration to allow efficient ligation.*

6. Quantify DNA samples using a DNA-specific fluorescent dye and fluorometer, or other accurate methodology. Digestion of RNA with DNase-free RNase A, followed by reprecipitation, and quantification using a spectrophotometer may also be used (see *APPENDIX 1K*).

## REAGENTS AND SOLUTIONS

*Use DNase-free water for all recipes. Sterilization is optional except for PCR buffers. For common stock solutions, see* ***APPENDIX 2A****; for suppliers, see* ***SUPPLIERS APPENDIX****.*

### *Alkaline phosphatase buffer*

900 ml $dH_2O$
12.1 g Tris base (0.1 M)
5.8 g NaCl (0.1 M)
2.0 g $MgCl_2 \cdot 6H_2O$ (10 mM)
Mix well, titrate pH to 9.5 using Tris·Cl crystals (requires ~1 to 2 g).
Adjust volume to 1 liter
Store solution indefinitely at room temperature

### *Alkaline phosphatase color substrate buffer*

Dilute 4-nitroblue tetrazolium chloride (NBT) liquid stock to 450 µg/ml and 5-bromo-4-chloro-3-indolyl-phosphate (BCIP) liquid stock to 17.5 µg/ml in alkaline phosphate buffer (see recipe). Make up 10 ml of solution fresh just before use.

*NBT/BCIP stocks are also commercially available (e.g., from Millipore or Roche).*

### *Blocking buffer*

100 ml MABS solution (see recipe)
1 g blocking reagent (Roche)
100 µl Triton X-100
Store indefinitely at −20°C

*Add blocking reagent to MABS. Heat in 60°C water bath to dissolve, vortex every 5 min until solubilized. Add Triton-X and stir gently to avoid foaming. [Alternative blocking solution: use 3 ml 1 mg/ml BSA (see recipe) or 5 g powdered milk.]*

***Bovine serum albumin (BSA; 1 mg/ml)***

90 ml $dH_2O$
100 mg bovine serum albumin (Fraction V, Sigma)
Adjust pH to 8.8 with 6 M HCl
Add 700 µl 2-mercaptoethanol (100 mM)
Adjust volume to 100 ml
Store indefinitely at −20°C

***Fixative (4% paraformaldehyde in 0.02M PBS, freshly depolymerized)***

200 ml 0.02 M PBS, pH 7.4, microwave until just near boiling
8 g powdered paraformaldehyde (e.g., Sigma)
Stir until completely dissolved (3 to 5 min)
Filter with filter paper
Prepare fresh daily

CAUTION: *Paraformaldehyde is toxic; prepare solution in a chemical fume hood.*

***ISEL+ TdT solution***

784 µl $dH_20$
200 µl 5× TdT buffer (Invitrogen)
10 µl DIG dUTP, 50 µM
10 µl 10% Triton X-100/$dH_2O$
6 µl TdT (Invitrogen; includes 5× buffer and enzyme)
Prepare fresh daily before use

***MABS (0.1 M maleic acid buffer saline, pH 7.5)***

980 ml $dH_20$
Add 11.61 g maleic acid (Sigma)
Add 8.76 g NaCl (Fisher)
Add 6 g NaOH pellets
Stir to equilibrate, and then fine-adjust with 10 N NaOH solution to pH 7.5
Store at 4°C to minimize bacterial growth

CAUTION: *Maleic acid is toxic; wear a dust mask when weighing powder.*

***MABST (MABS/0.1% Triton X-100)***

100 ml MABS (see recipe)
100 µl Triton X-100
Stir gently to mix thoroughly, but avoid foaming

***Nuclear fast red solution (0.1% w/v)***

500 ml $dH_2O$
Add 25 g $Al_2(SO4)_3$
Add 0.5 g nuclear fast red (Sigma, cat. no. N8002)

Heat water to boil, then stir and dissolve aluminum sulfate. Add nuclear fast red, and continue to stir at boiling temperature until color does not change (~10 min). Cool and filter before use. Store up to 1 year at room temperature.

***PCR buffer***

*Prepare 10× stock:*
8.1 g Tris·hydrochloride (670 mM)
0.41 g $MgCl_2 \cdot 6H_2O$ (20 mM)
2.11 g $(NH_4)_2SO_4$ (160 mM)

*continued*

$H_2O$ to 80 ml
Store up to 6 months at −20°C
*Just before use, dilute to 1×, adding:*
10 mM 2-mercaptoethanol
100 µg/ml BSA (from 1 mg/ml stock; see recipe)
32 µg/ml 10 mM 4-dNTP mix (320 µM final)

*Alternatively, buffer may be included with the purchased Taq enzyme.*

***SDS/proteinase K buffer***

80 ml $H_2O$
0.44 g NaCl (75 mM)
0.12 g Tris·hydrochloride (10 mM)
5 ml 0.5 M EDTA, pH 8.0 (*APPENDIX 2A*; 25 mM)
1 g SDS (1%)
Adjust pH to 8.0 with 1 M HCl
Add $H_2O$ to 100 ml
Store indefinitely at room temperature
Add 0.4 g proteinase K per ml buffer just prior to use

***SSPE/0.6% Triton X-100, 2×***

100 ml 20× SSPE (*APPENDIX 2A*; 2×)
6 g Triton X-100 (0.6%)
$H_2O$ to 1 liter
Store indefinitely at room temperature

***T4 DNA ligase buffer, 10×***

8 ml $H_2O$
0.80 g Tris·hydrochloride (660 mM)
0.10 g $MgCl_2 \cdot 6H_2O$ (50 mM)
0.1 ml 1 M DTT (10 mM)
0.055 g ATP, disodium salt (10 mM)
Adjust pH to 7.5 with concentrated HCl
Add $H_2O$ to 10 ml
Store up to 1 month at −20°C

*Alternatively, buffer may be included with the purchased enzyme.*

***Triethanolamine (TEA), 0.1 M***

295 ml $H_2O$
4 ml triethanolamine (Sigma, cat. no. T1377)
520 µl concentrated (12 M stock) HCl
Add 750 µl acetic anhydride (Fluka, cat. no. 45830) just prior to acetylation step
Mix until globules are gone and use immediately
Prepare fresh each time.

## COMMENTARY

### Background Information

Programmed cell death (PCD) is the physiological elimination of cells by death (Wyllie, 1981; Ucker, 1991). Apoptosis is the best-known form of PCD and is characterized morphologically by nuclear size reduction, blebbing of the cellular membrane, chromatin condensation, and the formation of nucleosome-sized fragments of genomic DNA, detectable by gel electrophoresis (Kerr et al., 1972, 1994; Morris et al., 1984). Other forms of PCD also exist. Autophagy (Bursch et al., 2000) is thought to be distinct from apoptosis by involving the combined destruction of

the Golgi apparatus, polyribosomes, and endoplasmic reticulum, but with preservation of mitochondrial and micro- and intermediate filaments. Caspase-independent forms of PCD also exist (Liang et al., 2008). Evidence for the occurrence of PCD has been found in every multicellular organism studied, from flies to worms to mammals (Oppenheim, 1985; Ellis and Horvitz, 1986; Raff et al., 1993; White et al., 1994; Blaschke et al., 1996; Staley et al., 1997). All forms of PCD involve some degree of DNA fragmentation.

A significant advance in the study of PCD has been the development of histological techniques that localize DNA strand breaks within dying cells (Gavrieli et al., 1992; Wijsman et al., 1993; Wood et al., 1993). The first such technique, TdT-mediated dUTP nick-end labeling (TUNEL; Gavrieli et al., 1992; Strater et al., 1995; Negoescu et al., 1996), employed the template-independent DNA polymerase terminal deoxynucleotidyl transferase (TdT) to attach biotin-labeled nucleotides to the free 3′ ends of fragmented DNA. These labeled nucleotides could then be recognized by a peroxidase-conjugated avidin molecule and visualized through a substrate reaction that produced a colored precipitate within the nucleus. TUNEL and related techniques have been used to demonstrate the presence of PCD in many organisms, as well as in tissue culture (Surh and Sprent, 1994; White et al., 1994). In the nervous system, techniques conceptually related to TUNEL, but employing different polymerases and/or visualization techniques, have also been used to show evidence of PCD in the granule cell layer of the cerebellum (Wood et al., 1993) and in neurodegenerative disorders such as Huntington's disease (Thomas et al., 1995).

Procedures like TUNEL, as originally published, were unable to identify dying cells to any significant degree within the embryonic cerebral cortex, which, combined with prevailing views at the time, led some to conclude that cell death did not occur there. This disparity led to the development of techniques with improved sensitivity over TUNEL, resulting in in situ end-labeling plus (ISEL+; Blaschke et al., 1996, 1998) and the associated but independent technique of ligation-mediated PCR [(LMPCR; Staley et al., 1997) of DNA ladders. These techniques have proved successful in both tissue preparations and cell cultures at identifying dying cells produced by PCD in the developing nervous system, as well as in other tissues (Staley et al., 1997; Weiner et al., 1998; Vaccarino et al., 1999; Weiner and Chun, 1999; Contos et al., 2000; Gu et al., 2000; Pompeiano et al., 2000; Yan et al., 2000; Kingsbury et al., 2003; McConnell et al., 2004; Chao et al., 2006; Rehen et al., 2006). Multiple technical differences exist between ISEL+ and the original TUNEL technique (Table 3.8.1; see also Strategic Planning) that result in a significant increase in sensitivity. Many current commercial kits are in fact hybrids of TUNEL and ISEL+.

It is important to make a distinction between dying versus dead cells. ISEL+ is optimized to detect the former, whereas the original TUNEL protocol generally identifies the latter, e.g., corresponding with pyknotic nuclei. An experiment to examine the latency between DNA fragmentation detected by ISEL+ and actual cell death and removal was conducted in the small intestine, utilizing BrdU birthdating to follow cells after their last cell division (Pompeiano et al., 1998). The epithelium of the small intestine turns over completely in several days, and the age of epithelial cells increases as one ascends the villus (into the intestinal lumen). Use of this well-defined model system demonstrated that cells destined to die commenced DNA fragmentation 2 to 3 days before they were actually eliminated as dead cells at the villus tip.

The increased level of sensitivity produced by ISEL+ identified significant levels of developmentally variable dying cells, averaging around 50%, within the embryonic cerebral cortex (Blaschke et al., 1996), as well as throughout the neuraxis (Blaschke et al., 1998). At the time, this was a surprising result, as it contrasted with prevailing views. However, independent studies using genetic deletion of the pro-apoptotic proteins caspase-3 (Kuida et al., 1996; Pompeiano et al., 2000) or caspase-9 (Kuida et al., 1998; Zaidi et al., 2001) resulted in a striking hyperplasia of embryonic brain cells, consistent with the proven functions of the caspases in cell death, and consistent with at least partial rescue of the PCD that had been identified by ISEL+ and LMPCR. These results have been further supported by deletion of more pro-cell death genes, resulting in "big brain" phenotypes like the caspase-null mutants: Apaf 1 (Cecconi et al., 1998; Yoshida et al., 1998), Bax and Bak (Lindsten et al., 2003), Pten (Groszer et al., 2001), as well as novel pathways involving the ephrins (Depaepe et al., 2005). Similarly, anti-cell-death genes, when genetically removed, resulted in smaller brains or progenitor pools, as observed for Bcl-X (Motoyama et al., 1995), Survivin (Jiang et al., 2005), and

Mcl-1 (Arbour et al., 2008). Further evidence supporting extensive neural cell death comes from examination of single clones identified using a transgenic, mutant *lacZ* reversion construct (Wilkie et al., 2004). An unanticipated, marked decrease in the proportion of embryos with labeled clones was found during early neurogenesis, which is consistent with significant cell death during this period, as identified by ISEL+.

### *Sensitivity of ISEL+*

The most significant advantage of ISEL+ is its sensitivity in detecting dying cells. ISEL+ is up to ten times more sensitive than TUNEL. Figure 3.8.2 shows a comparison between TUNEL and ISEL+ in an adult mouse thymus treated in vivo with the corticosteroid dexamethasone (DX). DX causes rapid apoptosis of all immature thymocytes within the cortex (outer portion) of the thymus (Surh and Sprent, 1994) and, under the employed experimental conditions, should kill the majority of thymic cortical cells. In identically treated thymi, TUNEL identified a number of dying cells in the thymic cortex (Fig. 3.8.2A), but ISEL+ labeling (Fig. 3.8.2B) showed many more dying thymocytes; thus, the extent of PCD was more accurately revealed by ISEL+. A parallel time-course study of TUNEL and ISEL+ labeling in DX-treated thymic cultures further demonstrated the relatively greater sensitivity of ISEL+ (Fig. 3.8.3). TUNEL (Fig. 3.8.3A-C) did not detect increased cell death until 4 hr after DX addition, while ISEL+ (Fig. 3.8.3 D-F) detected the occurrence of increased apoptosis within 30 min of treatment. These results demonstrate that ISEL+ identifies dying cells with greater sensitivity than does TUNEL.

To quantify the relative difference in sensitivity between ISEL+ and TUNEL, the number of fragmented DNA ends that are required for visualization of a dying cell using each technique was estimated. A 1013-bp linearized fragment of plasmid DNA was labeled in solution by either TUNEL or ISEL+. Known amounts of labeled fragment were electrophoresed on an agarose gel and transferred to nitrocellulose. Labeled fragments were then detected either by TUNEL or by ISEL+. Using this assay (Fig. 3.8.4), 10 ng of labeled DNA were barely detectable by TUNEL, but prominently detected by ISEL+, which has a limit of detection approaching 1 ng (DNA content measured using a fluorometer). A conservative estimate was obtained of the number of fragmented ends that are required in a single cell for labeling by ISEL+, based on the following calculation. The number of ends in one nanogram of 1013-bp DNA ($1.50 \times 10^{-15}$ mol) is $1.80 \times 10^{9}$. The area of the blotted DNA band was determined to be $2 \times 10^{-6}$ m$^2$; $6.37 \times 10^{5}$ cells (with a maximum cross-sectional diameter of $10^{-5}$ m, and an area of $3.14 \times 10^{-12}$ m$^2$ each) would fit into that area. Dividing the number of free ends by the number of cells equates to 3000 ends that

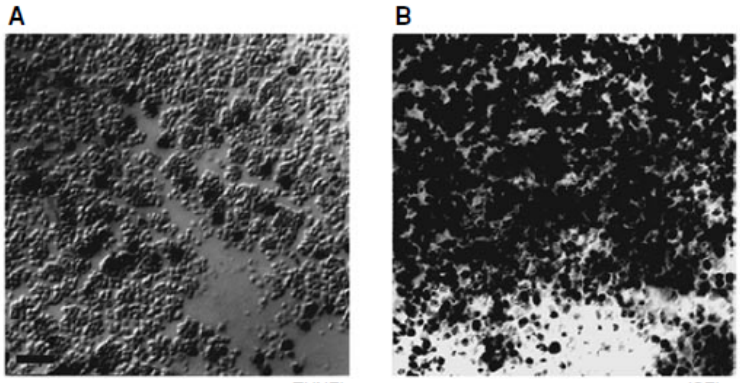


**Figure 3.8.2** ISEL+ is more sensitive than TUNEL in identifying dying cells. Data are for thymi from 4-week-old mice treated with dexamethasone for 8 hr to induce massive PCD of cortical thymocytes, and then fixed and processed for ISEL+ or TUNEL. (**A**) A number of dying cells were identified by TUNEL in the cortex of the thymus (dark stain). (**B**) The ISEL+ procedure identified significantly more dying cells in the thymic cortex (dark stain). Scale bar = 20 μm.

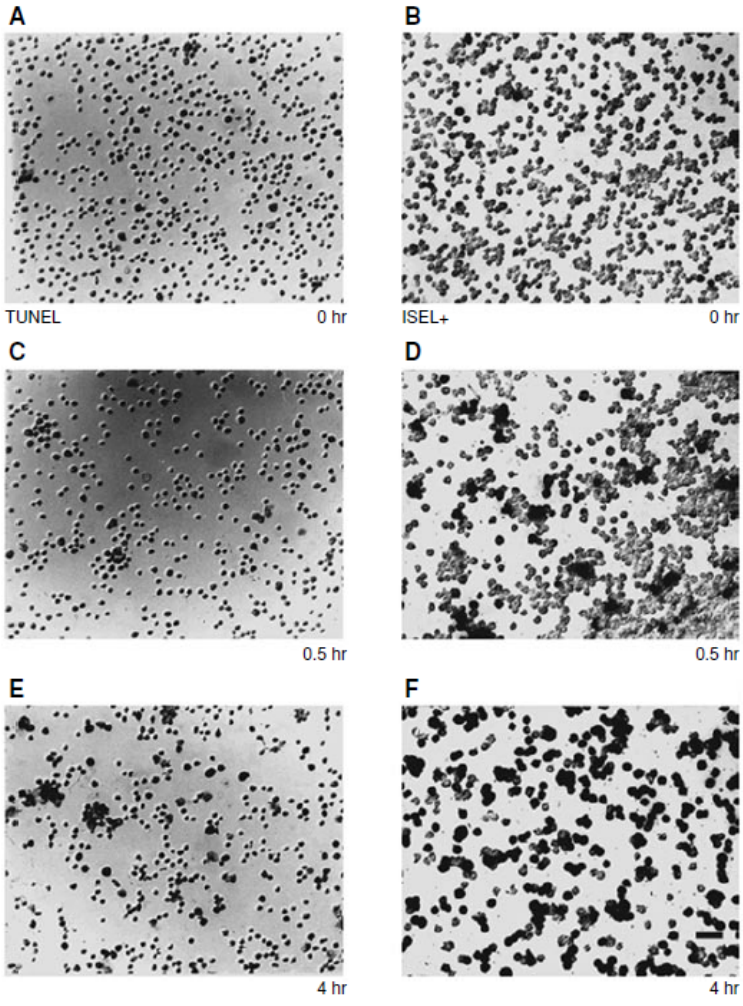


**Figure 3.8.3** ISEL+ identifies dying cells earlier than TUNEL following the induction of PCD. Data are for thymic cultures prepared from 4-week-old mouse thymi, then treated with dexamethasone to induce PCD and fixed for either ISEL+ or TUNEL at various times after PCD treatment. Dying cells were identified by either the TUNEL (**A, C, E**) or ISEL+ (**B, D, F**) procedure. (**A, B**) 0 hr (control). Neither ISEL+ nor TUNEL identified many dying cells before dexamethasone treatment of cultures. (**C, D**) 0.5 hr. Although TUNEL (**C**) did not show an increase in dying cells, ISEL+ (**D**) detected an increase in cells undergoing PCD. (**E, F**) 4 hr. At this timepoint, TUNEL (**E**) detected an increase in dying cells produced by the dexamethasone treatment (at 1 hr and 2 hr there was still no increase in TUNEL-labeled cells; data not shown). Labeling looked similar to that shown by ISEL+ at 0.5 hr (D). ISEL+ labeling at 4 hr (**F**), however, showed a massive increase in dying cells, reflecting its much higher sensitivity. Scale bar = 20 μm.

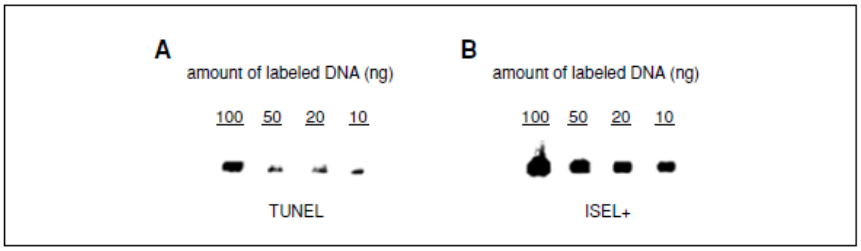


**Figure 3.8.4** Labeling by ISEL+ is ~10 times more sensitive than TUNEL. Known quantities of a 1013-bp DNA fragment were labeled by either ISEL+ or TUNEL and electrophoresed on an agarose gel, then transferred to nitrocellulose and detected by ISEL+ or TUNEL. (**A**) TUNEL required 10 ng of labeled DNA per well for threshold detection. (**B**) ISEL+ detection of 10 ng labeled DNA is shown for comparison. This observation is consistent with thymic in situ data (see Fig. 3.8.2).

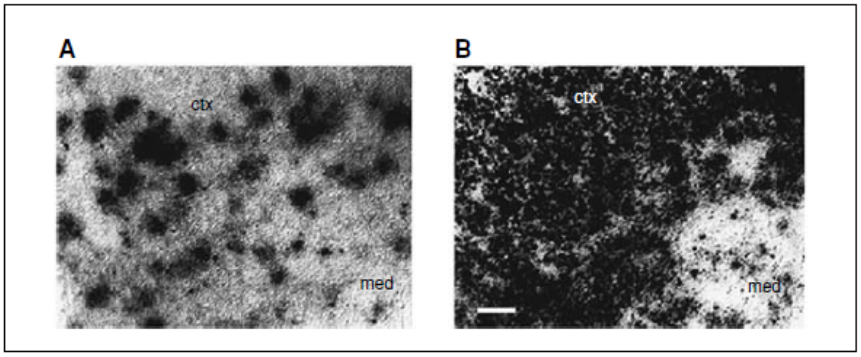


**Figure 3.8.5** ISEL+ is specific in its identification of cells undergoing PCD. (**A**) ISEL+ identified relatively small numbers of dying cells in the cortex of the normal thymus, consistent with the normal rate of PCD in this tissue (dark stain). (**B**) After cortical thymocytes were induced to undergo PCD en masse by dexamethasone (Wyllie, 1981), ISEL+ labeled virtually all the thymocytes in the cortex. Scale bar = 50 μm. Abbreviations: ctx, thymic cortex; med, thymic medulla.

are required per cell for labeling by ISEL+ at the 1-ng limit of detection, or 30,000 ends per cell at the 10-ng level. Therefore, ISEL+ is approximately ten times more sensitive than TUNEL.

*Specificity*

The specificity of ISEL+ in the detection of dying cells was examined using the thymus as a model. Under normal conditions, ~90% of immature thymocytes asynchronously undergo PCD in the cortex of the thymus (Egerton et al., 1990; Shortman et al., 1990). In vivo exposure of thymus to DX causes immature cortical thymocytes to undergo PCD en masse (Egerton et al., 1990; Shortman et al., 1990). This drug-induced apoptosis involves essentially all of the thymocytes in the cortex, which proceed synchronously through the cell death pathway. Mature thymocytes, located in the thymic medulla, are insensitive to DX and do not undergo massive PCD (Caelles et al., 1994; Blaschke et al., 1996; Staley et al., 1997). A normal mouse thymus labeled by ISEL+ identifies a number of labeled cells, consistent with the asynchronous nature of PCD (Fig. 3.8.5A). In contrast, a thymus treated in vivo with DX and then labeled by ISEL+ identifies a majority of cells (Fig. 3.8.5B), consistent with the large-scale synchronous cell death induced by DX, as can be seen by the intense labeling of most cells in the thymic cortex. Thus, cells identified by ISEL+ specifically increase in number after a treatment known to increase the number of dying cells.

As an additional example of the specificity of ISEL+, the medulla of a DX-treated thymus is shown (Fig. 3.8.5B). In this portion of the thymus, cells are insensitive to DX, and, as would be expected, very few cells were labeled by ISEL+. The specificity of ISEL+ has also been addressed in an in vitro paradigm of PCD, in which death was induced in P19 embryonal

carcinoma cells by UV irradiation (Staley et al., 1997). All of these paradigms also show parallel increases in DNA ladders, identified by both standard and LMPCR techniques (Pompeiano et al., 1998). Further validation in the small intestine, mentioned above, also supports the specificity of the assay (Blaschke et al., 1996). These combined data show that ISEL+ is specific in labeling apoptotic cells under the employed biological conditions. It is possible that artifactual or non-biological production of DNA double-strand breaks could produce false-positive signals, as could poor tissue conditions associated with extended post-mortem interval, physical damage, toxicity, etc. Use of independent means of assessing PCD (e.g., appropriate genetic mutants or LMPCR) can minimize errors. Additional controls are shown and discussed in Young (1984), Crespo et al. (1985), and Sengelaub et al. (1986). Some examples are presented below.

***Examples of PCD detected by ISEL+***

PCD has been studied in a number of neural cell types, and ISEL+ was designed to identify PCD in the nervous system, as shown in several examples from the murine nervous system (Fig. 3.8.6A-C).

The death of cells in the ganglion layer of the early postnatal rodent retina is well documented (Young, 1984; Sengelaub et al., 1986), and PCD is prominent during the first 11 days (Flanagan, 1969; Lance-Jones, 1982; Oppenheim, 1985, 1989). In the P1 retina, reportedly a site of high PCD, >60% of ganglion cells were labeled by ISEL+ (Fig. 3.8.6A), consistent with prior studies.

During the period of limb innervation, spinal cord motor neurons undergo PCD between embryonic days 13 (E13) and E18, and the peak of motor neuron cell death is on E14 (Davies and Lumsden, 1984; Buchman and Davies, 1993). Many cells are labeled by ISEL+ in the area where motor neurons are differentiating at E14 (Fig. 3.8.6B).

The developmental period of PCD for trigeminal ganglia is E13 to E18 (Pompeiano et al., 1998), which corresponds to the period during which synaptic connections are formed. A trigeminal ganglion at E16 shows a consistent amount of ISEL+ labeling (Fig. 3.8.6C).

## Critical Parameters and Troubleshooting

***ISEL+***

*Tissue isolation:* Once deprived of normal nutrient exchange, via diffusion or blood supply, tissues begin to die. It is critical, therefore, to minimize cell death produced by tissue handling. Rapid dissection and use of ice-cold buffers during tissue preparation can help to minimize damage produced during tissue isolation.

*Clearance time of labeled cells*: The sensitivity of ISEL+ allows one to identify dying cells sooner than with other techniques. Like other techniques, ISEL+ provides static information from a tissue section at a single age from a single animal. Rigorous determination of how a population of cells changes with time, which would require real-time analysis of the same cells in the same animal, cannot therefore be made. Within a tissue section, a cell observed to be labeled on a single day may be just starting to die, midway through its death, or about to be eliminated. The half-life of dying neuroblasts or post-mitotic neurons identified by ISEL+ could range from a few hours to several days, and therefore the actual number of cells eliminated on a given day is uncertain. Based on studies in the small intestinal villus (Pompeiano et al., 1998), cells labeled by ISEL+ can require up to several days to be eliminated following the onset of PCD, or can be eliminated within hours at the end of the cell death program, which currently serves as the best estimate for interpreting ISEL+ labeling.

*Tissue sectioning*: Cryostat sections must be of excellent quality. Sections should be cut with a sharp blade to minimize tissue damage and potential artifactual labeling. Thickness should be kept in the range of 10 μm; greater thickness may prevent access of labeling reagents into all cells. Other variables, such as sample and box temperatures within the cryostat, blade angle, anti-roll bar positioning, size of cut block, and ambient temperature and humidity outside the cryostat can all affect tissue sectioning.

*Fixation and permeabilization of tissue sections*: Over-fixation can block access of labeling reagents, while under-fixation can produce artifactual labeling. Using Basic Protocol 1, a wide variety of tissues has been examined with consistent results; however, fixation can be re-examined empirically to further optimize results. No proteinase treatments are used in this procedure (in contrast to the original TUNEL procedure); the Triton X-100 permeabilization step is therefore critical, because it allows access through both the outer cell and nuclear membranes for DNA labeling.

*Acetylation of tissue sections:* Background signal primarily arises from nonspecific retention of marker molecules (e.g., dUTP or

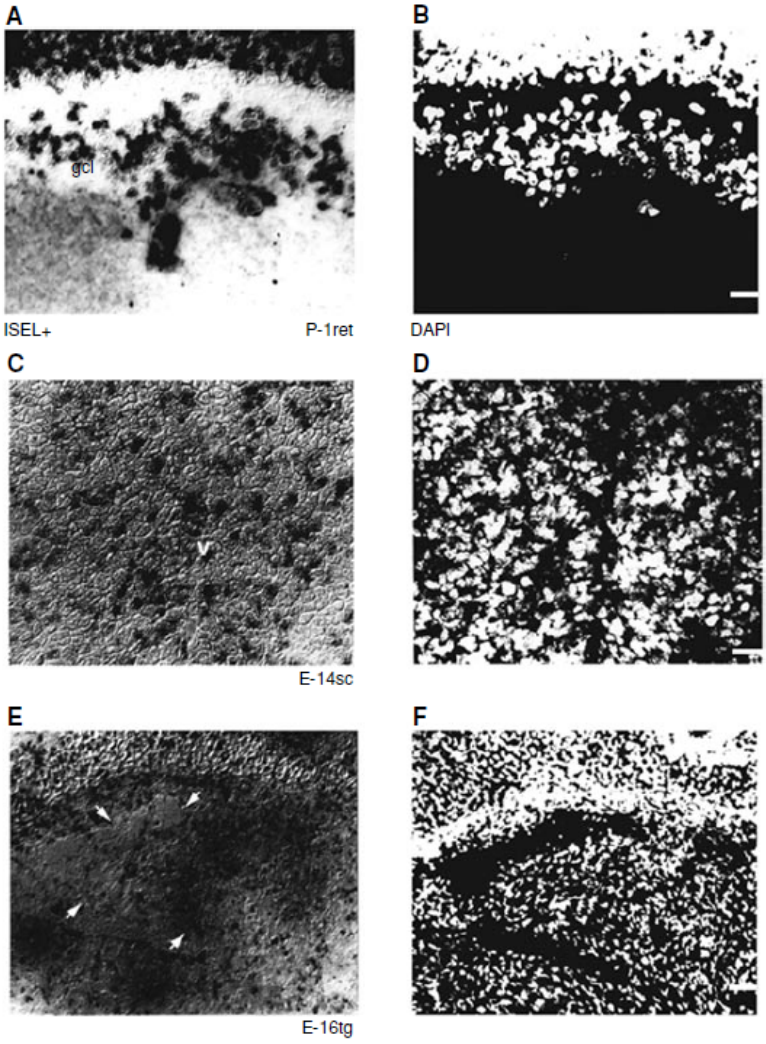


**Figure 3.8.6** ISEL+ identifies dying cells in known models of neuronal PCD. Slides were viewed by ISEL+ (**A, C, E**) and DAPI counterstaining (**B, D, F**) for comparison. (**A, B**) P1 is the peak of PCD in the ganglion cell layer, and here >60% of cells were labeled by ISEL+. (**C, D**) ISEL+ identified dying motor neurons in the embryonic mouse (E14) spinal cord. (E, F). In the trigeminal ganglion at E16, dying neurons were easily identified by ISEL+ despite their low incidence at this age. Arrowheads indicate ganglion borders. Scale bar = 20 μm. Abbreviations: ret, retina; gcl, ganglion cell layer; sc, spinal cord; v, ventricle; tg, trigeminal ganglion.

anti-DIG/AP antibody) in tissue sections. Several chemical functional groups in proteins (such as amine and carboxylate groups) are believed to promote nonspecific binding. In addition, marker molecules may become entrapped within the three-dimensional tissue structure. This source of background can be minimized by treating tissue slides with acetic anhydride to acetylate basic groups. Acetic anhydride is very hygroscopic and hydrolyzes in the presence of water to form acetic acid, thereby neutralizing its acetylation ability. Therefore, fresh acetic anhydride (preferably using newly opened vials) should be used during the preparation of TEA/acetic anhydride.

*Terminal deoxynucleotidyl transferase (TdT)*: The unit activity of TdT differs between suppliers; even different batches from one supplier can be quite variable. Enough TdT from the same supplier and batch should be obtained to complete an entire experiment without switching batches or suppliers. Like all enzymes, TdT should be stored in a reliable, non-defrosting −20°C freezer, and maintaining a dedicated stock of the enzyme is recommended.

*Immunohistochemical procedures*: Two steps are particularly important. First, overnight incubation with anti-digoxigenin gives a substantially stronger and cleaner signal than a 1 hr (or intermediate) incubation, and can be used for maximum sensitivity. Prolonged incubation for color development should be conducted in darkness. Second, alkaline phosphatase, especially associated with a bluish (versus reddish) reaction product, produces the best sensitivity. Other labels can be used (e.g., fluorescence, horseradish peroxidase), but they are less sensitive than the blue alkaline phosphatase product (Fig. 3.8.7A,B). Fluorescence labeling, however, does allow for detection and co-visualization of other proteins with tagged antibodies.

*Sample storage*: Embedded samples can be stored at −80°C for up to several weeks. Cut sections can be stored desiccated for at least several months, provided they are not repeatedly thawed and refrozen. Once reacted for alkaline phosphatase detection, samples should be coverslipped (see protocols above) and can be stored indefinitely.

*Labeling of DNA not associated with cell death*: In theory, any free DNA end could be labeled by ISEL+. Biologically relevant free ends such as Okazaki fragments do not appear to be labeled, as shown in studies comparing cells undergoing DNA synthesis (identified by BrdU incorporation) to cells labeled by ISEL+ (Blaschke et al., 1996; Staley et al., 1997). Mitochondrial DNA is circular and does not appear to be labeled. DNA cleavage by procedures like acid nicking (e.g., for anti-BrdU immunohistochemistry) can produce artifactual labeling and should be accounted for before using ISEL+.

***LMPCR***

All oligonucleotides should be gel-purified to ascertain their correct size before ligation; they may also need to be desalted. Of course, the primers must *not* be phosphorylated. Be sure to work from the same batch of primers for all the analyzed samples, as differences in ligation efficiency between batches of primers have been observed. It is advisable to use fresh ligase and dNTPs. DNA samples must be washed thoroughly in 70% ethanol to remove salts that can inhibit ligation. Be sure to resuspend the DNA completely after precipitation, washing, and drying. Various thermal cyclers may produce slightly different ramping profiles and they should be assessed accordingly. Use a standard DNA sample with which to compare the tissue in question. In the mouse, DNA from the adult small intestine always produces a very strong signal with 20 cycles or less, while DNA from 2.5-week-old thymus produces a signal after ~22 cycles.

## Anticipated Results

The ISEL+ procedure will result in the visualization of more PCD compared to TUNEL. As discussed above, the clearance time is not well defined for cells labeled by ISEL+. The seemingly high level of PCD identified by ISEL+ has been shown to be a more accurate description of PCD compared to other methodologies, as discussed above. In conjunction with ISEL+, LMPCR provides independent confirmation of the operation of apoptotic mechanisms. Clear nucleosomal ladders can be observed in nervous system tissue similar to those seen in the thymus (Fig. 3.8.8); the adult PCD reflects glial and/or subependymal cell PCD (A.J. Blaschke and J. Chun, unpub. observ.).

## Time Considerations

***ISEL+***

Starting in the morning, the entire procedure can be completed within 3 days; with optimization, and depending on the level of sensitivity required, this should be viewed as an upper limit.

Day 1: Tissue isolation and slide processing

Day 2: TdT polymerization and heat inactivation

Overnight 2: Anti-digoxigenin incubation

Day 3: Visualization of bound antibody and analysis.

***LMPCR***

Starting in the afternoon, the entire procedure can be completed in 3 days.

Day 1, p.m.: Tissue isolation

Overnight 1: SDS/proteinase K incubation

Day 2, a.m.: Organic extraction and precipitation

Day 2, p.m.: DNA resuspension

Overnight 2: Linker ligation

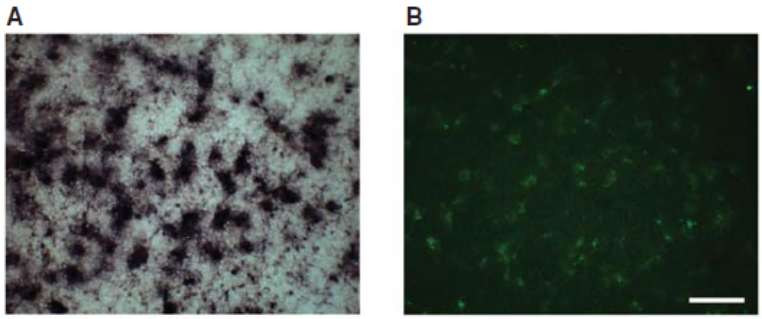


**Figure 3.8.7** ISEL+ using AP and NPT/BCIP colorimetric detection is more sensitive than fluorescence detection. ISEL+ was run in parallel for identical lengths of time using both (**A**) AP and NPT/BCIP colorimetric detection and using (**B**) an AlexaFluor 488 (green) tagged secondary antibody on E12 mouse fetal liver to detect clusters of lymphocytes. The signal strength was stronger, the background was cleaner, and more dying cells were detected using colorimetric detection. Positive signal is denoted by dark stain and green fluorescence in the left and right panels, respectively. Scale bar = 100 μm. For color version of this figure go to *http://www.currentprotocols.com/protocol/ns0308*.

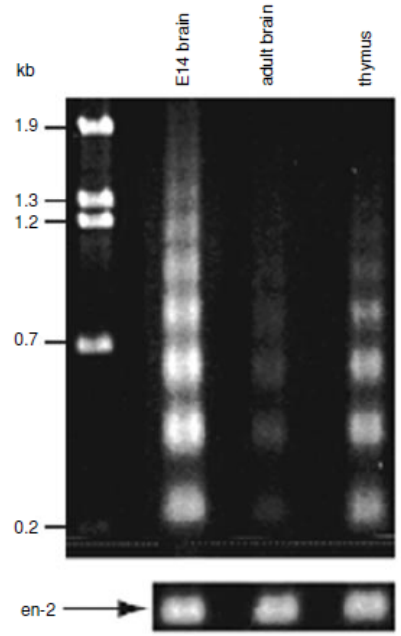


**Figure 3.8.8** Ligation-mediated PCR (LMPCR) identifies DNA nucleosomal ladders from tissues undergoing apoptosis. Mouse embryonic day E14 and adult brain tissue, as well as 4-week-old mouse thymus, were examined using LMPCR for the presence of nucleosomal ladder as an independent indication of apoptosis. Clear nucleosomal ladders can be seen for embryonic brain and adult thymus tissue, while adult brain showed significantly less intense laddering. A single-copy gene PCR control is also shown (for *engrailed, en*), confirming that equivalent amounts of genomic DNA were used for each sample. See Staley et al. (1997) for additional details.

Day 3: PCR, gel electrophoresis, and photographic documentation.

As with ISEL+, the procedure can be optimized and truncated to reduce the duration of the procedure.

## Acknowledgments

The authors thank Anne Blaschke and Kristina Staley for their contributions to the original protocols, Danielle Letourneau for careful reading of the manuscript, and all past and present members of the laboratory for their help in the refinement of these protocols. This work was supported by the NIH (NIMH, NINDS, NIDA, and NICHD to JC) and the NSF (YCY). YCY is also in the Biomedical Sciences Graduate Program, UCSD School of Medicine.

## Literature Cited

Arbour, N., Vanderluit, J.L., Le Grand, J.N., Jahani-Asl, A., Ruzhynsky, V.A., Cheung, E.C., Kelly, M.A., MacKenzie, A.E., Park, D.S., Opferman, J.T., and Slack, R.S. 2008. Mcl-1 is a key regulator of apoptosis during CNS development and after DNA damage. *J. Neurosci.* 28:6068-6078.

Blaschke, A.J., Staley, K., and Chun, J. 1996. Widespread programmed cell death in proliferative and post-mitotic regions of the fetal cerebral cortex. *Development* 122:1165-1174.

Blaschke, A.J., Weiner, J.A., and Chun, J. 1998. Programmed cell death is a universal feature of embryonic and postnatal neuroproliferative regions throughout the central nervous system. *J. Comp. Neurol.* 396:39-50.

Buchman, V.L. and Davies, A.M. 1993. Different neurotrophins are expressed and act in a developmental sequence to promote the survival of embryonic sensory neurons. *Development* 118:989-1001.

Bursch, W., Hochegger, K., Torok, L., Marian, B., Ellinger, A., and Hermann, R.S. 2000. Autophagic and apoptotic types of programmed cell death exhibit different fates of cytoskeletal filaments. *J. Cell Sci.* 113:1189-1198.

Caelles, C., Helmberg, A., and Karin, M. 1994. p53-dependent apoptosis in the absence of transcriptional activation of p53-target genes. *Nature* 370:220-223.

Cecconi, F., Alvarez-Bolado, G., Meyer, B.I., Roth, K.A., and Gruss, P. 1998. Apaf1 (CED-4 homolog) regulates programmed cell death in mammalian development. *Cell* 94:727-737.

Chao, C., Herr, D., Chun, J., and Xu, Y. 2006. Ser18 and 23 phosphorylation is required for p53-dependent apoptosis and tumor suppression. *EMBO J.* 25:2615-2622.

Contos, J.J., Fukushima, N., Weiner, J.A., Kaushal, D., and Chun, J. 2000. Requirement for the lpA1 lysophosphatidic acid receptor gene in normal suckling behavior. *Proc. Natl. Acad. Sci. U.S.A.* 97:13384-13389.

Crespo, D., O'Leary, D.D.M., and Cowan, W.M. 1985. Changes in the numbers of optic nerve fibers during late prenatal and postnatal development in the albino rat. *Dev. Brain Res.* 19:129-134.

Davies, A. and Lumsden, A. 1984. Relation of target encounter and neuronal death to nerve growth factor responsiveness in the developing mouse trigeminal ganglion. *J. Comp. Neurol.* 223:124-137.

Depaepe, V., Suarez-Gonzalez, N., Dufour, A., Passante, L., Gorski, J.A., Jones, K.R., Ledent, C., and Vanderhaeghen, P. 2005. Ephrin signalling controls brain size by regulating apoptosis of neural progenitors. *Nature* 435:1244-1250.

Egerton, M., Scollay, R., and Shortman, K. 1990. Kinetics of mature T-cell development in the thymus. *Proc. Natl. Acad. Sci. U.S.A.* 87:2579-2582.

Ellis, H.M. and Horvitz, H.R. 1986. Genetic control of programmed cell death in the nematode *C. elegans*. *Cell* 44:817-829.

Flanagan, A.E.H. 1969. Differentiation and degeneration in the motor column of foetal mouse. *J. Morphol.* 129:281-305.

Gavrieli, Y., Sherman, Y., and Ben-Sasson, S.A. 1992. Identification of programmed cell death in situ via specific labeling of nuclear DNA fragmentation. *J. Cell Biol.* 119:493-501.

Groszer, M., Erickson, R., Scripture-Adams, D.D., Lesche, R., Trumpp, A., Zack, J.A., Kornblum, H.I., Liu, X., and Wu, H. 2001. Negative regulation of neural stem/progenitor cell proliferation by the Pten tumor suppressor gene in vivo. *Science* 294:2186-2189.

Gu, Y., Sekiguchi, J., Gao, Y., Dikkes, P., Frank, K., Ferguson, D., Hasty, P., Chun, J., and Alt, F.W. 2000. Defective embryonic neurogenesis in Ku-deficient but not DNA-dependent protein kinase catalytic subunit-deficient mice. *Proc. Natl. Acad. Sci. U.S.A.* 97:2668-2673.

Jiang, Y., de Bruin, A., Caldas, H., Fangusaro, J., Hayes, J., Conway, E.M., Robinson, M.L., and Altura, R.A. 2005. Essential role for survivin in early brain development. *J. Neurosci.* 25:6962-6970.

Kerr, J.F.R., Wyllie, A.H., and Currie, A.R. 1972. Apoptosis: A basic biological phenomenon with wide-ranging implications in tissue kinetics. *Br. J. Cancer* 26:239-257.

Kerr, J.F., Winterford, C.M., and Harmon, B.V. 1994. Apoptosis. Its significance in cancer and cancer therapy. *Cancer* 73:2013-2026.

Kingsbury, M.A., Rehen, S.K., Contos, J.J., Higgins, C.M., and Chun, J. 2003. Non-proliferative effects of lysophosphatidic acid enhance cortical growth and folding. *Nat. Neurosci.* 6:1292-1299.

Kuida, K., Zheng, T.S., Na, S., Kuan, C., Yang, D., Karasuyama, H., Rakic, P., and Flavell, R.A.

1996. Decreased apoptosis in the brain and premature lethality in CPP32-deficient mice. *Nature* 384:368-372.

Kuida, K., Haydar, T.F., Kuan, C.Y., Gu, Y., Taya, C., Karasuyama, H., Su, M.S., Rakic, P., and Flavell, R.A. 1998. Reduced apoptosis and cytochrome c-mediated caspase activation in mice lacking caspase 9. *Cell* 94:325-337.

Lance-Jones, C. 1982. Motoneuron cell death in the developing lumbar spinal cord of the mouse. *Dev. Brain Res.* 4:473-479.

Liang, Q., Li, W., and Zhou, B. 2008. Caspase-independent apoptosis in yeast. *Biochim. Biophys. Acta* 1783:1311-1319.

Lindsten, T., Golden, J.A., Zong, W.X., Minarcik, J., Harris, M.H., and Thompson, C.B. 2003. The proapoptotic activities of Bax and Bak limit the size of the neural stem cell pool. *J. Neurosci.* 23:11112-11119.

McConnell, M.J., Kaushal, D., Yang, A.H., Kingsbury, M.A., Rehen, S.K., Treuner, K., Helton, R., Annas, E.G., Chun, J., and Barlow, C. 2004. Failed clearance of aneuploid embryonic neural progenitor cells leads to excess aneuploidy in the Atm-deficient but not the Trp53-deficient adult cerebral cortex. *J. Neurosci.* 24:8090-8096.

Morris, R.G., Hargreaves, A.D., Duvall, E., and Wyllie, A.H. 1984. Hormone-induced cell death. 2. Surface changes in thymocytes undergoing apoptosis. *Am. J. Pathol.* 115:426-436.

Motoyama, N., Wang, F., Roth, K.A., Sawa, H., Nakayama, K., Nakayama, K., Negishi, I., Senju, S., Zhang, Q., Fujii, S., and Loh, D.Y. 1995. Massive cell death of immature hematopoietic cells and neurons in Bcl-x-deficient mice. *Science* 267:1506-1510.

Negoescu, A., Lorimier, P., Labat-Moleur, F., Drouet, C., Robert, C., Guillermet, C., Brambilla, C., and Brambilla, E. 1996. In situ apoptotic cell labeling by the TUNEL method: Improvement and evaluation on cell preparations. *J. Histochem. Cytochem.* 44:959-968.

Oppenheim, R.W. 1985. Naturally occurring cell death during neural development. *Trends Neurosci.* 8:487-493.

Oppenheim, R.W. 1989. The neurotrophic theory and naturally occurring motoneuron death. *Trends Neurosci.* 12:252-255.

Pompeiano, M., Hvala, M., and Chun, J. 1998. Onset of apoptotic DNA fragmentation can precede cell elimination by days in the small intestinal villus. *Cell Death Differ.* 5:702-709.

Pompeiano, M., Blaschke, A.J., Flavell, R.A., Srinivasan, A., and Chun, J. 2000. Decreased apoptosis in proliferative and postmitotic regions of the Caspase 3-deficient embryonic central nervous system. *J. Comp. Neurol.* 423:1-12.

Raff, M.C., Barres, B.A., Burne, J.F., Coles, H.S., Ishizaki, Y., and Jacobson, M.D. 1993. Programmed cell death and the control of cell survival: lessons from the nervous system. *Science* 262:695-700.

Rehen, S.K., Kingsbury, M.A., Almeida, B.S., Herr, D.R., Peterson, S., and Chun, J. 2006. A new method of embryonic culture for assessing global changes in brain organization. *J. Neurosci. Methods* 158:100-108.

Sengelaub, D.R., Dolan, R.P., and Finlay, B.L. 1986. Cell generation, death, and retinal growth in the development of the hamster retinal ganglion cell layer. *J. Comp. Neurol.* 246:527-543.

Shortman, K., Egerton, M., Spangrude, G.J., and Scollay, R. 1990. The generation and fate of thymocytes. *Sem. Immunol.* 2:3-12.

Staley, K., Blaschke, A.J., and Chun, J. 1997. Apoptotic DNA fragmentation is detected by a semi-quantitative ligation-mediated PCR of blunt DNA ends. *Cell Death Differ.* 4:66-75.

Strater, J., Gunthert, A.R., Bruderlein, S., and Moller, P. 1995. Microwave irradiation of paraffin-embedded tissue sensitizes the TUNEL method for in situ detection of apoptotic cells. *Histochem. Cell Biol.* 103:157-160.

Surh, C.D. and Sprent, J. 1994. T-cell apoptosis detected in situ during positive and negative selection in the thymus. *Nature* 372:100-103.

Thomas, L.B., Gates, D.J., Richfield, E.K., O'Brien, T.F., Schweitzer, J.B., and Steindler, D.A. 1995. DNA end labeling (TUNEL) in Huntington's disease and other neuropathological conditions. *Exp. Neurol.* 133:265-272.

Ucker, D.S. 1991. Death by suicide: One way to go in mammalian cellular development? *New Biol.* 3:103-109.

Vaccarino, F.M., Schwartz, M.L., Raballo, R., Nilsen, J., Rhee, J., Zhou, M., Doetschman, T., Coffin, J.D., Wyland, J.J., and Hung, Y.T. 1999. Changes in cerebral cortex size are governed by fibroblast growth factor during embryogenesis. *Nat. Neurosci.* 2:848.

Weiner, J.A. and Chun, J. 1999. Schwann cell survival mediated by the signaling phospholipid lysophosphatidic acid. *Proc. Natl. Acad. Sci. U.S.A.* 96:5233-5238.

Weiner, J.A., Hecht, J.H., and Chun, J. 1998. Lysophosphatidic acid receptor gene vzg-1/lpA1/edg-2 is expressed by mature oligodendrocytes during myelination in the postnatal murine brain. *J. Comp. Neurol.* 398:587-598.

White, K., Grether, M.E., Abrams, J.M., Young, L., Farrell, K., and Steller, H. 1994. Genetic control of programmed cell death in Drosophila. *Science* 264:677-683.

Wijsman, J.H., Jonker, R.R., Keijzer, R., Van De Velde, C.J.H., Cornelisse, C.J., and Van Dierendonck, J.H. 1993. A New Method to Detect Apoptosis in Paraffin Sections: In Situ End-labeling of Fragmented DNA. *J. Histochem. Cytochem.* 41:7-12.

Wilkie, A.L., Jordan, S.A., Sharpe, J.A., Price, D.J., and Jackson, I.J. 2004. Widespread tangential dispersion and extensive cell death during early neurogenesis in the mouse neocortex. *Dev. Biol.* 267:109-118.

Wood, K.A., Dipasquale, B., and Youle, R.J. 1993. In situ labeling of granule cells for apoptosis-associated DNA fragmentation reveals different mechanisms of cell loss in developing cerebellum. *Neuron* 11:621-632.

Wyllie, A.H. 1981. Cell death: A new classification separating apoptosis from necrosis. *In* Cell Death in Biology and Pathology (I.D. Bowen and R.A. Lockshin, eds.) pp. 9-34. Chapman and Hall, London.

Yan, L., Herrmann, V., Hofer, J.K., and Insel, P.A. 2000. β-Adrenergic receptor/cAMP-mediated signaling and apoptosis of S49 lymphoma cells. *Am. J. Physiol.-Cell Physiol.* 279:C1665-1674.

Yoshida, H., Kong, Y.Y., Yoshida, R., Elia, A.J., Hakem, A., Hakem, R., Penninger, J.M., and Mak, T.W. 1998. Apaf1 is required for mitochondrial pathways of apoptosis and brain development. *Cell* 94:739-750.

Young, R.W. 1984. Cell death during differentiation of the retina in the mouse. *J. Comp. Neurol.* 229:362-373.

Zaidi, A.U., D'Sa-Eipper, C., Brenner, J., Kuida, K., Zheng, T.S., Flavell, R.A., Rakic, P., and Roth, K.A. 2001. Bcl-X(L)-caspase-9 interactions in the developing nervous system: Evidence for multiple death pathways. *J. Neurosci.* 21:169-175.

## Key References

Blaschke et al., 1996. See above.
*First use of ISEL+ and the detection of programmed cell death in the embryonic cortex.*

Gavrieli et al., 1992. See above.
*First technique to utilize labeling of DNA ends to detect programmed cell death.*

Raff et al., 1993. See above.
*An informative discussion of nervous system programmed cell death.*

Staley et al., 1997. See above.
*First use of ligation-mediated PCR to demonstrate apoptotic ladders in normal tissues.*

Wyllie, 1981. See above.
*First demonstration of nucleosomal ladders associated with apoptosis.*

The text of Appendix B is, in full, a reprint of material as it appears in the Current Protocols of Neuroscience. The dissertation author was the primary co-author of this work, and Dr. Jerold Chun supervised the research that forms the basis of this chapter. Appendix B is reprinted here with full permission of all the authors, and of the journal, as per its published copyright transfer agreement.

**References**


1. Raff, M.C., Barres, B.A., Burne, J.F., Coles, H.S., Ishizaki, Y., and Jacobson, M.D. (1993). Programmed cell death and the control of cell survival: lessons from the nervous system. Science *262*, 695-700.

2. Ross, M.E. (1996). Cell division and the nervous system: regulating the cycle from neural differentiation to death. Trends Neurosci *19*, 62-68.

3. Wyllie, A.H. (1981). Cell death: A new classification separating apoptosis from necrosis. In Cell Death in Biology and Pathology, I.D. Bowen and R.A. Lockshin, eds. (London: Chapman and Hall).

4. Ucker, D.S. (1991). Death by suicide: one way to go in mammalian cellular development? The New biologist *3*, 103-109.

5. Baehrecke, E.H. (2002). How death shapes life during development. Nat Rev Mol Cell Biol *3*, 779-787.

6. Kerr, J.F., Winterford, C.M., and Harmon, B.V. (1994). Apoptosis. Its significance in cancer and cancer therapy. Cancer *73*, 2013-2026.

7. Kerr, J.F., Wyllie, A.H., and Currie, A.R. (1972). Apoptosis: a basic biological phenomenon with wide-ranging implications in tissue kinetics. British journal of cancer *26*, 239-257.

8. Morris, R.G., Hargreaves, A.D., Duvall, E., and Wyllie, A.H. (1984). Hormone-induced cell death. 2. Surface changes in thymocytes undergoing apoptosis. Am J Pathol *115*, 426-436.

9. Davies, A.M. (1996). The neurotrophic hypothesis: where does it stand? Philos Trans R Soc Lond B Biol Sci *351*, 389-394.

10. Cowan, W.M. (2001). Viktor Hamburger and Rita Levi-Montalcini: the path to the discovery of nerve growth factor. Annu Rev Neurosci *24*, 551-600.

11. Yung, Y.C., Kennedy, G., and Chun, J. (2009). Identification of neural programmed cell death through the detection of DNA fragmentation in situ and by PCR. Curr Protoc Neurosci *Chapter 3*, Unit 3 8.

12. Blaschke, A.J., Staley, K., and Chun, J. (1996). Widespread programmed cell death in proliferative and postmitotic regions of the fetal cerebral cortex. Development *122*, 1165-1174.

13. Blaschke, A.J., Weiner, J.A., and Chun, J. (1998). Programmed cell death is a universal feature of embryonic and postnatal neuroproliferative regions throughout the central nervous system. J Comp Neurol *396*, 39-50.

14. Kuida, K., Zheng, T.S., Na, S., Kuan, C., Yang, D., Karasuyama, H., Rakic, P., and Flavell, R.A. (1996). Decreased apoptosis in the brain and premature lethality in CPP32-deficient mice. Nature *384*, 368-372.

15. Pompeiano, M., Blaschke, A.J., Flavell, R.A., Srinivasan, A., and Chun, J. (2000). Decreased apoptosis in proliferative and postmitotic regions of the Caspase 3-deficient embryonic central nervous system. J Comp Neurol *423*, 1-12.

16. Kuida, K., Haydar, T.F., Kuan, C.Y., Gu, Y., Taya, C., Karasuyama, H., Su, M.S., Rakic, P., and Flavell, R.A. (1998). Reduced apoptosis and cytochrome c-mediated caspase activation in mice lacking caspase 9. Cell *94*, 325-337.

17. Zaidi, A.U., D'Sa-Eipper, C., Brenner, J., Kuida, K., Zheng, T.S., Flavell, R.A., Rakic, P., and Roth, K.A. (2001). Bcl-X(L)-caspase-9 interactions in the developing nervous system: evidence for multiple death pathways. J Neurosci *21*, 169-175.

18. Cecconi, F., Di Bartolomeo, S., Nardacci, R., Fuoco, C., Corazzari, M., Giunta, L., Romagnoli, A., Stoykova, A., Chowdhury, K., Fimia, G.M., et al. (2007). A novel role for autophagy in neurodevelopment. Autophagy *3*, 506-508.

19. Yoshida, H., Kong, Y.Y., Yoshida, R., Elia, A.J., Hakem, A., Hakem, R., Penninger, J.M., and Mak, T.W. (1998). Apaf1 is required for mitochondrial pathways of apoptosis and brain development. Cell *94*, 739-750.

20. Lindsten, T., Golden, J.A., Zong, W.X., Minarcik, J., Harris, M.H., and Thompson, C.B. (2003). The proapoptotic activities of Bax and Bak limit the size of the neural stem cell pool. J Neurosci *23*, 11112-11119.

21. Groszer, M., Erickson, R., Scripture-Adams, D.D., Lesche, R., Trumpp, A., Zack, J.A., Kornblum, H.I., Liu, X., and Wu, H. (2001). Negative regulation of neural stem/progenitor cell proliferation by the Pten tumor suppressor gene in vivo. Science *294*, 2186-2189.

22. Motoyama, N., Wang, F., Roth, K.A., Sawa, H., Nakayama, K., Negishi, I., Senju, S., Zhang, Q., Fujii, S., and et al. (1995). Massive cell death of immature hematopoietic cells and neurons in Bcl-x-deficient mice. Science *267*, 1506-1510.

23. Jiang, Y., de Bruin, A., Caldas, H., Fangusaro, J., Hayes, J., Conway, E.M., Robinson, M.L., and Altura, R.A. (2005). Essential role for survivin in early brain development. J Neurosci *25*, 6962-6970.

24. Arbour, N., Vanderluit, J.L., Le Grand, J.N., Jahani-Asl, A., Ruzhynsky, V.A., Cheung, E.C., Kelly, M.A., MacKenzie, A.E., Park, D.S., Opferman, J.T., et al. (2008). Mcl-1 is a key regulator of apoptosis during CNS development and after DNA damage. J Neurosci *28*, 6068-6078.

25. Vanderhaeghen, P., and Cheng, H.J. (2010). Guidance molecules in axon pruning and cell death. Cold Spring Harb Perspect Biol *2*, a001859.

26. Llambi, F., Causeret, F., Bloch-Gallego, E., and Mehlen, P. (2001). Netrin-1 acts as a survival factor via its receptors UNC5H and DCC. EMBO J *20*, 2715-2722.

27. Bloch-Gallego, E., Ezan, F., Tessier-Lavigne, M., and Sotelo, C. (1999). Floor plate and netrin-1 are involved in the migration and survival of inferior olivary neurons. J Neurosci *19*, 4407-4420.

28. Furne, C., Rama, N., Corset, V., Chedotal, A., and Mehlen, P. (2008). Netrin-1 is a survival factor during commissural neuron navigation. Proc Natl Acad Sci U S A *105*, 14465-14470.

29. Ben-Zvi, A., Manor, O., Schachner, M., Yaron, A., Tessier-Lavigne, M., and Behar, O. (2008). The Semaphorin receptor PlexinA3 mediates neuronal apoptosis during dorsal root ganglia development. J Neurosci *28*, 12427-12432.

30. Depaepe, V., Suarez-Gonzalez, N., Dufour, A., Passante, L., Gorski, J.A., Jones, K.R., Ledent, C., and Vanderhaeghen, P. (2005). Ephrin signalling controls brain size by regulating apoptosis of neural progenitors. Nature *435*, 1244-1250.

31. Kingsbury, M.A., Rehen, S.K., Contos, J.J., Higgins, C.M., and Chun, J. (2003). Non-proliferative effects of lysophosphatidic acid enhance cortical growth and folding. Nat Neurosci *6*, 1292-1299.

32. Estivill-Torrus, G., Llebrez-Zayas, P., Matas-Rico, E., Santin, L., Pedraza, C., De Diego, I., Del Arco, I., Fernandez-Llebrez, P., Chun, J., and De Fonseca, F.R. (2008). Absence of LPA1 signaling results in defective cortical development. Cereb Cortex *18*, 938-950.